จุฬาลงกรณ์มหาวิทยาลัย
ทุนวิจัย
กองทุนรัชดาภิเษกสมโภช

รายงานวิจัย

การพัฒนาสมรรถนะการสื่อสารระยะไกล ผ่านเส้นใยแก้วนำแสง โดยใช้อุปกรณ์คอนจูเกต สัญญาณที่กึ่งกลาง

โดย

พสุ แก้วปลั่ง

มีนาคม ๒๕๔๖

ทุนวิจัย

กองทุนรัชดาภิเษกสมโภช

รายงานผลการวิจัย

การพัฒนาสมรรถนะการสื่อสารระยะไกลผ่านเส้นใยแก้วนำแสง โดยใช้อุปกรณ์คอนจูเกตสัญญาณที่กึ่งกลาง

PERFORMANCE IMPROVEMENT OF LONG-HAUL ULTRA-HIGH-SPEED OPTICAL TRANSMISSION USING MIDWAY OPTICAL PHASE CONJUGATION

โดย

พสุ แก้วปลั่ง

มีนาคม 2546

ACKNOWLEDGEMENT

At first, I wish to express my utmost gratitude to Associated Prof. Tuptim Angkaew and Prof. Dr. Kazuro Kikuchi, my research advisors for providing me fruitful advice together with valuable discussion. Without their professional guidance and continuous encouragement throughout the course of present study, this work can hardly be completed.

I should thank for my assistance: Mr. Anutarapun Pakdeechart for his helps in running programs, analyzing calculated results, plotting a lot of graphs, working on documentary works and making a number of helpful discussion together with stimulated suggestion to this study.

Finally, I would like to give a special thank with all of my heart to my beloved one for her forbearance and encouragement, my wife, Dr. Orapin Kaewplung and my daughter, Miss Alisara Kaewplung.

ชื่อโครงการวิจัย การพัฒนาสมรรถนะการสื่อสารระยะไกลผ่านเส้นใยแก้วนำแสงโดยใช้อุปกรณ์คอนจูเกตสัญญาณที่กึ่งกลาง

ชื่อผู้วิจัย พสุ แก้วปลั่ง

เดือนและปีที่ทำวิจัยเสร็จ มีนาคม 2546

บทคัดย่อ

สมรรถนะของระบบสื่อสารผ่านเส้นใยแก้วนำแสงซึ่งใช้อุปกรณ์คอนจูเกตสัญญาณที่กึ่งกลางระบบถูกจำกัดด้วยปัญหาหลักคือดิสเพอร์ชั่นอันดับสามของเส้นใยแก้วนำแสงและปรากฏการณ์เรโซแนนท์ผ่านความไม่เป็นเชิงเส้นของเส้นใยแก้วนำแสงที่เกิดขึ้นที่ความถี่ไซด์แบนด์ค่าเฉพาะเจาะจงของสัญญาณ ซึ่งเรียกว่าปรากฏการณ์ความไม่เสถียรของไซด์แบนด์

โครงงานนี้นำเสนอทฤษฎีการวิเคราะห์ความไม่สเถียรของไซด์แบนด์ที่สมบูรณ์ที่สุดในกรณีที่นำเส้นใยแก้วนำแสงสองเส้นที่มีคุณสมบัติต่างกันมาต่อกันเพื่อทำการจัดการกับดิสเพอร์ชั่นเป็นครั้งแรก ผลจากการวิเคราะห์พบว่าอัตราการเพิ่มขนาดของความไม่เสถียรของไซด์แบนด์ลดลงเมื่อเพิ่มค่าดิสเพอร์ชั่นของเส้นใยแก้วนำแสงที่นำมาทำการจัดการดิสเพอร์ชั่น

โครงงานนี้ได้จับประเด็นเฉพาะสำหรับกรณีที่การจัดการดิสเพอร์ชั่นใช้เส้นใยแก้วนำแสงโหมดเดียวแบบทั่วไปกับเส้นใยแก้วนำแสงแบบกลับดิสเพอร์ชั่น ซึ่งการจัดการดิสเพอร์ชั่นแบบนี้ได้ถูกใช้ทั่วไปเพื่อกำจัดดิสเพอร์ชั่นอันดับสองและสามในเวลาเดียวกัน จากการคำนวณด้วยวิธีเชิงเลขพบว่าความไม่เสถียรของไซด์แบนด์สามารถก่อให้เกิดความผิดเพี้ยนอย่างชัดเจนของสัญญาณที่เดินทางในระบบสื่อสารมัลติเพล็กซ์เชิงความถี่ที่มีช่องสัญญาณหนาแน่นมากได้ถ้าช่องสัญญาณถูกวางที่ความถี่ที่เกิดความไม่เสถียรของไซด์แบนด์ เมื่อช่องสัญญาณถูกเรียงใหม่เพื่อหลีกเลี่ยงความถี่ที่เกิดความไม่เสถียรของไซด์แบนด์ พบว่าสมรรถนะของระบบดีขึ้นอย่างชัดเจน

ต่อจากนั้นโครงการนี้ได้เสนอวิธีกำจัดทั้งดิสเพอร์ชั่นอันดับสามและความไม่เสถียรของไซด์แบนด์พร้อมกันในระบบคอนจูเกตสัญญาณโดยใช้เส้นใยแก้วนำแสงโหมดเดียวแบบทั่วไปกับเส้นใยแก้วนำแสงแบบกลับดิสเพอร์ชั่นมาทำการจัดการกับดิสเพอร์ชั่นเป็นครั้งแรก จากการคำนวณด้วยวิธีเชิงเลขพบว่าระบบที่ใช้วิธีที่นำเสนอนี้สามารถส่งสัญญาณความเร็วสูงถึงสองร้อยกิกะบิตต่อวินาทีในระยะทางหนึ่งหมื่นกิโลเมตรเป็นผลสำเร็จ เมื่อค่าความถี่ของการจัดการกับดิสเพอร์ชั่นและค่ากำลังของสัญญาณได้รับการเลือกให้อยู่ในค่าที่เหมาะสมที่สุด

Project Title Performance improvement of long-haul ultra-high-speed optical transmission using midway optical phase conjugation

Name of the Investigators Pasu Kaewplung

Year March 2003

Abstract

In optical phase conjugation (OPC) systems, the third-order dispersion (TOD) of optical fibers and the nonlinear resonance at well-defined signal sideband frequencies called sideband instability (SI) mainly limit the transmission performance.

We present for the first time a complete theoretical analysis of sideband instability (SI) that occurs when two kinds of fibers with different characteristics are concatenated to form a dispersion-managed fiber link. We find that the magnitude of the SI gain reduces with the increase in strength of dispersion management.

Next, we focus on the fiber link using the combination of standard single-mode fiber (SMF) and reverse dispersion fiber (RDF), which is widely used for simultaneously compensating second-order dispersion (SOD) and third-order dispersion (TOD). By computer simulation, it is shown that, in wavelength-division-multiplexed (WDM) systems, SI still induces significant degradation in channels located at frequencies where SI induced from other channels arises. By re-allocating the channel frequency to avoid the SI frequency, the transmission performance is improved significantly.

Then we propose for the first time, a scheme for simultaneous suppression of both TOD and SI in OPC systems using a higher-order dispersion-managed link consisting of SMFs and RDFs. Computer simulation results demonstrate the possibility of 200-Gbit/s transmission over 10,000 km in the higher-order dispersion-managed OPC system, where the dispersion map is optimized by our system design strategies.

CONTENTS

List of Figures

1. INTRODUCTION

1.1 General background

Four-wave mixing (FWM) and cross-phase modulation (XPM) in optical fibers have been recognized as the main problems that cause signal waveform distortion in wavelength-division-multiplexed (WDM) systems [1]-[3]. FWM induces signal energy transfer among channels, while, through XPM, temporal intensity variation of every channel modulates the phase of other copropagating channels. In fact, the use of non-zero dispersion for signal transmission yields relatively different propagating group-velocity among channels, referred as walk-off, which dramatically results in the reduction of channel crosstalk induced from both FWM and XPM. For this purpose, the second-order dispersion (SOD) management method has been proposed and demonstrated [4]-[7]. Through this method, fiber sections are periodically arranged in such a way that the signal carrier wavelengths alternatively fall in normal and anomalous dispersion region, while, for each period, the total fiber exhibits zero or near zero dispersion on average. Therefore, signal pulse propagating in the link will always experience non-zero dispersion while its width is almost preserved at each compensation period due to low average dispersion.

However, such an approach can manage only SOD in only one channel. Therefore, in WDM systems, signal channels far from the average zero-dispersion wavelength experience different amount of dispersion accumulation along the entire system length because of the existence of the dispersion slope or third-order dispersion (TOD).

It has been predicted that the existence of TOD limits the available passband of the WDM systems with the data rates of over 10Gbit/s [8]-[10]. For further expansion both in capacity and distance, dispersion management to eliminate both SOD and TOD will be one of the key issues. For this purpose, the special dispersion compensating fibers called reverse dispersion fiber (RDF) [11], [12] has been proposed and demonstrated its potential. Since RDF exhibits low negative TOD with large negative SOD, we can achieve the dispersion flattened fiber link with low average SOD by combining RDF with standard single-mode fiber (SMF) in each compensation interval. The use of such higher-order dispersion compensation fiber link in combination with the optimization of channel spacing realizes the

simultaneously reduction of FWM, XPM, and TOD. Transmission experiment shows that using the combination of SMF and RDF can achieve the data rate as high as 1Tbit/s (104x10Gbit/s) WDM transmission over 10,000km [13].

On the other hand, in ultra-high bit-rate optical-time-division multiplexed (OTDM) transmission systems, the SOD of fibers for transmission must be completely compensated. With SOD averaged to zero, the TOD also shows up and influences transmission characteristics. Moreover, TOD interplays with the self-phase modulation (SPM) of optical pulses, causing severe distortion of both signal waveform and signal spectrum [1].

In the dispersion-managed system using non-return-to-zero (NRZ) pulse format, the bit rate of the 10,000-km transmission system is limited only about 10 Gbit/s because of the interplay of the TOD with the SPM. For further expansion both in capacity and distance, dispersion management to eliminate both SOD and TOD will also be one of the key issues. For this purpose, the use of a special dispersion compensating fiber link composed of SMF and RDF will play a significant role in the realization of the dispersion flattened fiber link with low average SOD for simultaneously compensating both SOD and TOD.

Several recent OTDM transmission experiments have demonstrated very attractive results of this SMF+RDF combination based systems such as the transmission of 640 Gbit/s over 92 km [14] and even the data bit rate as high as 1.28 Tbit/s over 70 km [15].

As an alternative approach for ultrahigh-bit-rate long-haul transmission, midway optical phase conjugation (OPC) is an attractive solution to compensating for the distortion induced from the interplay between SOD and SPM [16]. However, the ultimate performance of OPC systems is also limited by TOD together with a nonlinear resonance at well-defined signal sideband frequencies induced by periodic amplification process called sideband instability (SI) effect [16]. Recently, we have demonstrated by a numerical simulation that the single-channel OTDM 100 Gbit/s, 10,000 km transmission can be made possible by using the optimum signal power in the OPC system incorporated with TOD compensation [17]. For the SI effect, Watanabe and Shirasaki have given a condition for perfect SI compensation [18]. In order to satisfy the condition, a dispersion-decreasing fiber (DDF), whose dispersion-decreasing

coefficient is proportional to a fiber loss coefficient, must be installed throughout the entire OPC system length. A good transmission result of 20 Gbit/s over 3,000 km [18] was demonstrated by using a quasi-DDF in which short fibers with different dispersion values were concatenated to form the dispersion-decreasing profile. However, such an approach sounds too impractical to be employed in real systems. Moreover, uncompensated TOD will show up to affect the long-haul transmission with the bit rate higher than 40 Gbit/s. Recently, our analysis has demonstrated a more practical way to suppress SI by only applying strong dispersion management [19], [20]. Therefore, by using such combination of SMF and RDF in the OPC system, the simultaneous suppression of both SI and TOD can be expected.

1.2 Purpose of this project

The aim of this project is to improve the performance of OPC transmission system by simultaneously suppressing both two main problems which limit ultra-high-bit-rate long-haul transmission performance, TOD and SI, using SMF+RDF-based dispersion compensation. We will find out the most suitable dispersion profile for installing such SMF+RDF combination on OPC systems by calculating the numerical bit error rate (BER) of the transmitted signal. The most suitable installing scheme should result the minimum BER comparing the other possible schemes. Next we will derive theoretical optimum system design strategies in order to achieve system maximum performance.

In this study, we will use both mathmetical approach based on solving the nonlinear Schrodinger equation (NLSE) with small signal approximation, together with numerical approach based on solving the NLSE with the split-step Fourier method [1]. It should be noted that the numerical method will be mainly used to prove our derived theory and to evaluate our designed systems. The anticipated speed of 10,000km OPC system where both TOD and SI are suppressed may reach a value as high as 200Gbit/s.

1.3 Studying Steps

To this report, this project has been done step by step as shown below.

1. Deriving complete mathematical expression of SI gain concerning periodic dispersion management fiber link when two different fibers are connected together.
2. Writing computer simulation programs to evaluate the proposed theory.
3. Studying the effect of SI on higher-order dispersion-managed WDM transmission systems and how the problem can be avoided.
4. Summarizing the results, submitting the works to IEEE/OSA periodical journal of lightwave technology.
5. Writing computer simulation programs based on SMF+RDF-dispersion-managed OPC system model for simulating the optical signal propagation in this dispersion-managed OPC system.
6. Using the computer simulation to confirm the reduction of SI gain with the proposed scheme and how it affects the linear TOD compensation.
7. Theoretically comparing the advantages and disadvantages of two possible ways to install the SMF+RDF combination in OPC system. One is symmetric dispersion profile with respect to midway OPC and the other is asymmetric dispersion profile with respect to midway OPC. Then, find the suitable scheme from these two possible ways. Then, find the most suitable scheme between these two schemes.
8. Confirming the comparison between these two schemes by computer simulations, together with using computer simulations to evaluate the performance improvement of 100 Gbit/s 10,000 km OPC transmission system employing the combination of SMF and RDF to simultaneously suppress TOD and SI.
9. Summarizing the results, submitting the result to conferences, and writing this progress report
10. Focusing on OPC systems with transmission length of 10,000km and with data rate higher than 100Gbit/s, theoretically studying the optimum OPC system design strategies in terms of designing system operating parameters such as the optimum dispersion map, average dispersion value, etc. to achieve maximum system performance.
11. Writing computer simulation programs based on SMF+RDF-dispersion-managed OPC system model for simulating the optical signal propagation in this dispersion-managed OPC system.

12. Using computer simulations to evaluate the performance improvement of 10,000km OPC transmission system with data rate higher than 100Gbit/s using our proposed optimum system design strategies.
13. Summarizing the results, writing a final report, and presenting the work in conferences and publishing the work in periodical journal

1.4 Organization of this report

This paper is organized as follows. Chapter 2 reviews some previous works about the OPC system and its limitations. The TOD compensation scheme in OPC system is also discussed. Our main contributions presented here commence from chapter 3. In chapter 3, the complete theoretical analysis of SI focusing on the case when two different characteristic fibers connected together is made. In our analysis, not only the periodic power variation but the periodic dispersion management, periodic fiber loss coefficient variation, and periodic nonlinear coefficient variation are also included. We derive the analytical SI gain and the SI frequency considering three cases: (a) when a dispersion management period is larger than an amplifier spacing, (b) when the two lengths are equal, and (c) when an amplifier spacing is larger than a dispersion management period. The derived theory is evaluated its accuracy by computer simulations.

We also focuses on dispersion managed transmission system consisting of SMF and RDF. Our computer simulation results show that, when two or more channels produce SI at the same frequency, SI significantly causes a serious problem to the channel whose carrier is positioned just at that superposition resonance frequency. We also demonstrate that, by re-arranging the channel position or channel spacing in such a way that none of the SI resonance frequency falls inside the channel signal bandwidth, the transmission performance is significantly improved.

In chapter 4, the reduction of the SI gain by employing the combination of SMF and RDF is shown. We then discuss an implementation of dispersion management in OPC systems. We suggest that a symmetric dispersion profile with respect to the mid-point of the system is preferable in order to avoid nonlinear accumulation of amplifier noise when the system operates with relatively high signal intensity. The performance improvement of the dispersion-managed

100-Gbit/s OPC system using the symmetric dispersion profile is confirmed by numerical simulations even when the dispersion map is not optimized.

Next, we discuss the optimum dispersion map design for obtaining the maximum performance in OPC systems. We demonstrate that, a 200-Gbit/s data transmission over a 10,000 km distance can be achieved by simultaneously suppressing TOD and SI in OPC systems using the dispersion-managed fiber link consisting of SMF and RDF whose dispersion map is properly designed. Finally, the summary of this report, together with the suggestion for future work are presented in chapter 5.

2. OPTICAL TRANMISSION SYSTEM USING MIDWAY OPTICAL PHASE CONJUGATION

Since we have been so far originally studied the optical phase conjugation (OPC) systems and the effect of SI. First, we should summarize the main limitations of OPC systems. Next, we discuss the accumulation characteristic of TOD in OPC systems and demonstrate that the performance of the OPC system can be improved beyond TOD limitation only by linearly compensating TOD. Numerical simulation results show that 100Gbit/s, 10,000km transmission is made possible by assuming linear TOD compensation [20].

2.1 OPC system and its limitation

Figure 2.1 shows schematically the midway OPC system. Under the condition that all of the system characteristics are symmetric with respect to the midway OPC, generating the conjugate signal of the first-half-transmitted signal at the midway of the system, all of the phase distortions induced in the first half are completely compensated via the self-recovery effect of the conjugate signal when transmitting through the second half of the system. However, in real transmission, three problems including one from an asymmetric system characteristic occur and limit a performance of OPC systems.

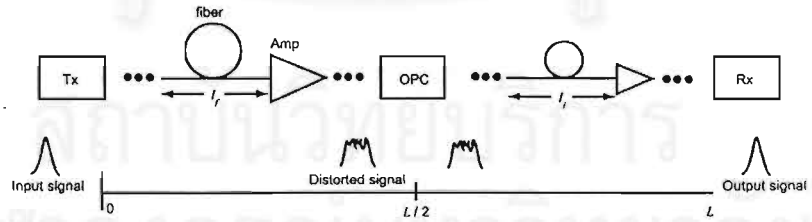

Fig. 2.1: Midway OPC system

According to the nonlinear Schrodinger equation (NLSE) which governs the propagation of signal pulses in an optical fiber [1]

$$\frac{\partial A}{\partial z} = -\frac{\alpha}{2}A - \frac{i}{2}\beta_2 \frac{\partial^2 A}{\partial T^2} + \frac{1}{6}\beta_3 \frac{\partial^3 A}{\partial T^3} + i\gamma |A|^2 A, \qquad (2.1)$$

where A denotes the complex amplitude of the signal, z the propagation distance, α the attenuation coefficient, β_2 the GVD

coefficient, β_3 the TOD coefficient, γ the fiber nonlinearity coefficient, and $T = t - z/v_g$ the time measured in a frame of reference moving with the pulse at the group velocity v_g. Take the complex conjugation of NLSE, we obtain

$$-\frac{\partial A^*}{\partial z} = +\frac{\alpha}{2}A^* - \frac{i}{2}\beta_2\frac{\partial^2 A^*}{\partial T^2} - \frac{1}{6}\beta_3\frac{\partial^3 A^*}{\partial T^3} + i\gamma\left|A^*\right|^2 A^*, \qquad (2.2)$$

where * denotes the complex conjugate operation. Eq. (2.2) describes the complex conjugate amplitude of the signal A propagating in backward direction through the fiber which exhibit reverse sign of α and β_3. According to Eq. (2.1) and (2.2) indicates that if we generate the complex conjugate of the distorted pulses at the midway of a transmission link and let them travel through the second half of the link, we will obtain the complex conjugate of the undistorted input pulses at the output end. The nonlinear waveform distortion caused by the fiber nonlinearity and the dispersion is thus perfectly compensated at the output end. However, to achieve the perfect compensation two conditions are needed. First, the transmission fiber of the second half must have negative β_3 while its β_2 still keeps the same sign as that of first half. Second, the propagation of signal through the second half requires a distributed gain instead of distributed loss since the sign of α must be reversed.

According to the first requirement, the widely-used transmission fibers such as SMF and dispersion-shifted fiber (DSF) both exhibit positive TOD. Therefore, similar to other systems, the TOD in OPC systems cannot be compensated by OPC but it just accumulates along the system length and will also cause the signal waveform distortion. On the other hand, the second condition can be satisfied only in an ideal lossless medium. In real system with long distance transmission, a periodic lumped amplification must be used for maintain signal power in order to obtain good signal-to-noise ratio (SNR) at receiver. The fiber loss and this periodic amplification forms a periodic signal power distribution along the system length and at the same time produces a periodic variation of fiber refractive index through the nonlinear Kerr effect of an optical fiber. By this process, it seems like a grating is virtually constructed in the transmission fiber. As

shown in Fig. 2.2, a resonance between the virtual grating and the signal will occur at the signal sideband component whose wave vector matches the wave vector of this virtual grating resulting in exponential growth of that component with transmission length. This phenomenon is known as the sideband instability (SI), which causes signal waveform distortion if SI arises at frequency inside the signal bandwidth, which cannot be eliminated by using optical bandpass filter [24]. Quanlitatively, SI can be considered as four-wave mixing (FWM) effect which is quasi-phase-matched by the assistance of the periodic power variation induced virtual grating as the condition

$$k_+ + k_- = 2k_0 + k_f . \tag{2.3}$$

In Eq. (2.3), k_0 denote the wave number of the signal which acts as a pump, $k_\pm$ the sideband wave numbers, and k_f the wave number of the virtual grating which is given as

$$k_f = \frac{2\pi n}{l_f}, \tag{2.4}$$

where $n = 0,\pm1,\pm2,...,$ and l_f is the amplifier spacing. The sideband frequency ω_n shifted from the carrier frequency, at which SI arises is obtained from Eq. (2.3) and (2.4) as

$$\omega_n = \pm\sqrt{\frac{1}{|\beta_2|}\left(k_f n - 2\,\mathrm{sgn}(\beta_2)\overline{P}\right)}. \tag{2.5}$$

where $\overline{P}$ is the path-averaged signal power. The power gain $\lambda(\omega_n)$ of SI at each *n*-order resonance frequency is

$$\lambda(\omega_n) = 2P_0|F_n|, \tag{2.6}$$

where P_0 denotes the signal input power and F_n the *n*-order of the Fourier series coefficient of the periodic function $\alpha(z)$ whose period is equal to l_f.

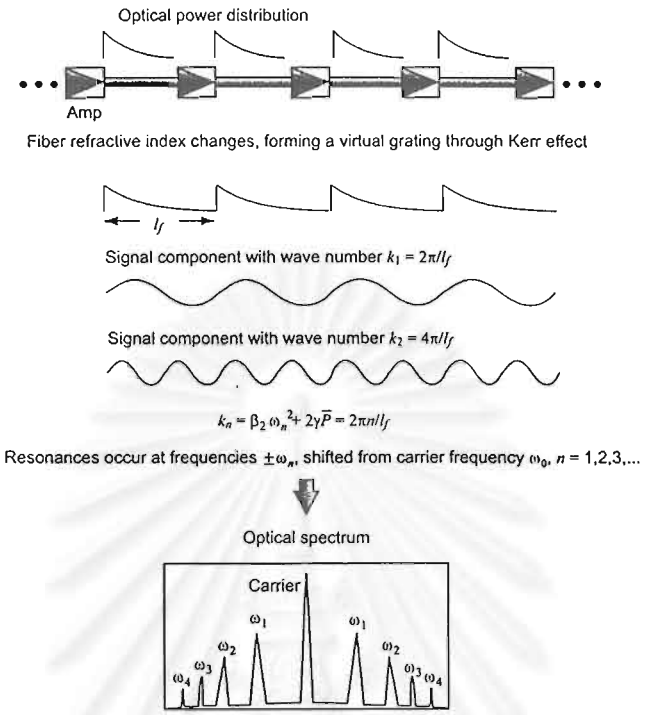

Fig. 2.2: The occurrence of SI in chain of periodic amplification

2.2 TOD compensation for OPC Systems

First, it should be noted that, to discuss the accumulation of TOD in OPC systems, it is necessary to use three characteristic scales: the SOD length L_{d2}, the TOD length L_{d3}, and the nonlinear length L_{nl}, which are defined in [1] for forecasting signal behaviors in optical fiber transmission systems. The effect whose scale becomes the shortest plays a dominant role in limiting the system performance.

Dispersion-managed NRZ transmission systems require the GVD compensation interval, which is quite shorter than L_{nl}, in order to avoid the interaction of the SOD and SPM. If the SOD compensation interval becomes much shorter than L_{d3}, which is usually the case, the pulse behaves in the TOD scale as if it propagates through a uniformly zero-dispersion fiber. In such a system, in order to prevent the interaction between the TOD and the SPM, it is necessary to place TOD compensators at the interval much shorter than L_{nl} so that TOD can be compensated before interacting with SPM.

Also in OPC systems, TOD cannot be compensated by OPC and it just accumulates along the system length. However, the accumulation of TOD in OPC systems has different characteristics from the above system. In OPC systems, SOD exists along the entire transmission length; therefore, L_{d2} becomes many times shorter than L_{n1} for the case of high bit-rate transmission. When L_{d2} is much shorter than L_{n1} and L_{d3}, the signal pulses are rapidly broadened by the SOD effect, and their peak power decreases after transmitting for several L_{d2}. This means that the broadened pulses almost do not experience the effect of the fiber nonlinearity, and we can thus expect that the accumulation of the TOD-induced phase shift increases almost linearly with the transmission length.

However, if L_{n1} becomes comparable to L_{d2}, both the pulses and spectrum will first be distorted by the interaction between SPM and SOD and subsequently being attacked by TOD. In this case, even though the pulse waveform and spectrum can be restored to their initial shapes at the end of the system, since OPC can compensated for the SPM+SOD interaction, the amount of TOD-induced phase shift is no longer linearly proportional to the transmission length because the spectral shape changes during the transmission. However, to obtain the condition $L_{n1} \approx L_{d2}$, we need an extremely high input signal power which will not be practically used in ordinary operating states. Thus, we can conclude from this fact that the TOD accumulation in OPC systems is almost linear. The linear TOD accumulation enables us to place only one TOD compensator at any point in the link instead of periodically placing TOD compensators at the interval much shorter than L_{n1}.

To confirm the prediction, the computer simulations have been performed. The main parameters used in the simulation are typical dispersion-shifted fiber parameters: SOD: D = -1ps/km/nm, TOD = 0.06ps/km/nm, and the nonlinear coefficient γ = $2.6W^{-1}km^{-1}$. The fiber loss and amplification process are neglected in order to focus only on the TOD accumulation characteristics. The TOD compensator used in simulations is assumed to be an ideal device that multiplies the complex amplitude of the signal with a negative amount of linearly accumulated phase shift caused by TOD. This compensator is placed only at the end of system. The optical pulse at the midway of the system is conjugated by an ideal infinite-bandwidth optical phase conjugator. The propagation of

the optical pulse is calculated by solving the nonlinear Schrodinger (NLS) equation by the split-step Fourier method [1]. In the first calculation, L_{n1} is set at 280km which is equal to L_{d3} and is approximately 40times longer than L_{d2} (≈ 7 km). Figures 2.3(a) and (b) shows the waveform and spectrum of a single 5ps FWHM optical pulse. The dotted curves show those of input pulse, whereas the dash-dotted curves those of the input pulse which propagates a 2000-km distance in the OPC system with the effect of TOD. The pulse waveform is distorted after propagation, while any change in its spectrum is not observed. The solid curves are those of 2,000-km transmitted pulse after compensating TOD. The pulse waveform recovers to the initial shape by TOD compensation. The results shown in Fig. 2.3 indicate that the accumulation of TOD is linear and the compensation is done perfectly as we expected in the previous section.

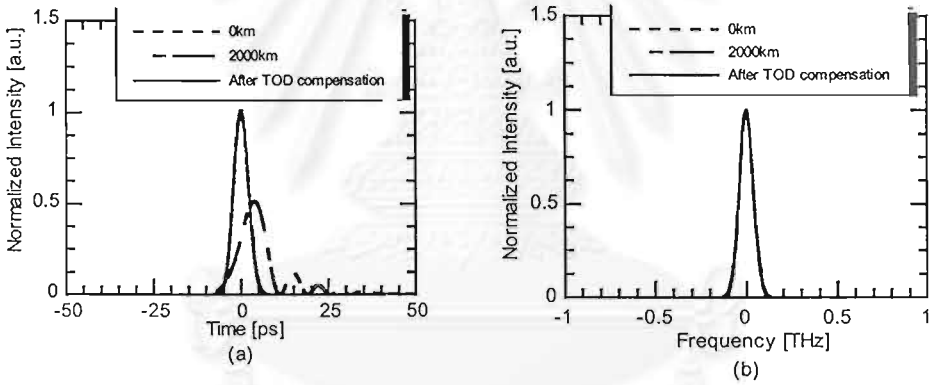

Fig. 2.3: Waveform and spectrum of an optical pulse propagating a 2,000-km distance in the OPC system where the nonlinear length is set equal to the TOD length; (a) optical pulse, (b) optical spectrum. The dotted curves show those of the input pulse, the dash-dotted curves those of the pulse transmitted with the effect of TOD, and the solid curves are those of the transmitted pulse after compensating the TOD.

Figures 2.4(a) and (b) show the calculated results of the case when L_{n1} is equal to L_{d2} (≈ 7 km). As we have mentioned, the interaction between TOD and SPM appears in OPC systems. Both the pulse shape and spectrum becomes distorted and the TOD compensation is almost failed.

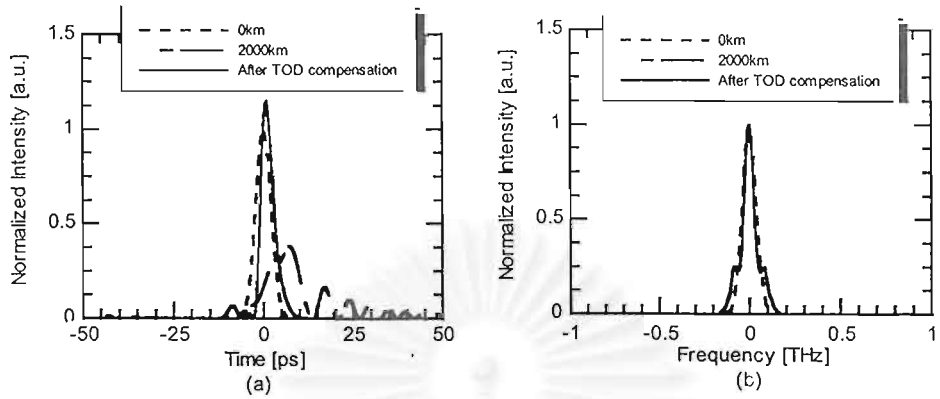

Fig. 2.4: Waveform and spectrum of an optical pulse propagating a 2,000-km distance in the OPC system where the nonlinear length is equal to the GVD length; (a) optical pulse, (b) optical spectrum. The dotted curves show those of the input pulse, the dash-dotted curves those of the pulse transmitted with the effect of TOD, and the solid curves are those of the transmitted pulse after compensating the TOD.

Figure 2.5 shows the calculated bit-error rate (BER) of the TOD compensated OPC system. The input power of all curves is set at 3mW. In this case, L_{nl} becomes almost equal to L_{d3} at 280km while L_{d2} is around 7km. An input optical signal consists of a pseudorandom 32-bit Gaussian RZ pulse train whose bit rate is equal to 100Gbit/s. The fiber loss of 0.2dB/km and amplification of 8dB at every 40km interval are included in the calculations. The optical amplifier produces ASE noise through a process of amplification with noise figure of 5.3dB (n_{sp} = 1.7). The ideal infinite bandwidth TOD compensator is placed at the output end of the fiber. We assume the use of an optical band-pass filter with a 1THz bandwidth in front of a receiver with a bandwidth of 50GHz-cutoff-low-pass filter. The system performance is evaluated in terms of the bit-error rate (BER) calculated by repeating 128times the transmission of the same pulse train and assuming Gaussian noise distribution [2].

According to the calculation results, the BER curve obtained from the TOD compensated OPC system (shown by squares) almost fits with that obtained from the system that neglects TOD (shown by diamonds), showing that the accumulation of the TOD is almost linear even L_{d3} is comparable to L_{nl} so that the linear TOD

compensation is done perfectly. Without TOD compensation (shown by circles) the maximum achievable length for 100Gbit/s OPC transmission is limited about 2,500km at BER=10^{-9} as shown by the across line. The TOD compensated OPC system gains more 4,000km transmission length up to 6,500km. This proves the effectiveness of TOD compensation on improving transmission performance in OPC systems.

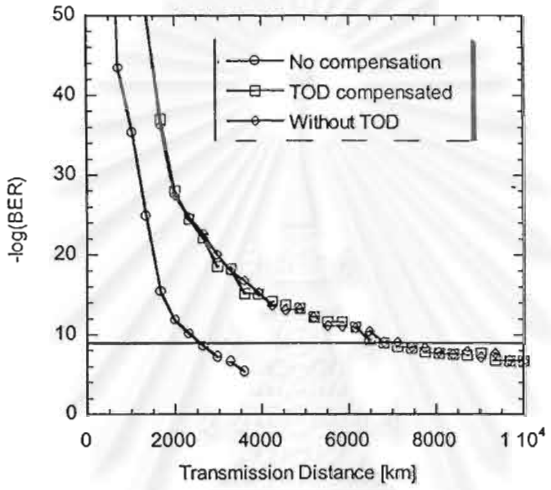

Fig. 2.5: BER of the 100-Gbit/s TOD compensated OPC systems where the nonlinear length becomes equal to the TOD length. The BER of TOD compensated OPC system is shown by squares, that of the system neglecting the TOD is shown by diamonds, and that of the system without TOD compensation is shown by circles.

If we increase the power of the signal, the achievable transmission distance will increase due to the improvement of SNR. At the same time, the increase in power gives rise to the degradations from the SI effect and the reduction of the corresponding nonlinear length. Therefore, the improvement and degradation will balance each other at an optimum input power in which the system can reach the maximum performance. To find the optimum power, we perform the simulations by increasing the input power of the same system as Fig. 2.6 from 3mW to 20mW. Figure 2.6 shows the BER calculated as a function of the transmission distance. The optimum power obtained from the result is approximately 7 mW, and with this input power, we can achieve over 10,000-km transmission at BER=10^{-9}.

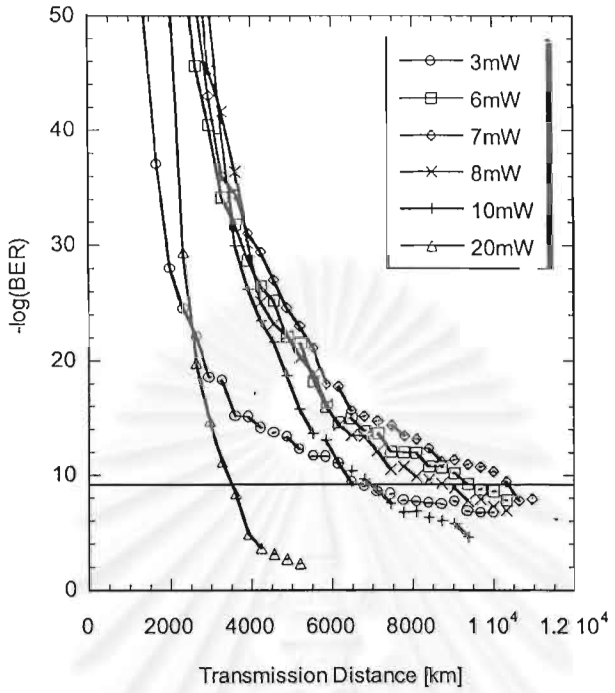

Fig. 2.6: BER curves of 100-Gbit/s TOD compensated OPC systems when an input power increases from 3 to 20 mW. We find that 100-Gbit/s, 10,000-km transmission is achieved by the optimum input power of 7mW when TOD is compensated in the OPC system.

3. COMPLETE ANALYSIS OF SIDEBAND INSTABILITY IN CHAIN OF PERIODIC DISPERSION-MANAGED FIBER LINK AND ITS EFFECT ON HIGHER-ORDER DISPERSION-MANAGED LONG-HAUL WAVELENGTH DIVISION MULTIPLEXED SYSTEMS

In this chapter, we demonstrate that the additional signal distortion to long-haul higher-order-dispersion-managed WDM systems can occur via the quasi FWM phase-match process assisted by periodic variation of the signal power in the chain of lossy fiber intervals and lumped amplifiers incorporated with periodic dispersion management. This parametric process, which occurs in both normal and anomalous dispersion region, is called sideband instability (SI). Through this process, signal carrier transfers its energy to specific sideband frequencies which grow up exponentially with transmission distance.

It has been shown theoretically that in order to avoid the XPM-induced signal waveform distortion for 10Gbit/s-based 10,000km WDM transmission, the use of channel spacing larger than 100GHz is preferable [21]. Several long-haul transmission experiments also demonstrate attractive results using the channel spacing around this value [8], [13], [22]. With this relatively large channel spacing, the first order SI, which usually exhibits large gain than higher orders, will not arise inside one's channel bandwidth. Therefore, the problem induced from SI has not been yet appeared and can be ignored for such transmissions.

However, with system distance shorter than 10,000km, the possibility of using smaller channel spacing for signal transmission has been shown [23]-[25]. In this situation, if two different channels produce SI at the same frequency, SI will cause a serious problem to the channels whose carriers are placed just at that frequency, especially for the frequency where the first order SI arises.

Historically, Matera et al. first theoretically showed the occurrence of SI in long distance systems through the periodic signal

amplification [26]. Kurtzke and Peterman briefly discussed the impact of SI on multichannel long-distance optical communication systems [27], [28]. In their works, by computer simulations, a serious channel signal distortion was observed when the SI resonance frequency superpositions on the channel frequency. Kikuchi, et al. experimentally observed SI in optical amplifier chain using a recirculating fiber loop [29]. Smith and Doran predicted that the periodic dispersion management also leads to the occurrence of SI. They also demonstrated that the gain of SI could be reduced by strong dispersion management [30]. Recently, we have presented a part of the derivation of SI under the existence of both periodic power variation and periodic dispersion variation [19].

However, all of the previous works have not yet included the periodic variation of fiber parameters such as fiber loss coefficient and fiber nonlinear coefficient, which is practically necessary to consider when two different fibers are connected together to form a dispersion-managed transmission line. Moreover, to avoid the problem of SI in WDM systems, it is important to study SI more details and the exact analytical expression of SI must be derived.

3.1 Derivation of Sideband Instability in The Presence of Periodic Power Variation and Periodic Dispersion Management

In long haul and high-capacity fiber transmission systems, the power of the optical signal must be kept high in order to obtain good signal-to-noise ratio (SNR) at a receiver. In such high power systems, by amplification process, the periodic power variation produces a periodic variation of fiber refractive index through the nonlinear Kerr effect of an optical fiber. By this process, it seems like a grating is virtually constructed in the transmission fiber. As shown in Fig. 3.1, a parametric resonance between the virtual grating and the signal will occur at the signal sideband component whose wave number is half of the wave number of this virtual grating resulting in exponential growth of that component with transmission length [26]. This phenomenon is known as the sideband instability (SI), which causes signal waveform distortion if SI arises at frequency inside the signal bandwidth since it cannot be eliminated by using optical bandpass filter.

I. Analytical Expression of SI gain

Quantitatively, the occurrence of SI can be explained in terms of quasi-phase-matched FWM process that is assisted by the virtual grating induced by the periodic power variation as the condition [9]

$$k_+ + k_- = 2k_0 + k_f . \tag{3.1}$$

In Eq. (3.1), the wave number of the signal, which acts as a pump, is $k_0 = -\gamma\overline{P} + \beta(\omega_0)$, the sideband wave numbers are $k_+ = k_- = \frac{1}{2}\beta_2\omega_n^2 + \beta(\omega_0)$, where $\beta(\omega_0)$ is the wave number at the central carrier frequency ω_0. k_f is the wave number of the virtual grating which is given as

$$k_f = \frac{2\pi n}{l_f}, \tag{3.2}$$

where $n = 0,\pm1,\pm2,...,$ and l_f is the amplifier spacing. The sideband frequency ω_n shifted from the carrier frequency, at which SI arises is obtained from Eq. (3.1) and (3.2) as

$$\omega_n = \pm\sqrt{\frac{1}{|\beta_2|}\left(k_f n - 2\,\mathrm{sgn}(\beta_2)\gamma\overline{P}\right)}. \tag{3.3}$$

where $\overline{P}$ is the path-averaged signal power. The power gain $\lambda(\omega_n)$ of SI at each *n*-order resonance frequency is

$$\lambda(\omega_n) = 2P_0|F_n|, \tag{3.4}$$

where P_0 denotes the signal input power and F_n the *n*-order of the Fourier series coefficient of the periodic function $\alpha(z)$ whose period is equal to l_f.

In fact, not only the periodic power variation, but also all of the periodic perturbation under the Kerr effect, such as the periodic dispersion variation, the periodic fiber loss coefficient variation, and the periodic fiber nonlinear coefficient variation, can also lead to the occurrence of SI. To obtain the general expression of SI considering all of the periodic perturbation, we should start the analytical derivation based on the models of dispersion management systems illustrated in Fig. 3.1. In Fig. 3.1, the signal power and the fiber dispersion is assumed to change periodically with transmission length. As we aim to concentrate to dispersion managed

transmission system consisting of SMF and RDF, the fiber link is composed of two different characteristic fibers with the same length. Therefore, the dispersion profile is the simplest type where the dispersion varies every half of period with the same amount plus and minus around a given average dispersion value. Each fiber has its own nonlinear coefficient and the fiber loss, which is assumed periodic by the period equivalent to the dispersion management period. We consider here three possible cases: (a) when the dispersion management period is longer than the amplifier span, (b) when the two scales become equal, and (c) when the dispersion management period is shorter than the amplifier span.

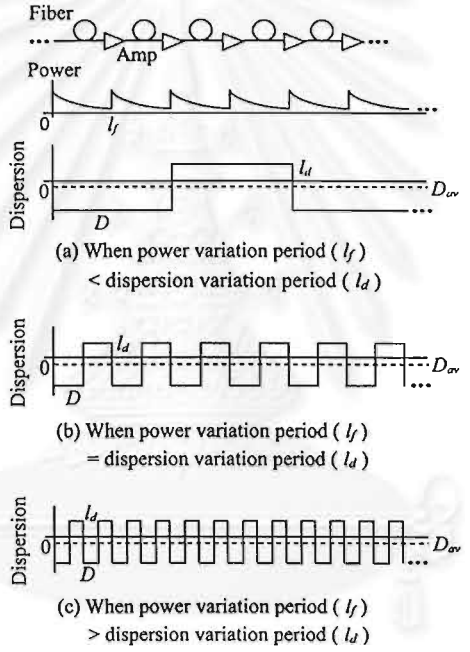

Fig. 3.1: Models of dispersion management system used for the analytical derivation. The signal power and fiber dispersion change periodically with transmission length. The fiber link consists of two different characteristic fibers with the same length. Three possible cases are modeled: (a) when the dispersion compensation period l_d is longer than the amplifier span l_f, (b) when the two scales become equal, and (c) when $l_d < l_f$.

The analysis starts from the nonlinear Schrodinger equation [1] for the signal envelope function $U(z,t)$

$$\frac{\partial U}{\partial Z} = -\frac{\alpha(z)}{2}U - \frac{j}{2}\left(\beta_{2av} + \beta_{2fl}(z)\right)\frac{\partial^2 U}{\partial t^2} + j\gamma(z)|U|^2 U. \qquad (3.5)$$

In Eq. (3.5), The GVD is separated in two parts: the constant average β_{2av} and the fluctuation part $\beta_{2fl}(z)$. The fiber loss coefficient $\alpha(z)$, the nonlinear coefficient $\gamma(z)$ and $\beta_{2fl}(z)$ are the functions of z which are assumed periodic with the same period equivalent with the dispersion management period. It should be noted that the GVD parameter β_2 relates to the common dispersion parameter D by

$$D = -\frac{\omega_0}{\lambda_0}\beta_2, \qquad (3.6)$$

where ω_0 denotes the carrier frequency and λ_0 the carrier wavelength.

At each amplifier, the span loss is compensated so that we can assume the optical field propagating in each amplification period has the form

$$U(z,t) = u(z,t)\exp\left(-\frac{1}{2}\alpha(z)z\right). \qquad (3.7)$$

Inserting Eq. (3.7) into Eq. (3.5), we obtain

$$\frac{\partial u}{\partial Z} = -\frac{j}{2}\left(\beta_{2av} + \beta_{2fl}(z)\right)\frac{\partial^2 u}{\partial t^2} + jf(z)|u|^2 u, \qquad (3.8)$$

where $f(z) = \gamma(z)\exp(-\alpha(z)z)$ is the periodical function whose period is equal to the amplifier spacing. Next, we perturb Eq. (3.8) by a small amplitude fluctuation a added to the steady solution of Eq. (3.8),

$$u(z,t) = \left(\sqrt{P_0} + a\right)\exp\left(jP_0\int_0^z f(z')dz'\right) \qquad (3.9)$$

where P_0 denotes the input peak power and a is defined as

$$a(z,t) = \frac{1}{2}\left\{a(z,\omega)\exp(j\omega t) + a(z,-\omega)\exp(-j\omega t)\right\}. \qquad (3.10)$$

Substituting Eq. (3.9) and (3.10) back to Eq. (3.8), then we obtain one set of two differential equations

$$\frac{\partial}{\partial Z}\begin{bmatrix} a(z,\omega) \\ a^*(z,-\omega)\end{bmatrix} = j\begin{bmatrix} \frac{1}{2}\left(\beta_{2av} + \beta_{2fl}(z)\right)\omega^2 + f(z)P_0 & f(z)P_0 \\ -f^*(z)P_0 & -\frac{1}{2}\left(\beta_{2av} + \beta_{2fl}(z)\right)\omega^2 - f^*(z)P_0\end{bmatrix}\begin{bmatrix} a(z,\omega) \\ a^*(z,-\omega)\end{bmatrix} \qquad (3.11)$$

where the subscript * indicates the counterpart complex conjugate. By introducing the transformation

$$\begin{bmatrix} a(z,\omega) \\ a^*(z,-\omega) \end{bmatrix} = \begin{bmatrix} \exp\left(j\frac{\omega^2}{2}\int_0^z \beta_{2,n}(z')dz' \right) & 0 \\ 0 & -\exp\left(j\frac{\omega^2}{2}\int_0^z \beta_{2,fl}(z')dz' \right) \end{bmatrix} \begin{bmatrix} b(z,\omega) \\ b^*(z,-\omega) \end{bmatrix} \quad (3.12)$$

Eq. (3.11) becomes

$$\frac{\partial}{\partial Z}\begin{bmatrix} b(z,\omega) \\ b^*(z,-\omega) \end{bmatrix} = j\begin{bmatrix} \frac{1}{2}\beta_{2av}\omega^2 + f(z)P_0 & g(z)P_0 \\ -g^*(z)P_0 & -\frac{1}{2}\beta_{2av}\omega^2 - f^*(z)P_0 \end{bmatrix} \begin{bmatrix} b(z,\omega) \\ b^*(z,-\omega) \end{bmatrix} \quad (3.13)$$

where

$$g(z) = f(z)\exp\left(-j\omega^2 \int_0^z \beta_{2,fl}(z')dz' \right). \quad (3.14)$$

By this transformation, we can remove the fast oscillations in the field envelope, so that only those changes that accumulate over the period of $\beta_{2,fl}(z)$ is left. The key step of this analysis is to expand $f(z)$ and $g(z)$ as complex Fourier series:

$$f(z) = \sum_{n=-\infty}^{\infty} F_n \exp(jk_f nz), \qquad g(z) = \sum_{n=-\infty}^{\infty} G_n \exp(jk_g nz), \quad (3.15)$$

where k_f and k_g are the fundamental wave constants of $f(z)$ and $g(z)$, and F_n and G_n denote the Fourier series coefficients of $f(z)$ and $g(z)$.

A. The case when the dispersion compensation period is larger than the amplifier spacing

First, we consider the case (a) when the dispersion management period l_d is larger than the amplifier spacing l_f. The wave constant k_g in this case can be written as $k_g = 2\pi/l_d = k_d$, where $l_d = 2pl_f$, so that $k_f = 2pk_d$ and p = 1, 2, 3, ... In order to get close to the resonance of the n-th Fourier component of the perturbation, we introduce the variable transformation

$$\begin{bmatrix} b(z,\omega) \\ b^*(z,-\omega) \end{bmatrix} = \begin{bmatrix} \exp\left(j\frac{1}{2}k_d nz \right) & 0 \\ 0 & \exp\left(-j\frac{1}{2}k_d nz \right) \end{bmatrix} \begin{bmatrix} c(z,\omega) \\ c^*(z,-\omega) \end{bmatrix} \quad (3.16)$$

Inserting Eq. (3.15) and (3.16) into Eq. (3.13) and equating only the coefficients of $\exp(jk_d nz/2)$ and $\exp(-jk_d nz/2)$ (for the complex conjugate counterpart), we obtain

$$\frac{\partial}{\partial Z}\begin{bmatrix} c(z,\omega) \\ c^*(z,-\omega) \end{bmatrix} = j\begin{bmatrix} -\frac{1}{2}k_d n + \frac{1}{2}\beta_{2av}\omega^2 + P_0F_0 & P_0G_n \\ -P_0G_n^* & \frac{1}{2}k_d n - \frac{1}{2}\beta_{2av}\omega^2 - P_0F_0^* \end{bmatrix}\begin{bmatrix} c(z,\omega) \\ c^*(z,-\omega) \end{bmatrix}, \quad (3.17)$$

where F_0 and G_n denote the fundamental and the n-th order coefficient of Fourier series of $f(z)$ and $g(z)$, respectively.

From the eigen values of Eq. (3.17), we obtain the power gain $\lambda(\omega)$ for the n-order SI effect as

$$\lambda(\omega) = \sqrt{4P_0^2|G_n|^2 - \left(k_d n - \beta_{2av}\omega^2 - P_0|F_0|\right)^2}\,. \quad (3.18)$$

At each order of SI, λ appears its peak at frequencies defined by

$$\omega_n = \pm\sqrt{\frac{1}{|\beta_{2av}|}\left(k_d n - 2\,\mathrm{sgn}(\beta_{2av})P_0|F_0|\right)}. \quad (3.19)$$

It is remarkable from Eq. (3.19) that SI occurs at frequencies determined by the dispersion management period l_d and by the averaged GVD β_{2av} independent of the fluctuation part β_{2fl}. For larger l_d, the SI gain position moves closer to signal carrier frequency, which may cause more severe signal waveform distortion. On the other hand, the peak of SI gain at the n-order resonance frequency $\lambda(\omega_n)$ depends on β_{2av} through ω_n in $|G_n|$ according to Eq. (3.14) and (3.19).

In order to obtain the expression of the SI gain, F_0 and G_n have to be derived. F_0 can be calculated from

$$F_0 = \frac{1}{l_d}\int_0^{l_d} f(z)dz = \frac{1}{l_d}\int_0^{l_d}\gamma(z)\exp(-\alpha(z)z)dz. \quad (3.20)$$

Since this paper considers the periodical dispersion compensation, which is constructed by the combination of two fibers in equal length. Each fiber exhibits different values of α and γ which are assumed to be constant along each fiber length. In each compensation interval, let α_1 and γ_1 represent the fiber loss coefficient and the nonlinear coefficient of the first fiber and α_2 and γ_2 represent the fiber loss coefficient and the nonlinear coefficient of the second fiber, respectively, F_0 is obtained through

$$F_0 = \frac{1}{l_d}\sum_{i=0}^{p-1}\left\{\int_{\frac{il_d}{2p}}^{\frac{l_d}{2p}+\frac{il_d}{2p}}\gamma_1\exp(-\alpha_1 z)dz + \int_{\frac{l_d}{2}+\frac{il_d}{2p}}^{\frac{l_d}{2}+\frac{l_d}{2p}+\frac{il_d}{2p}}\gamma_2\exp(-\alpha_2 z)dz\right\} = p\left\{\gamma_1\left(\frac{1-\exp\left(-\alpha_1\frac{l_d}{2p}\right)}{\alpha_1 l_d}\right)+\gamma_2\left(\frac{1-\exp\left(-\alpha_2\frac{l_d}{2p}\right)}{\alpha_2 l_d}\right)\right\} \quad (3.21)$$

By assuming that $\beta_{2fl}(z)$ follows the profile shown in Fig. 3.1, we have

$$\int_0^z \beta_{2fl}(z')dz' = \begin{cases} \beta_{2fl} z, z = \left[0, \frac{l_d}{2}\right) \\ \beta_{2fl}(l_d - z), z = \left[\frac{l_d}{2}, l_d\right] \end{cases} \quad (3.22)$$

Substituting Eq. (3.22) to the exponential part of Eq. (3.14), G_n can be analytically obtained through the Fourier integration

$$\begin{aligned} G_n = &\frac{1}{l_d}\sum_{i=0}^{p-1}\int_{\frac{il_d}{2p}}^{\frac{ld}{2p}+\frac{il_d}{2p}}\gamma_1\exp(-\alpha_1 z)\exp(-j\beta_{2fl}\omega^2 z)\exp(-jk_d n z)dz \\ &+\frac{1}{l_d}\sum_{i=0}^{p-1}\int_{\frac{l_d}{2}+\frac{il_d}{2p}}^{\frac{l_d}{2}+\frac{ld}{2p}+\frac{il_d}{2p}}\gamma_2\exp(-\alpha_2 z)\exp(-j\beta_{2fl}\omega^2(l_d - z))\exp(-jk_d n z)dz. \end{aligned} \quad (3.23)$$

Because $f(z)$ is periodical over each fiber length with the period of $\left[i\frac{l_d}{2p}, i\frac{l_d}{2p}+\frac{l_d}{2p}\right)$ for i = 0,1,2,..., it satisfies the following relations

$$f\left(\frac{il_d}{2p}\right) = \gamma\exp\left(-\alpha\frac{il_d}{2p}\right) = 1, \quad f\left(\frac{l_d}{2p}+\frac{il_d}{2p}\right) = \gamma\exp\left(-\alpha\frac{l_d}{2p}\right),$$

$$f\left(\frac{l_d}{2}+\frac{il_d}{2p}\right) = \gamma\exp\left(-\alpha\left(\frac{l_d}{2}+\frac{il_d}{2p}\right)\right) = 1, \quad f\left(\frac{l_d}{2}+\frac{l_d}{2p}+\frac{il_d}{2p}\right) = \gamma\exp\left(-\alpha\frac{l_d}{2p}\right) \quad (3.24)$$

Applying the above conditions to Eq. (3.23), we obtain

$$\begin{aligned} G_n = &\gamma_1\left\{\frac{1-\exp\left(-\alpha_1\frac{l_d}{2p}\right)\exp\left(-j\left(\beta_{2fl}\omega^2+k_d n\right)\frac{l_d}{2p}\right)}{\alpha_1 l_d + j\left(\beta_{2fl}\omega^2+k_d n\right)l_d}\right\}\sum_{i=0}^{p-1}\exp\left(-j\left(\beta_{2fl}\omega^2+k_d n\right)\frac{il_d}{2p}\right) \\ &+\gamma_2\left\{\frac{\exp\left(j\left(\beta_{2fl}\omega^2-k_d n\right)\frac{l_d}{2}\right)-\exp\left(-\alpha_2\frac{l_d}{2p}\right)\exp\left(j\left(\beta_{2fl}\omega^2-k_d n\right)\left(\frac{l_d}{2}+\frac{l_d}{2p}\right)\right)}{\alpha_2 l_d - j\left(\beta_{2fl}\omega^2-k_d n\right)l_d}\right\}\sum_{i=0}^{p-1}\exp\left(j\left(\beta_{2fl}\omega^2-k_d n\right)\frac{il_d}{2p}\right) \end{aligned} \quad (3.25)$$

At resonance frequency ω_n where the n-order SI occurs, the n-order SI gain becomes $2P_0|G_n|$. Figure 3.2 plots the n = 1, 2, and 3-order SI gain peaks at ω_n as a function of local SOD D, calculated by Eq. (3.25) with l_f = 40 km, l_d = 80 km. P_0 is assumed to be 5 mW,

At resonance frequency ω_n where the *n*-order SI occurs, the *n*-order SI gain becomes $2P_0|G_n|$. Figure 3.2 plots the *n* = 1, 2, and 3-order SI gain peaks at ω_n as a function of local SOD *D*, calculated by Eq. (3.25) with l_f = 40 km, l_d = 80 km. P_0 is assumed to be 5 mW, D_{av} is -5 ps/km/nm, α_1 and γ_1 of the fiber#1 are 0.2 dB and 1.6 $W^{-1}km^{-1}$, for the fiber#2, α_2 , γ_2 are 0.25 dB and 4.8 $W^{-1}km^{-1}$, respectively. It should be noted that *D* exhibits a negative value when the arrangement of fiber link changes the order of fiber installation to fiber#2-fiber#1 instead of fiber#1-fiber#2.

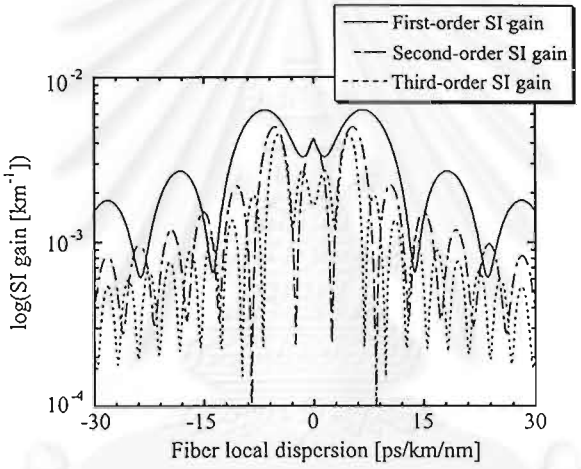

Fig. 3.2: Theoretical *n* = 1, 2, and 3-order SI gain peaks at resonance frequency ω_n as a function of local SOD *D*, calculated with l_f = 40 km, l_d = 80 km, P_0 = 5 mW, and D_{av} = -5 ps/km/nm. *D* exhibits a negative value when the arrangement of fiber link changes the order of fiber installation to RDF-SMF instead of SMF-RDF. The gain characteristics for all three orders appear to be decreased and periodically reduced to minimum points with the increase in *D*.

The gain characteristics shown in Fig. 3.2 for all three orders appear to be decreased and periodically reduced to minimum points with the increase in fiber local SOD. The reduction of SI gain with the increase of local SOD has been predicted by Smith and Doran [10]. However, the reason for explaining this phenomena has not been clearly mentioned yet. According to Eq. (3.23), it is obvious that the reduction of SI gain does not come from the linear addition and cancellation of the two Fourier components: one induced from the

$$|G_n| = \left| \frac{2}{l_f} \int_0^{l_f} \gamma_1 \exp(-\alpha_1 z) \exp\left(-j\frac{(c+n)}{2} k_f z\right) dz + \frac{2}{l_f} \exp(-j(c+n)\pi) \int_0^{l_f} \gamma_2 \exp(-\alpha_2 z) \exp\left(j\frac{(c-n)}{2} k_f z\right) dz \right| \quad (3.26)$$

Eq. (3.26) indicates that, for the n-order SI, by increasing the local GVD $|\beta_{2fl}|$, the corresponding c is increased, resulting in the increase of wave constant k_f by the factor of $(c+n)/2$ for the first term and $(c-n)/2$ for the second term, respectively. Each order of the SI gain, which becomes smaller for large k_f, is correspondingly reduced. Saying in other words, the first term of Eq. (3.26) is similar to the formula of Fourier integration using for obtaining the $(c+n)/2$ -order Fourier coefficient of $f(z)$ when the period is l_f, and for the second term, the $(c-n)/2$ -order Fourier coefficient. Therefore, this can be also interpreted that the increase of local GVD $|\beta_{2fl}|$ virtually shifts the order of SI induced from the power variation to higher order which exhibits lower gain than the lower order. Furthermore, the SI gain falls down to minimum points when the virtual order number $(c+n)/2$ and $(c-n)/2$ together become an integer. In Fig. 3.2, agreeing with our prediction, the SI gain reduces to minimum points when $(c+n)/2$ and $(c-n)/2$ becomes $|c|$ = 3, 5, 7,..., for the first-order, $|c|$ = 4, 6, 8,..., for the second-order, and $|c|$ = 5, 7, 9,...., for the third-order, respectively.

B. The case when the dispersion compensation period becomes equal to, or shorter than the amplifier spacing

In this subsection, we consider the case when l_d is equal to, or shorter than l_f. The wave constant k_g for this case becomes $k_f = 2\pi / l_f$. l_f is assumed to satisfy $l_f = pl_d$, where p = 1, 2, 3,.... The analysis approach for this case is almost similar to that of previous

subsection. By only replacing k_d in Eq. (3.15) with k_f. The power gain $\lambda(\omega)$ for n-order SI effect becomes

$$\lambda(\omega)=\sqrt{4P_0^2|G_n|^2-\left(k_f n-\beta_{2av}\omega^2-P_0|F_0|\right)^2}\,, \tag{3.27}$$

which exhibit each peak of the SI order at frequencies determined by

$$\omega_n=\pm\sqrt{\frac{1}{|\beta_{2av}|}\left(k_f n-2\,\mathrm{sgn}(\beta_{2av})P_0|F_0|\right)}. \tag{3.28}$$

From Eq. (3.28), the frequencies where SI arises are determined by the wave constant k_f which is constant even the dispersion management period l_d is changed. This means that, for $l_d \le l_f$, SI will almost arise at the same frequencies independent of the change in l_d, which is different from the previous case. For this case, F_0 can be obtained by

$$F_0=\frac{1}{l_f}\sum_{i=0}^{p-1}\left\{\int_{il_d}^{\frac{l_d}{2}+il_d}\gamma_1\exp(-\alpha_1 z)dz+\int_{\frac{l_d}{2}+il_d}^{l_d+il_d}\gamma_2\exp(-\alpha_2 z)dz\right\}$$

$$=\sum_{i=0}^{p-1}\left\{\gamma_1\left(\frac{\exp(-\alpha_1 il_d)-\exp\left(-\alpha_1\left(\frac{l_d}{2}+il_d\right)\right)}{\alpha_1 l_f}\right)+\gamma_2\left(\frac{\exp\left(-\alpha_2\left(\frac{l_d}{2}+il_d\right)\right)-\exp(-\alpha_2(l_d+il_d))}{\alpha_2 l_f}\right)\right\}. \tag{3.29}$$

It should be noted that, in fact, ω_n slightly depends on the change of l_d through F_0 in Eq. (3.28) and (3.29). For example, computing the first order SI frequency by substituting the same fiber parameters as the calculation of Fig. 3.2 into Eq. (3.28) and (3.29), when we reduce l_d from 40 km (= l_f) to 1 km, the first order SI frequency only moves 0.3 GHz closer to the carrier frequency. Therefore, such small amount of frequency shift is negligible comparing to the shift of SI position caused by the change of k_f.

G_n, for this case, can be analytically obtained through the series of Fourier integration

$$\begin{aligned}G_n=&\frac{1}{l_f}\sum_{i=0}^{p-1}\int_{il_d}^{\frac{l_d}{2}+il_d}\gamma_1\exp(-\alpha_1 z)\exp\left(-j\beta_{2fl}\omega^2 z\right)\exp\left(-jk_f nz\right)dz\\&+\frac{1}{l_f}\sum_{i=0}^{p-1}\int_{\frac{l_d}{2}+il_d}^{l_d+il_d}\gamma_2\exp(-\alpha_2 z)\exp\left(-j\beta_{2fl}\omega^2(l_d-z)\right)\exp\left(-jk_f nz\right)dz\,.\end{aligned} \tag{3.30}$$

As $\exp\left(-j\beta_{2fl}\omega^2 z\right)$ in $g(z)$ repeats periodically p times over each l_f,

$$\exp\left(-j\beta_{2fl}\omega^2 il_d\right)=1,\quad \exp\left(-j\beta_{2fl}\omega^2\left(\frac{l_d}{2}+il_d\right)\right)=\exp\left(-j\beta_{2fl}\omega^2\frac{l_d}{2}\right),$$

$$\exp\left(-j\beta_{2fl}\omega^2\left(l_d-\left(\frac{l_d}{2}+il_d\right)\right)\right)=\exp\left(-j\beta_{2fl}\omega^2\frac{l_d}{2}\right),\quad \exp\left(-j\beta_{2fl}\omega^2\left(l_d-\left(l_d+il_d\right)\right)\right)=1. \qquad (3.31)$$

Carrying out the integration in Eq. (3.30) by the assistance of the relations in Eq. (3.31) gives

$$G_n=\gamma_1\left\{\frac{1-\exp\left(-\alpha_1\frac{l_d}{2}\right)\exp\left(-j\left(\beta_{2fl}\omega^2+k_f n\right)\frac{l_d}{2}\right)}{\alpha_1 l_f+j\left(\beta_{2fl}\omega^2+k_f n\right)l_f}\right\}\sum_{i=0}^{p-1}\exp\left(-\alpha_1 il_d\right)\exp\left(-jk_f nil_d\right)$$
$$+\gamma_2\left\{\frac{\exp\left(-\alpha_2\frac{l_d}{2}\right)\exp\left(j\left(\beta_{2fl}\omega^2-k_f n\right)\frac{l_d}{2}\right)-\exp\left(-\alpha_2 l_d\right)\exp\left(-jk_f nl_d\right)}{\alpha_2 l_f-j\left(\beta_{2fl}\omega^2-k_f n\right)l_f}\right\}\sum_{i=0}^{p-1}\exp\left(-\alpha_2 il_d\right)\exp\left(-jk_f nil_d\right) \qquad (3.32)$$

Figure 3.3 shows the relations between the n = 1, 2, and 3-order SI gains and D at resonance frequency ω_n. All parameters used in Fig. 3.3 are the same as the plot in Fig. 3.2 except l_d is set equal to l_f at 40 km. The gain characteristics in Fig. 3.3 are in similar shapes to Fig. 3.2 where the gain decreases and periodically reduces to minimum points with the increase in D.

The similar characteristic is also obtained for the case of $l_d < l_f$ as shown in Fig. 3.4 where l_d is reduced to 10 km. However, in order to achieve the magnitude of SI gain as low as those of the above two cases, relatively large D is required.

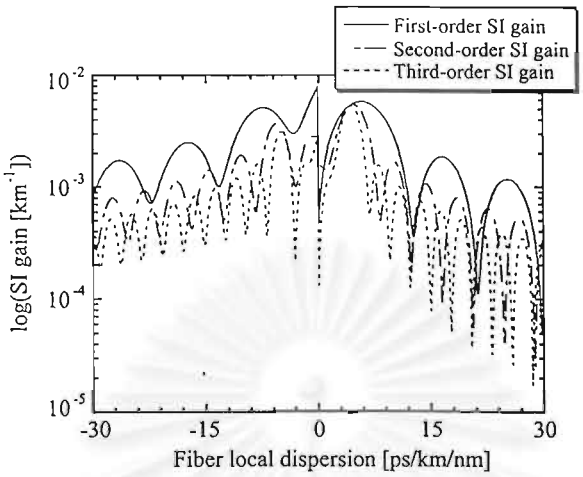

Fig. 3.3: Relations between the n = 1, 2, and 3-order SI gain peaks and D at resonance frequency ω_n. All parameters used in this figure are the same as the plot in Fig. 3.2 except l_d is set equal to l_f at 40 km. The SI gain characteristics for all three orders are similar to Fig. 3 where the gain decreases and periodically reduces to minimum points with the increase in D.

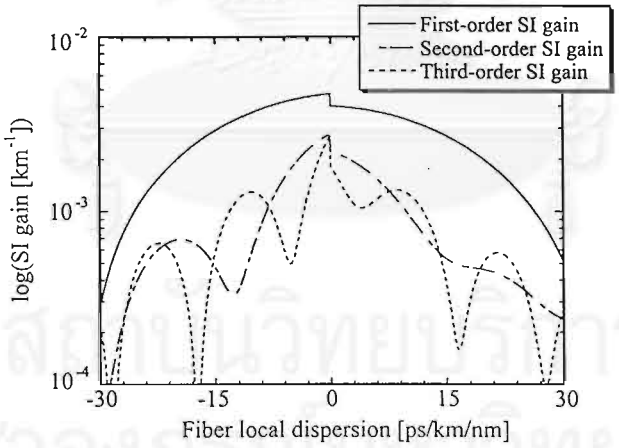

Fig. 3.4: Theoretical n = 1, 2, and 3-order SI gain peaks at resonance frequency ω_n as a function of D when l_d is set at 10 km and l_f is still 40 km. Other parameters are the same as used for Fig. 3.2. All three orders are similar to Fig. 3.2 and Fig. 3.3 where the gain decreases and periodically reduces to minimum points with the increase in D. However, in order to achieve the magnitude of SI gain as low as those of the above two cases, relatively large D is required.

One interesting thing observed from Fig. 3.2 ($l_d > l_f$), Fig. 3.3 ($l_d = l_f$), and Fig. 3.4 ($l_d < l_f$) is the gain characteristic in Fig. 3.2 is symmetrical with respect to D = 0 while those of Fig. 3.3 and Fig. 3.4 are not symmetrical. This can be explained as follows. As described above, when the sign of D is reversed, the order of the fiber installation is changed from fiber#1-fiber#2 to fiber#2-fiber#1. For the case of Fig. 3.3 and Fig. 3.4, at least two pieces of fibers is used for constructing the transmission line between two amplifiers. This means that the fiber which locates at the output of amplifier where the signal power is still high is replaced with the other fiber which has different α, different γ, and different sign of D. Therefore, the gain characteristics in Fig. 3.3 and Fig. 3.4 become asymmetrical when the order of the two fibers is changed. On the other hand, for the case of Fig. 3.2, only one fiber is installed over the entire length of one amplifier spacing. Therefore, the arrangement of the two fibers will not result any differences in the gain characteristic.

Quantitatively, $|G_n|$ calculated from Eq. (3.25) by replacing α_1 and γ_1 with α_2 and γ_2, and replacing α_2, γ_2, and β_{2fl} with α_1, γ_1, and $-\beta_{2fl}$ is equivalent to that obtained directly from Eq. (3.25). On the other hand, the replacement between α_1, γ_1, β_{2fl} and α_2, γ_2, $-\beta_{2fl}$ in Eq. (3.32) yields different $|G_n|$ comparing to $|G_n|$ obtained directly from Eq. (3.32) without the replacement. Furthermore, for the case of $l_d \leq l_f$, even both fiber#1 and fiber#2 possess equivalent values of α and γ, when the order of the two fibers is reversed, only the difference in the sign of D also leads to the different magnitude of SI gain since the power variation on each fiber is not the same.

It should be emphasized that, in this work, we focus only on the higher-order dispersion managed transmission line consisting of SMF and RDF. Since SMF and RDF possess almost equivalent absolute values of SOD and TOD with opposite signs, our analysis model shown in Fig. 3.1 is well matched with the practical transmission line composed of SMF and RDF. However, it is still worth studying SI induced from the dispersion-managed line which consists of fibers

with different lengths and different amount of dispersion shifted from the average dispersion value.

Figure 3.5(a) shows the model of the dispersion-managed fiber link composed of fiber#1 and fiber#2 whose lengths are unequal. The most practical case where $l_d = l_f$ is considered. In Fig. 3.5(a), x is the length of fiber#1 and $l_f - x$ is the length of fiber#2. D_1 and D_2, respectively, denote the local dispersion of the fiber#1 and the fiber#2 shifted from the average dispersion D_{av}. To make the accumulated dispersion vanished at each l_d, D_2 can be written as the function of D_1 and x as

$$D_2 = -\frac{D_1 x}{l_f - x}. \tag{3.33}$$

Following the above derivation for the case $l_d \le l_f$, we found that SI also occurs at the frequency determined by Eq. (3.28) but, for this case, F_0 is obtained as

$$\begin{aligned} F_0 &= \frac{1}{l_f}\left\{\int_0^x \gamma_1 \exp(-\alpha_1 z)dz + \int_x^{l_f} \gamma_2 \exp(-\alpha_2 z)dz\right\} \\ &= \gamma_1\left(\frac{1-\exp(-\alpha_1 x)}{\alpha_1 l_f}\right) + \gamma_2\left(\frac{\exp(-\alpha_2 x)-\exp(-\alpha_2 l_f)}{\alpha_2 l_f}\right). \end{aligned} \tag{3.34}$$

On the other hand, G_n can be obtained as

$$\begin{aligned} G_n = &\frac{1}{l_f}\int_0^x \gamma_1 \exp(-\alpha_1 z)\exp(-j\beta_{21}\omega^2 z)\exp(-jk_f nz)dz \\ &+ \frac{1}{l_f}\int_x^{l_f} \gamma_2 \exp(-\alpha_2 z)\exp\left(-j\omega^2\{(\beta_{21}-\beta_{22})x + \beta_{22}z\}\right)\exp(-jk_f nz)dz, \end{aligned} \tag{3.35}$$

where β_{21} and β_{22} are local GVD parameters of fiber#1 and fiber#2, respectively. Completing the integrations in Eq. (3.35) by using Eq. (3.6) and (3.33), we have

$$\begin{aligned} G_n = &\gamma_1\left\{\frac{1-\exp(-\alpha_1 x)\exp\left(-j\left(\beta_{21}\omega^2 + k_f n\right)x\right)}{\alpha_1 l_f + j\left(\beta_{21}\omega^2 + k_f n\right)l_f}\right\} \\ &+ \gamma_2 \exp\left(-j\omega^2\left(\frac{\beta_{21} l_f}{l_f - x}\right)x\right)\left\{\frac{\exp(-\alpha_2 x)\exp\left(j\left(\omega^2\left(\frac{\beta_{21}x}{l_f - x}\right) - k_f n\right)x\right) - \exp(-\alpha_2 l_f)\exp\left(j\left(\omega^2\left(\frac{\beta_{21}x}{l_f - x}\right) - k_f n\right)l_f\right)}{\alpha_2 l_f - j\left(\omega^2\left(\frac{\beta_{21}x}{l_f - x}\right) - k_f n\right)l_f}\right\}. \end{aligned} \tag{3.36}$$

Assuming both fiber#1 and fiber#2 exhibit equivalent α and γ, then G_n depends on D_1 and x. To see the variation of SI gain with the change of both D_1 and x, the gain contour map should be used. Figure 6(b) shows the contour map of the first order SI gain peak as functions of D_1 and x. For obtaining Fig. 3.5(b), D_{av} = -0.5 ps/km/nm, α = 0.2 dB/km, γ = 2.6 $W^{-1}km^{-1}$, and $l_d = l_f$ = 40 km are used. The gain map in Fig. 3.5(b) indicates that the use of fiber#1 that has large local dispersion with relatively long length can significantly reduce the SI gain. Quantitatively, the length of the fiber#1 should be longer than 10 km and the local dispersion $|D_1|$, which can be both normal and anomalous dispersion, should be larger than 5 ps/km/nm to assure the first order SI gain smaller than 10^{-3} km^{-1}.

For all cases, it should be noted that when D_{av} is set in anomalous dispersion region the modulation instability (MI), which can be interpreted as the 0-order SI, occurs and also only be slightly reduced by relatively large D.

Recently, the fabrication of optical fiber with designed dispersion value has been realized [31]. This enables us constructing a dispersion-managed transmission fiber with appropriate value of dispersion in order to suppress SI effect for a given system.

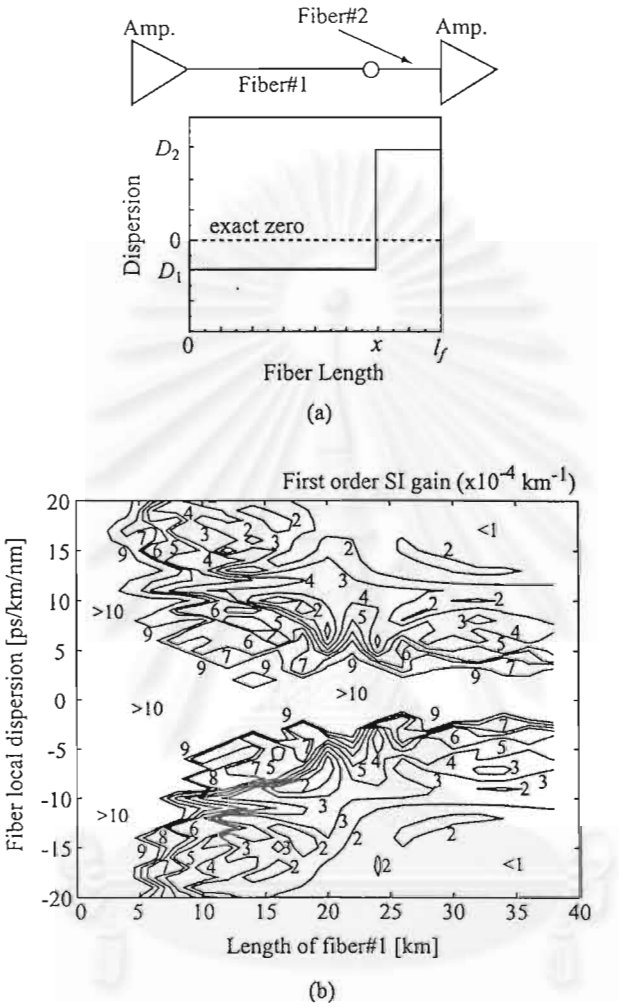

Fig. 3.5: Model of dispersion-managed transmission line and its corresponding SI gain contour map. (a) shows the model of dispersion-managed transmission line composed of fiber#1 and fiber#2 whose lengths are unequal. (b) shows the contour map of the first order SI gain peak as functions of D_1 and x. The gain map indicates that the use of fiber#1 that has large local dispersion with relatively long length can significantly reduce the SI gain.

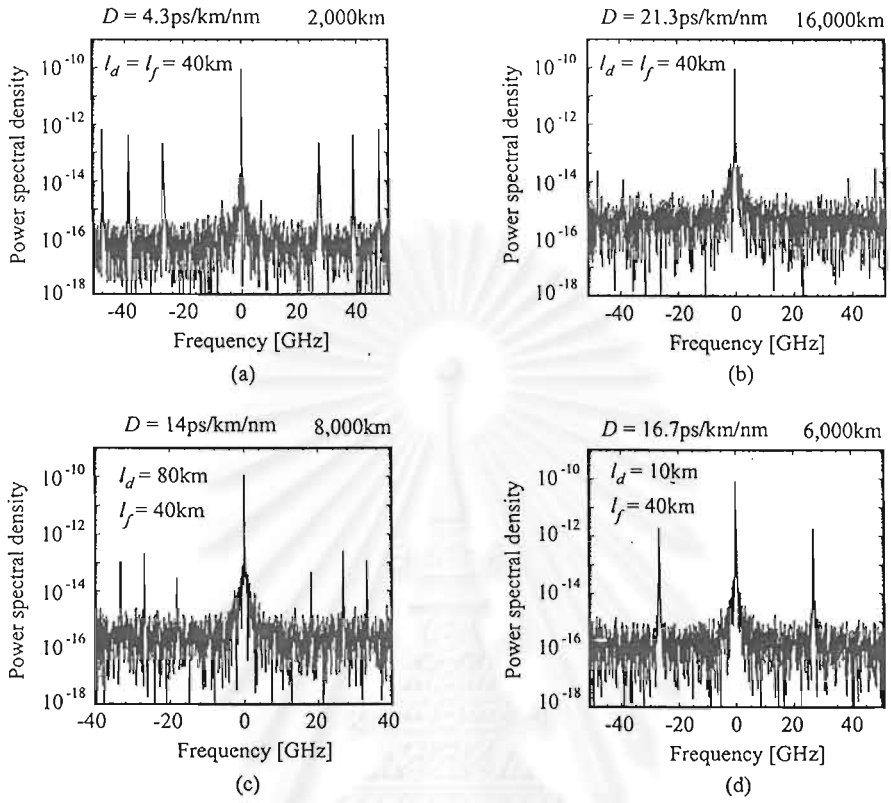

Fig. 3.6: Numerical simulation results show the spectrums of optical CW signal and amplified spontaneous emission (ASE) noise transmitted in dispersion management transmission line using SMF and RDF with periodic signal amplification. (a) 2,000-km-transmitted CW spectrum for $l_d = l_f$ = 40 km with D = 4.3 ps/km/nm, (b) 16,000-km-transmitted CW spectrum for $l_d = l_f$ = 40 km with D = 21.3 ps/km/nm, (c) 8,000-km-transmitted CW spectrum for l_f = 40 km, l_d = 80 km with D = 14 ps/km/nm, and (d) 6,000-km-transmitted CW spectrum for l_f = 40 km, l_d = 10 km with D = 16.7 ps/km/nm. All simulation results, for both SI gain and SI frequency, are in a good agreement with the theoretical gain shown in Fig. 3.2, 3.3 and 3.4.

When l_d is determined, then, it is helpful to use SI gain contour map to design the operating D_{av} and P_0 at the point where the SI gain becomes as low as possible. If we consider a practical case when $l_d = l_f$, assuming that the local SOD is fixed at a given value, the magnitude of SI gain now only depends on P_0 and D_{av}. Figure 8 shows

the gain contour map of the first order of SI concerning the dispersion managed transmission line using the combination of SMF and RDF. It should be noted that we should concentrate to the first order SI because, practically, the low order of SI is easier to be phase-matched and causes problem in the long haul transmission than other high orders. The SMF and RDF parameters used for the calculation are the same as those have been used for fiber#1 and fiber#2, respectively. In the contour map, $|D|$ is assumed to be 17ps/km/nm with positive sign for the SMF and minus sign for the RDF.

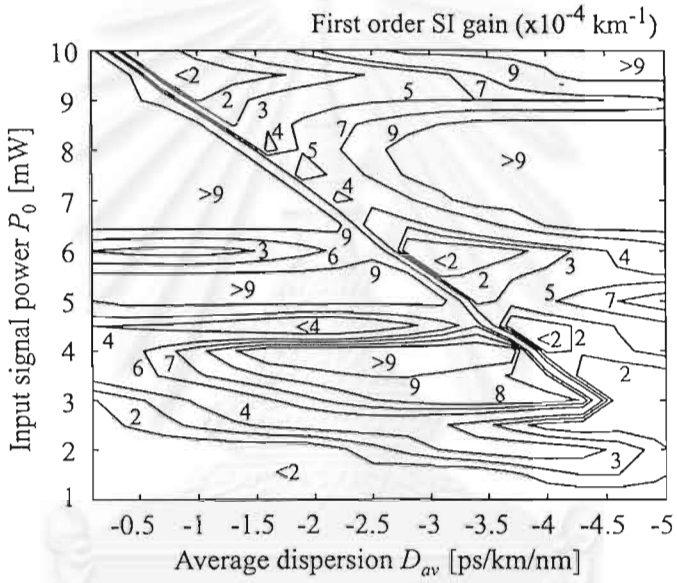

Fig. 3.7: Gain contour map of the first order of SI concerning the dispersion managed transmission line consisting of SMF and RDF for $l_d = l_f$ = 40 km and $|D|$ = 17 ps/km/nm with positive sign for the SMF and minus sign for the RDF.

In Fig. 3.7, for low P_0, which is referred to relatively short transmission, SI possesses relatively low gain over a wide range of D_{av}. For high power transmission, using low D_{av} can avoid the SI gain and, at the same time, move the SI position out of the signal carrier. However, at some points of P_0, the SI gain exhibits large value even at very low D_{av}, for examples, SI gain as high as 9 x 10^{-4}

km^{-1} arises from P_0 = 5 mW at D_{av} = −0.5 ps/km/nm. In order to achieve the maximum performance of the system, these operating points should be avoided. It should be noted when this periodic dispersion management using SMF and RDF is not applied to the system, the first order SI induced from only periodic amplification in dispersion-shifted fiber chain exhibits high gain larger than 10^{-3} km^{-1} even P_0 > 2 mW is used.

3.2 Effect of SI on Long Haul WDM Transmission Systems

In dispersion managed transmission system consisting of SMF and RDF, all channels experience almost the same amount of D_{av}. Thus, each channel produces its own SI that occurs at frequency shifted from carrier frequency by the same amount of frequency shift with almost the same gain. If two different channels produce SI at the same frequency, SI will cause a serious problem to the channels whose carriers are placed just at that frequency especially for the frequency where the first order SI arises.

In order to confirm our mention, we perform computer simulations of the transmission of 4-wavelength CW signal and ASE noise. In the first calculation, we focus on the case when the first order SI gain generated from two separated channels enhances each other and positions on the other two channels. In the calculations, l_d is set equal to l_f at 40 km and other SMF and RDF parameters are the same as those used in other calculations described above. According to the contour map in Fig. 8, to investigate the problem of SI even the system is operating with condition that yields relatively low SI gain, we select P_0 = 3 mW and D_{av} = -0.5 ps/km/nm, which yields the first order SI gain about 2 x 10^{-4} km^{-1}. Using Eq. (3.28) and the calculation parameters, the first order SI will arise at ± 77.4 GHz shifted from each carrier frequency. Next, we place four channels at the frequencies -116.1 GHz, -38.7 GHz, 38.7 GHz, and 116.1 GHz shifted from the zero-dispersion wavelength 1,550 nm respectively. By this arrangement, SI produced from channel#1 and channel#3 will arise just at the position of channel#2 carrier. Similarly, SI induced from channel#2 and channel#4 will occurs just at the position of channel#3.

Figure 3.8(b) shows the spectrum of the 4-channel CW signal transmitted over 4,000 km comparing with its initial shape shown in Fig. 3.8(a). By this channel allocation, the serious distortion of CW spectrum is clearly observed. In order to avoid this problem, it is necessary to arrange the channel allocation in such a way that none of the channel is placed on the SI frequency.

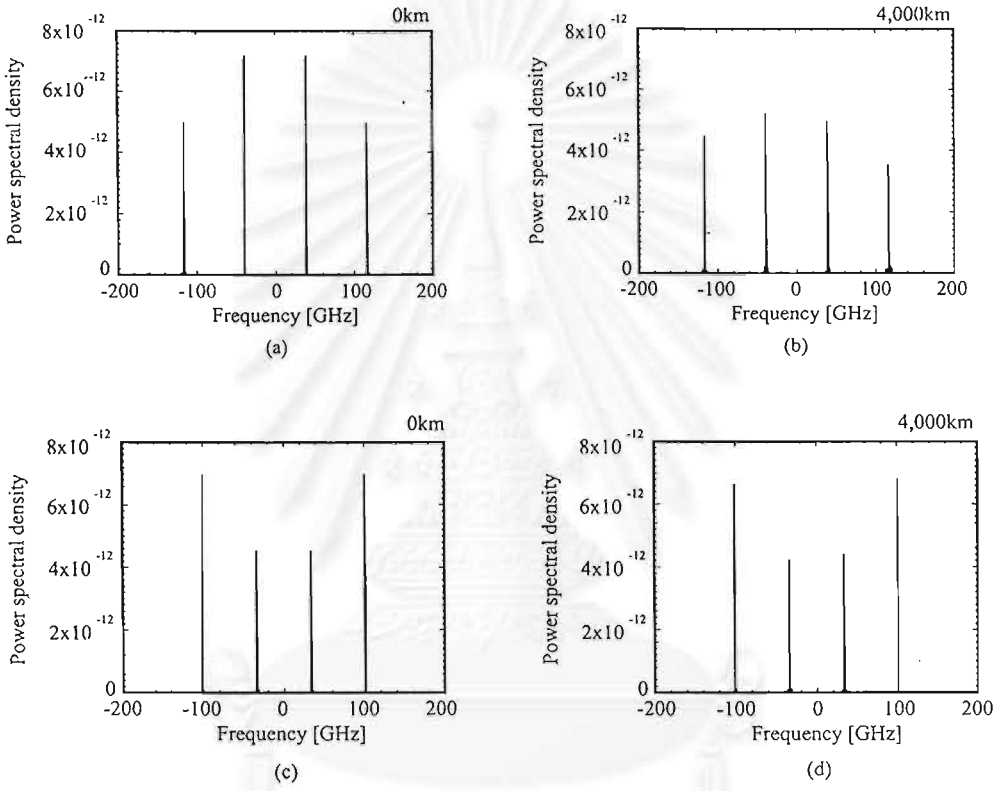

Fig. 3.8: Optical spectrum of 4-channel CW signal shown in linear scale. l_d is set equal to l_f at 40 km, P_0 = 3 mW and D_{av} = -0.5 ps/km/nm. In (a) and (b) the channel spacing is set at $\pm$ 77.4 GHz where two of the first order SI from neighbor channels arise just at channel#2 and channel#3 carrier positions. (a) initial shape and (b) 4,000-km-transmitted spectrum. By this channel allocation, serious distortion of CW spectrums is clearly observed. (c) and (d), respectively, shows the initial and 4,000-km-transmitted CW spectrums simulated by decreasing 10 GHz to shift SI frequency out of signal bandwidth. The transmitted spectrum in (b) appears in more severe distorted shape than (d) because of SI.

Figure 3.8(c) and (d) respectively shows the initial four-channel CW signal spectrum and its shape after 4,000 km transmission simulated by the same parameters as Fig. 3.8(b). The channel spacing in this calculation is decreased 10 GHz resulting in the shift of SI frequency out of signal bandwidth. Comparing to Fig. 3.8(b) where the SI occurs just at the channel position, the output spectrum in Fig. 3.8(d) appears in similar shape to the initial than the case of Fig. 3.8(b), confirming the achievement of avoiding the effect of SI. In fact, as FWM among channels is easy to be phase-matched when the channel spacing becomes smaller [1], the decrease in channel spacing should have led to more signal distortion. However, the transmitted spectrum in Fig. 3.8(b) appears in more severe distorted shape than that of Fig. 3.8(d). This can be interpreted that the effect of SI plays a significant role in determining the transmission performance than the inter-channel FWM for this condition.

To explore the effect of SI on WDM transmission more details, we perform the calculation of the bit-error rate (BER) of the 4-channel WDM system using pseudorandom 32-bit Gaussian RZ pulse train as an input optical signal whose bit rate of each channel is equal to 10 Gbit/s. At the end of the system, the accumulated D_{av} is post-compensated by multiplying the complex amplitude of the signal with a negative amount of linearly accumulated phase shift caused by D_{av}. We assume the use of a bandwidth-adjustable optical band-pass filter (OBPF) in front of the receiver to select the passband channel. This OBPF is also always adjusted to obtain minimum BER. The receiver is modeled by 6.5-GHz-cutoff sixth-order Bessel-Thompson low-pass filter following by BER detector. For obtaining the numerical BER of the detected signal, the simulation is repeated 128 times for the same pseudo-random pulse train. The numerical Q factor of every bit is then individually calculated at the maximum eye-opening point of the bit period. Based on the assumption of Gaussian noise distribution, the numerical BER's are computed from the bit numerical Q factors and averaged over the entire bits [7].

Figure 3.9(a) and (b), respectively, shows the calculated BER curves of channel#2 and 3 as a function of transmission distance simulated by P_0 = 3 mW and D_{av} = -0.5 ps/km/nm with different channel spacing setting. The BER curves obtained from the system whose signal carriers are placed on the position where the SI arises (shown

by circles) drop more rapidly than those obtained from 10-GHz-decreased channel spacing (shown by squares).

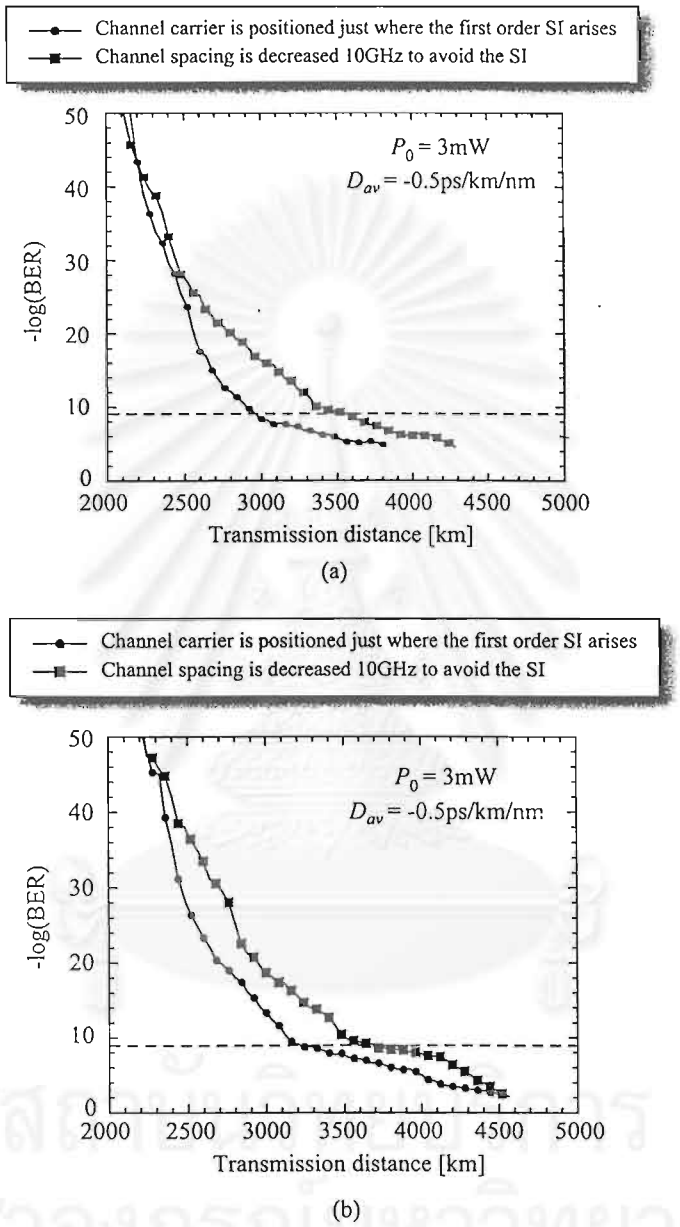

Fig. 3.9: BER as a function of transmission distance calculated from the (4 x 10)-Gbit/s-32-bit RZ signal for different channel spacings. (a) and (b) show BER curves of channel#2 and channel#3, respectively. In both (a) and (b), circles show BER obtained from the system whose signal carriers are placed on the position where the SI arises while squares show BER obtained from 10-GHz-decreasing channel spacing. At BER = 10^{-9} (shown by an across dotted line) the systems where the channel allocation is re-arranged to avoid the position of SI give significantly longer transmission length.

If we defined the maximum transmission distance obtained at the distance where the BER reaches 10^{-9} as shown by the across dotted line, the systems where the channel allocation is arranged to avoid the position of SI yield significantly longer transmission length. We also simulated the system with P_0 = 5mW and D_{av} = -0.5 ps/km/nm that yields high SI gain. The result showed more severe degradation of BER for channel carriers positioned just on SI frequency and, on the contrary, an obvious improvement when a channel allocation is done to avoid the SI frequency. This confirms the necessity of avoiding SI in higher-order dispersion management long-haul WDM transmission systems.

4. SIMULTANEOUS SUPPRESSION OF TOD AND SI IN OPC TRANSMISSION SYSTEMS BY COMBINATION OF SMF AND RDF

As described in chapter 2, the performance of OPC transmission systems is mainly limited by TOD and SI effect. Without TOD compensation, a 10,000-km transmission with data rate of 40 Gbit/s was achieved by following optimum design strategies to avoid the effect of SI [16]. To increase the transmission bit-rate of the 10,000-km OPC system, it is necessary to suppress both TOD and SI.

The accumulation characteristic of TOD in OPC systems can be discussed through three characteristic scales: the SOD length L_{d2}, the TOD length L_{d3}, and the nonlinear length L_{nl}, which are defined in [1]. In OPC systems, SOD exists along the entire transmission length; therefore, L_{d2} becomes many times shorter than L_{nl} for the case of high bit-rate transmission. When L_{d2} is much shorter than L_{nl} and L_{d3}, the signal pulses are rapidly broadened by SOD, and their peak power decreases after transmitting for several L_{d2}. This means that the broadened pulses almost do not experience the effect of fiber nonlinearity. Thus, in ultra-high-speed OPC systems, the accumulation of the TOD-induced phase shift increases almost linearly with the transmission length at an ordinary operating signal power. The linear TOD accumulation enables us to achieve perfect TOD compensation by placing only one compensator at any point in the line, or even freely installing distributed compensators without the necessity of concerning their intervals.

When TOD is perfectly compensated in OPC systems, the 100-Gbit/s data transmission over 10,000 km [17] can be made possible at the balance point of the improvement of signal-to-noise ratio (SNR) and the degradation from SI effect. In order to further improve the transmission performance of the TOD-compensated OPC system, the waveform distortion induced from SI effect must be overcome.

4.1 Reduction of Sideband instability gain by strong dispersion management

As shown in previous chapter, the gain of SI can be practically reduced by using a strong periodic dispersion-managed transmission

line such as the combination of SMF and RDF, instead of uniform dispersion line [19], [20]. This is because the increase in the local fiber dispersion virtually shifts the order of SI to higher orders resulting in the difficulty of phase-match process. Furthermore, the frequency where SI arises depends on the larger period between the amplifier spacing (l_f) and the dispersion management period (l_d). The larger the variation period becomes, the closer to the carrier frequency the SI frequency arises.

In order to show the reduction of SI gain through a periodic dispersion-managed line, here we calculate the gain contour map of the first-order SI focusing on the dispersion-managed transmission line consisting of SMF and RDF. The dispersion management profile is the simple type where one SMF and one RDF with an equivalent length are only connected together. In each dispersion management period, SMF is placed before RDF at the output end of the amplifier. The placement of signal carrier frequency determines the values of the operating average dispersion D_{av} and the local dispersion D. In Fig. 4.1, the gain map is obtained as a function of l_d and an input signal power P_0 when D_{av} and D are given. It should be noted that we should concentrate to the first order SI because, practically, the low order of SI is easier to be phase-matched and causes more serious signal distortion in long haul transmission systems than higher order SI. The fiber loss coefficient α_1 and the fiber nonlinear coefficient γ_1 of SMF used for calculating the gain map are 0.2 dB and 1.6 $W^{-1}km^{-1}$, respectively, while α_2, γ_2 representing those of RDF are 0.25 dB and 4.8 $W^{-1}km^{-1}$, respectively. D_{av} is set at -1 ps/km/nm and $|D|$ = 17 ps/km/nm. Comparing with these gain maps, the magnitudes of the first, second, and third-order SI gains of a non-dispersion management system as a function of the input power is shown in Fig. 12. In this case, the transmission fiber is assumed to be a dispersion-shifted fiber (DSF) with α = 0.2 dB and γ = 2.6 $W^{-1}km^{-1}$.

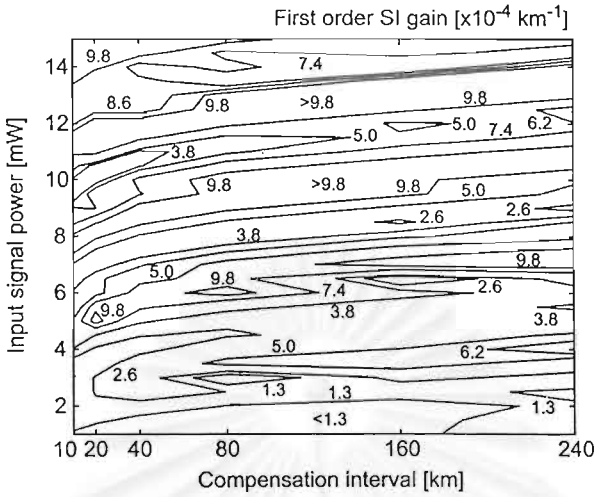

Fig. 4.1: Gain contour map of the first-order SI focusing on the dispersion-managed transmission line consisting of SMF and RDF. The gain is calculated as a function of l_d and an input signal power P_0 when an average dispersion D_{av} and a fiber local dispersion $|D|$ are set at -1 ps/km/nm and 17 ps/km/nm, respectively.

In Fig. 4.1, for low P_0 (< 3 mW), SI possesses very low gain over a wide range of l_d ; thus, SI may not affect the signal transmission for relatively short distance systems. Even in high power transmission (from 3 mW to 15 mW), SI still exhibits relatively low gain (< 10^{-3} km^{-1}) comparing with the gain shown in Fig. 4.2 at the same P_0 . Without dispersion management, Fig. 4.2 indicates that the SI gain almost linearly increases with P_0 and exhibits a value larger than 10^{-3} km^{-1} even for P_0 = 2 mW for the first-order SI.

The linear accumulation of TOD, together with the reduction of SI gain through strong dispersion management open a possibility of simultaneously suppressing TOD and SI in OPC systems by using the higher-order dispersion management transmission line such as the combination of SMF and RDF.

Assuming that TOD and SI are perfectly suppressed in OPC systems, there remains the problem originated from the accumulation of the transmission of amplified spontaneous emission (ASE) noise

which is enhanced during the transmission by parametric interaction between SOD and SPM [32]. As shown in Fig. 4.3, the transmission of the ASE noise is not symmetrical with respect to the midpoint of the system. Thus, only part of the nonlinear enhancement can be compensated by OPC while there still exists the accumulated ASE noise, which is enhanced by the nonlinear interaction.

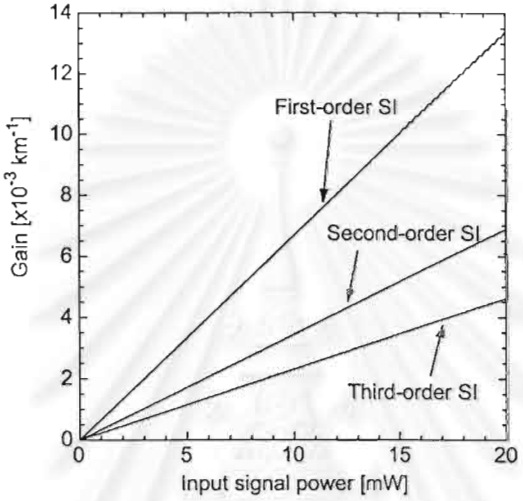

Fig. 4.2: Magnitudes of the first, second, and third-order SI gains arising from a non-dispersion management system. The gains are obtained as a function of signal input power. The transmission fiber is assumed to be only DSF with α = 0.2 dB and γ = 2.6 W^{-1}km^{-1}.

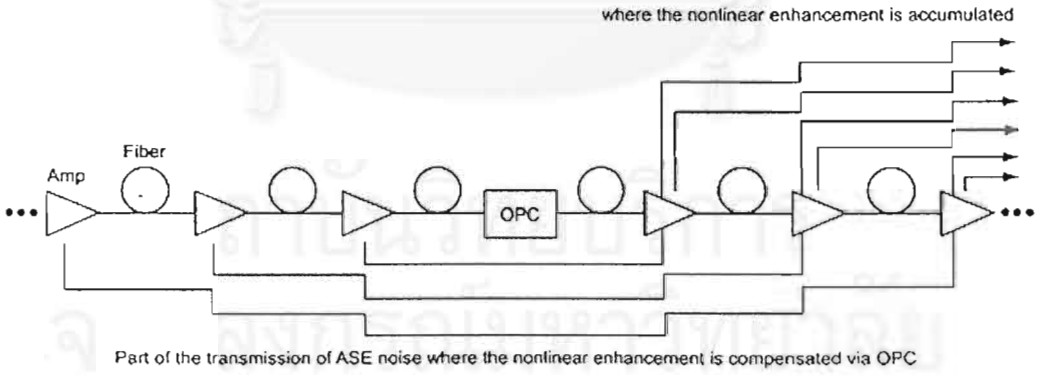

Fig. 4.3: Transmission of ASE noise in OPC system. ASE noise produced from each optical amplifier is enhanced during the transmission by parametric interaction between SOD and SPM, and will accumulate to the end of system. Since the transmission of ASE noise is not symmetric with respect to the system mid-point, therefore, only part of the nonlinear enhancement can be compensated by OPC while their remains an amount of ASE noise that is enhanced by the nonlinear interaction and accumulates to the end of system.

It should be noted that this fiber nonlinearity-enhanced ASE noise cannot be suppressed by the combination of SMF and RDF. However, its harm is expected to reduce through large fiber local dispersion with sufficiently large compensation period. This is because the signal pulses are rapidly broadened by SOD, therefore, they almost do not experience the effect of fiber nonlinearity.

4.2 Implementation of Dispersion Management on OPC Systems

The most practical way available now to compensate TOD for ultra-high bit-rate long-haul transmission is probably the use of the dispersion-managed fiber link such as the combination of SMF and RDF. In the previous section, we have shown that SI induced from the periodic power variation can be suppressed by using periodic dispersion management with large local dispersion. Therefore, by using such combination of SMF and RDF in OPC systems, the simultaneous compensation of both TOD and SI can be expected. Moreover, the accumulation of D_{av} will be automatically compensated by OPC without post compensation used in ordinary dispersion management systems.

I. Possible Installing Dispersion Profiles

Figure 4.4 illustrates two possible schemes to install dispersion management in the OPC transmission system. In Fig. 4.4(a), both periodic dispersion variation and periodic power variation are in uniform distributions along the entire system length. On the other hand, in Fig. 1.4(b), the order of SMF-RDF is reversed to RDF-SMF after the midway OPC yielding the symmetric distribution of the periodic dispersion variation with respect to the system mid-point.

We suggest that the symmetric dispersion profile in Fig. 4.4(b) gives better transmission performance than the other profile especially for high power transmission. The reasons can be explained as follows: First, when the nonlinear length L_{nl} is longer than the periods of the variations, due to the uniform distributions in Fig. 4.4(a), each order of SI arises from one frequency determined by the two periodic perturbations and experiences the gain whose magnitude

exponentially increases with the transmission length. On the other hand, for the dispersion management profile in Fig. 4.4(b), the system in the first half and second half produce their own SI at different frequencies whose separation depends on the difference in the nonlinear coefficient and the fiber loss coefficient between SMF and RDF. However, each resonance frequency experiences the SI gain only half of the system length, the signal distortion may not be so severe as that occurs from the dispersion profile in Fig. 14(a).

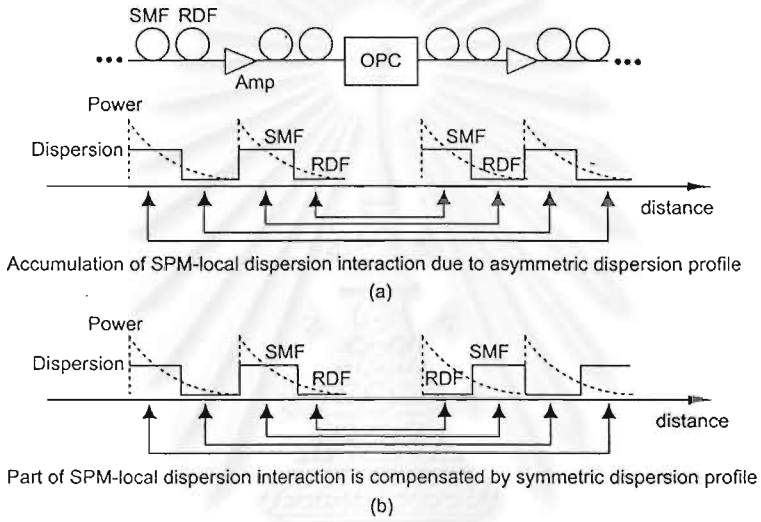

Fig. 4.4: Two possible ways for implementing the dispersion management in OPC transmission system. In (a) both periodic dispersion variation and periodic power variation are in uniform distributions along the entire system length. On the other hand, in (b), the order of SMF-RDF is reversed to RDF-SMF after the system mid-point, forming the symmetric distribution of the periodic dispersion variation with respect to the system mid-point. The symmetric dispersion profile in (b) gives better transmission performance than profile (a) especially when the systems operates with high signal power because part of the interaction between SPM and fiber local dispersion is compensated by OPC.

Second, for high power transmission, when L_{nl} becomes comparable or shorter than the compensation interval, the interplay between SPM and the local dispersion of each fiber occurs and causes additional signal waveform distortion. With this consideration, by constructing the symmetric dispersion compensation profile as shown in Fig. 4.4(b), part of the interaction between SPM and local dispersion of the fiber will be compensated by OPC whether the power

variation distribution remains unchanged. Oppositely, for the profile in Fig. 4.4(a), this interaction will accumulate along the transmission length due to the asymmetric distribution with respect to mid-point of both periodic power variation and periodic dispersion compensation.

II. Computer Simulations

In order to evaluate our proposed SI suppression method in OPC systems, we perform a computer simulation of the transmission of 100-Gbit/s data composed of 32-bit pseudorandom Gaussian RZ pulses based on the system models in Fig. 4.4. In the calculation, we set l_d = l_f = 40 km. TOD is assumed to be 0.06 ps/km/nm for SMF and -0.06 ps/km/nm for RDF. Other SMF and RDF parameters used in this simulation are the same as used above. The optical amplifier produces ASE noise with noise figure of 5.3 dB (n_{sp} = 1.7). The optical pulse at the midway of the system is conjugated by an ideal infinite-bandwidth optical phase conjugator.

When the combination of SMF and RDF is not applied for TOD compensation, the TOD compensator, placed only at the end of system, is assumed to be an ideal device that multiplies the complex amplitude of the signal with a negative amount of linearly accumulated phase shift caused by TOD. Also, for signal transmission in this case, DSF with the same parameters as the calculation above is used.

To see the efficiency of the SI suppression more obviously, the input signal power P_0 is set at 21 mW giving L_{nl} becomes equivalent to l_f. Also for all other cases, P_0 will be set at this value. Since SMF and RDF exhibit different values of α and γ, we calculate L_{nl} of the system employing SMF and RDF by using the average values of those parameters. With P_0 = 21 mW, L_{nl} of the system constructed by SMF and RDF becomes approximately 36 km, which is slightly shorter than that of DSF.

The bandwidth of the optical band-pass filter, which is placed at the output end of the fiber, is always adjusted to obtain the minimum BER. The propagation of the optical pulse is calculated by solving the nonlinear Schrodinger (NLS) equation by the split-step Fourier method [1]. The receiver is modeled by 65-GHz-cutoff sixth-

order Bessel-Thompson low-pass filter followed by a BER detector. The system performance is evaluated in terms of the bit-error rate (BER) calculated by repeating 128 times the transmission of the same pulse train and assuming the Gaussian distribution of the amplifier noise.

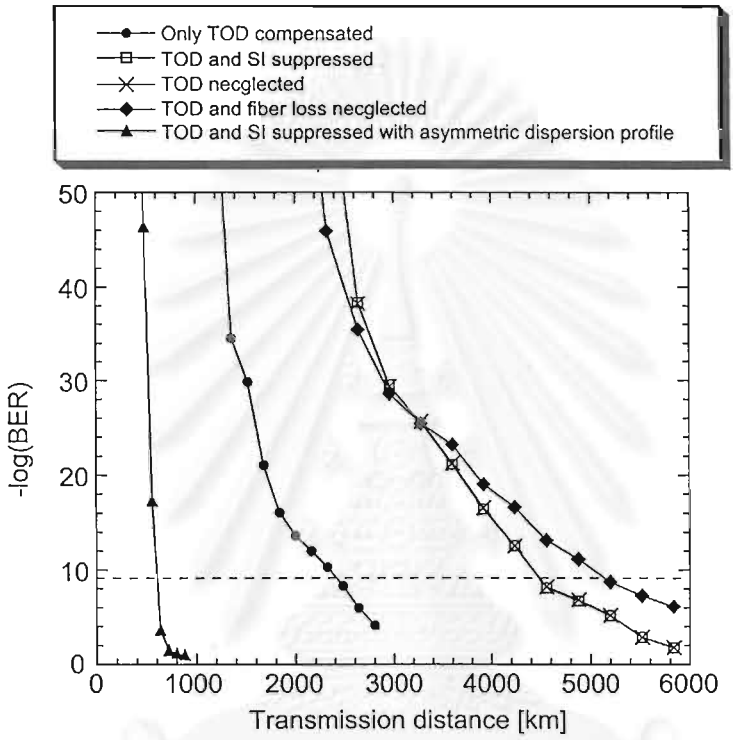

Fig. 4.5: BER of several OPC systems, calculated as a function of transmission distance. For all OPC systems, the input signal power is adjusted to give L_{nl} equivalent to l_f at 40 km. Circles show BER obtained from the system where only TOD is compensated. Squares show BER of the system using SMF and RDF as transmission fiber with the symmetric dispersion management profile of Fig. 4.4(b), while triangles show BER of the system employing the asymmetric dispersion profile of Fig. 4.4(a). Crosses show BER of the system where TOD is neglected. Diamonds show BER obtained from the system where both TOD and SI are neglected. At BER = 10^{-9}, the achievable transmission length of the system using symmetric dispersion increases 2,000 km longer than the system where only TOD is compensated without using SMF and RDF. Furthermore, BER of the system employing the asymmetric dispersion becomes the worst due to the accumulation of the nonlinear interaction between SPM and local fiber dispersion.

Figure 4.5 shows the calculated BER as a function of transmission distance. According to the condition $L_{nl} = l_f$, when only TOD is compensated (shown by circles), the performance of the system is limited by SI and the nonlinear distortion from the interaction between SPM and local dispersion in each segment of fiber. Thus, BER of the system in this case rapidly decreases. When the dispersion management profile in Fig. 4.4(b) is employed to the system (shown by squares), BER curve drops significantly slow. Comparing to the case without the combination of SMF and RDF, by using SMF and RDF, the achievable transmission length at BER = 10^{-9} can be further extended approximately 2,000 km. Moreover, the BER curve of the system where TOD is neglected (shown by crosses) almost fits with that obtained from TOD-compensated system. This result mentions that this SI suppression method does not affect accumulation characteristics of TOD since l_d is still much shorter than the TOD length L_{d3} ($\approx$ 280 km) so that in the TOD scale, the signal propagates as if there is no dispersion management ever be installed.

On the other hand, BER of the system employing the dispersion profile of Fig. 4.4(a) (shown by triangles) obviously becomes worse than others due to the reasons described above. Furthermore, the difference in transmission distance between the BER curve obtained from the system using the dispersion profile of Fig. 4.4(b) and the BER curve obtained from the system neglecting TOD and SI (shown by diamonds) mainly comes from part of the interaction between SPM and local fiber dispersion that cannot be perfectly compensated by OPC.

4.3 Optimum Dispersion Map for Higher-Order Dispersion-Managed OPC Systems Using SMF and RDF

When the combination of SMF and RDF is employed to a given system, the fiber local dispersion and the average dispersion are almost automatically determined by the placement of operating signal wavelength. In this case, the maximum system performance will be achieved by determining the optimum l_d and signal power. Below, we discuss the optimum dispersion map design considering the OPC systems using $l_d > l_f$, $l_d = l_f$, and $l_d < l_f$.

I. OPC Systems using $l_d > l_f$

For given l_d ($l_d > l_f$), the increase in the signal power can help improving SNR. At the same time, when the signal power is increased until L_{nl} becomes comparable to, or shorter than l_d, the signal pulse will experience the local dispersion rather than its periodic variation. In this case, SI determined by the period of l_f on each local fiber length also arises. Additionally, the signal will also be attacked by the interaction between SPM and the local dispersion. Therefore, for given l_d ($l_d > l_f$), the maximum system performance will be achieved by using an optimum input power which yields the balance of the improvement in SNR and the degradation described above.

Even the use of very large l_d ($l_d > l_f$) can also help reducing the nonlinear enhancement of the ASE noise since the signal and the ASE noise will transmit through large local dispersion which repeats for long length [32]. Additional to the problems discussed above, the larger l_d we use, SI, whose position is determined by l_d in this case, will occur at the frequency closer to the signal carrier. Therefore, even only a small SI gain may cause serious signal distortion. As a result, for larger l_d, the optimum signal power will exhibit lower value than that of shorter l_d. Futhermore, the system may give a good result close to the linear SNR limit for relatively low power transmission. However, the system performance will degrade very immediately after reaching the optimum signal power.

Comparing to ordinary dispersion management systems, in OPC systems, such optimum power will be found at relatively high value since dispersion exists along the transmission yielding L_{d2} several times shorter than L_{nl}, especially for the case of high bit-rate transmission.

II. OPC Systems using $l_d = l_f$

When $l_d = l_f$, the transmission of signal is expected to give a good result since SI occurs at the furthest frequency from the signal carrier. However, the signal, in this case, keeps its high peak power during the transmission because the signal almost restores its shape at each l_f due to low average dispersion. Therefore, it is easy to be affected by the nonlinear effect. When $L_{nl} > l_d = l_f$, the

nonlinear enhancement of ASE noise by the interaction between SPM and average dispersion, which is more severe than that of system with $l_d > l_f$, becomes a main problem that limits the system. Moreover, in the second half of the system, RDF, which exhibits larger nonlinear coefficient than SMF, is installed near the output of the optical amplifier according to the symmetric dispersion distribution. This results in more serious enhancement of ASE noise since, in the second half, the signal and the accumulated noise will propagate through the highly nonlinear RDF where their power are still intense. When L_{nl} approaches l_d by the use of high signal power, the interaction between SPM and fiber local dispersion also arises and causes additional signal waveform distortion. By these reasons, the system constructed with $l_d = l_f$ may not be expectable to give good transmission performance comparing to $l_d > l_f$ case and even $l_d < l_f$ case.

III. OPC Systems using $l_d < l_f$

For the system with $l_d < l_f$, SI will arise at the same frequencies as those of the $l_d = l_f$ case since the position of the resonance frequency depends on the larger period between l_d and l_f. With increasing the signal input power, similar to the case of $l_d = l_f$, the problem which limits the performance of the system comes from the enhancement of the amplifier noise by the interaction between SPM and average dispersion. However, even if we reverse the order of fibers after the mid-point to form symmetric dispersion profile, the nonlinear accumulation of amplifier noise will not be so severe as the case of $l_d = l_f$. This is because the signal at high peak power does not propagate on highly nonlinear RDF for a long length.

Even L_{nl} becomes very short by using relatively high input power, the interaction between the local dispersion and SPM will not be so serious as the case of $l_d = l_f$. This is because the signal does not too much feel the local dispersion as long as L_{nl} is still not

comparable to l_d . This makes the systems with $l_d < l_f$ may yield a significant tolerance to high power transmission comparing to other cases. At given l_d ($l_d < l_f$), the optimum power will exhibit relatively high value than the case of $l_d > l_f$. However, for a low input power, the system may not give good performance comparing to the case of $l_d > l_f$ according to the interaction of SPM and average dispersion.

From the above discussion, for each l_d , the optimum input power for achieving maximum transmission performance will be found at different values. One will be relatively low input power obtained for the case $l_d > l_f$. The longer l_d is, the lower the optimum power becomes. The other one will be found at relatively high value for the case $l_d < l_f$ and will be higher value with the reduction in l_d . However, the system operating with $l_d = l_f$ may not give as good result as the others.

4.4 Ultimate Performance of Higher-Order Dispersion-Managed OPC Systems

To explore the ultimate performance of the higher-order dispersion-managed OPC systems employing the combination of SMF and RDF when the systems are operating in optimum conditions, we perform extensive computer simulations of the systems with data rate of 100 Gbit/s, 160 Gbit/s, and 200 Gbit/s. The dispersion profile used in the simulations is the symmetric profile shown in Fig. 4.4(b). The system parameters and fiber parameters are all the same as above calculations.

Figures 4.6, 4.7, and 4.8, respectively, show the calculated BER at 10,000 km of OPC transmission systems with data rate of 100 Gbit/s, 160 Gbit/s, and 200 Gbit/s as a function of the signal input power P_0 for several l_d (10 km, 40 km, 80 km, 160 km, and 240 km). In each figure, BER of the same OPC system neglecting the nonlinear coefficient γ is also calculated to show the linear SNR limit for comparison.

According to the simulated results of the 100-Gbit/s OPC systems shown in Fig. 4.6, for low P_0, BER of the systems with larger l_d appears in a value closer to the SNR limit because the use of large l_d can help avoiding the effect of fiber nonlinearity. For higher P_0, BER of the systems using large l_d start decaying rapidly while that of system using l_d = 10 km still shows a good result due to its tolerance to fiber nonlinearity. As discussed above, the system with l_d is set equivalent to l_f at 40 km shows the worst result. However, with defining a maximum transmission distance at BER = 10^{-9}, all 100-Gbit/s systems can achieve 10,000-km transmission for a wide range of P_0. In comparison with these results, the system using DSF incorporated with TOD compensation can only reach 10,000 km by only P_0 = 7 mW [17]. This mentions the significant improvement of the OPC system by using the higher-order dispersion management transmission line consisting of SMF and RDF.

For the 10,000-km transmission result of 160-Gbit/s data shown in Fig. 4.7, the existence of the optimum P_0 can be observed more obviously. The systems with l_d = 240 km, 160 km, 80 km, and 10 km reach maximum performance, at BER smaller than 10^{-9}, with their own optimum P_0 at 9 mW, 10 mW, 14 mW, and 15 mW, respectively. As predicted, the optimum P_0 for longer l_d is found at lower value. However, system with l_d = 40 km no longer succeeds BER = 10^{-9} for all range of P_0.

According to this ultimate performance of dispersion-managed OPC systems, further increase in transmission bit-rate can be expected. The calculated BER of 200-Gbit/s data transmission at 10,000 km shown in Fig. 4.8 indicates the possibility of this ultra-high bit-rate long-haul transmission at BER = 10^{-9} using l_d = 240 km with P_0 = 11 mW or l_d = 10 km with P_0 = 15 mW.

To extend the bit-rate more than 200 Gbit/s in 10,000-km transmission, the easiest way may be the optimization of the average dispersion value D_{av}. The increase in D_{av} can reduce the effect of

fiber nonlinearity, at the same time, moving the SI which is not completely suppressed to occur more inner signal bandwidth. The optimum D_{av} will be found under the balance of these two effects.

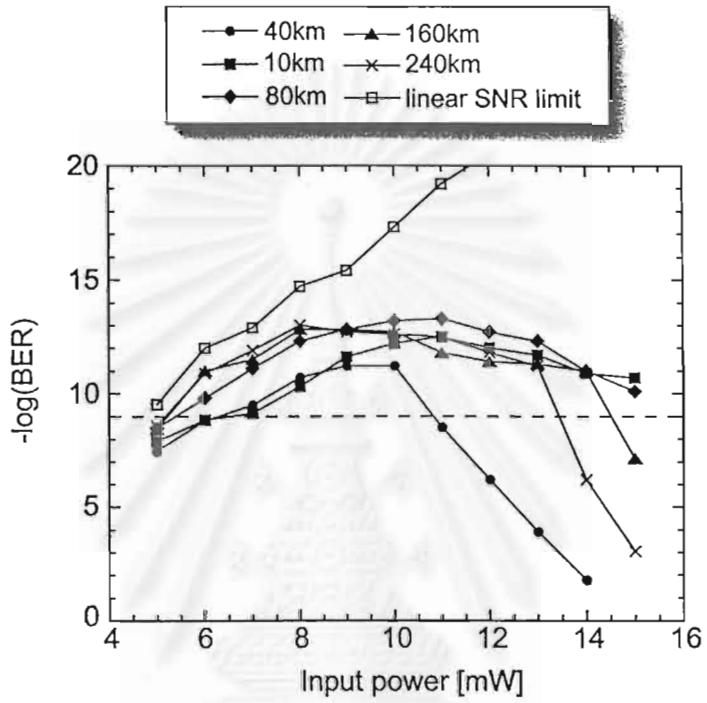

Fig. 4.6: BER of higher-order dispersion-managed 100-Gbit/s OPC transmission systems at 10,000 km as a function of the signal input power P_0 for several l_d (10 km, 40 km, 80 km, 160 km, and 240 km), comparing with the linear SNR-limited BER. At BER = 10^{-9}, all systems can achieve 10,000-km transmission for a broad range of P_0. Since the OPC system using DSF where TOD is compensated can only reach 10,000 km by only P_0 = 7 mW [10], these results show the significant improvement of OPC system by using the higher-order dispersion management transmission line consisting of SMF and RDF to eliminate both TOD and SI.

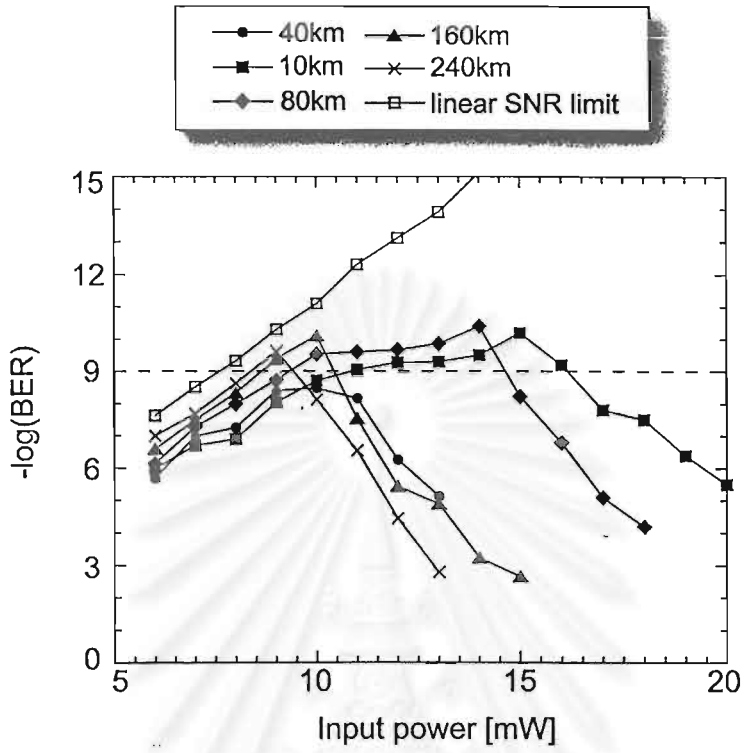

Fig. 4.7: BER of higher-order dispersion-managed 160-Gbit/s OPC transmission systems at 10,000 km as a function of the signal input power P_0 for several l_d (10 km, 40 km, 80 km, 160 km, and 240 km), comparing with the linear SNR-limited BER. The systems with l_d = 240 km, 160 km, 80 km, and 10 km reach maximum performance, with BER smaller than 10^{-9}, with the optimum P_0 at 9 mW, 10 mW, 14 mW, and 15 mW, respectively. However, system with $l_d = l_f$ = 40 km does not achieve BER = 10^{-9} for all range of P_0.

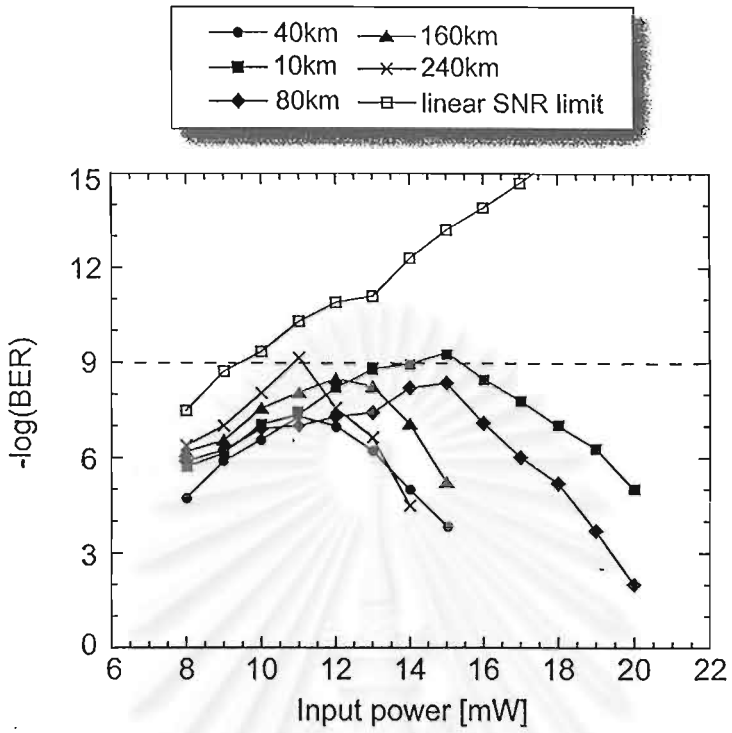

Fig. 4.8: BER of higher-order dispersion-managed 200-Gbit/s OPC transmission systems at 10,000 km as a function of the signal input power P_0 for several l_d (10 km, 40 km, 80 km, 160 km, and 240 km), comparing with the linear SNR-limited BER. The 10,000-km transmission of the data rate as high as 200 Gbit/s becomes possible at BER = 10^{-9} by using l_d = 240 km with P_0 = 11 mW or l_d = 10 km with P_0 = 15 mW in the higher-order dispersion-managed OPC transmission system.

Since polarization mode dispersion (PMD) has been recognized as a significant problem limiting the transmission of such ultra-high bit-rate data, in this paper, we do not take PMD into account in the calculations. However, as it has been shown that, without compensation, PMD of the dispersion-managed transmission fiber using SMF and RDF is as small as 0.03 ps/$\sqrt{\text{km}}$ [14]. Thus, by incorporating with PMD compensation, the performance of the dispersion-managed OPC systems may not be degraded too much.

In all calculations shown above, we assume that the RDF exhibits the complete reverse dispersion characteristic of that of the SMF. In fact, commonly the cancellation of the TOD of the SMF by the RDF reduces the total TOD in each link to be lower than 10^{-4}

ps/km/nm^2. Such very low TOD may slightly affect the transmission of ultra-high capacity WDM data that consumes extremely large band width. Since our highest transmission data rate used in the simulation is only 200 Gbit/s, the TOD length of the fiber consisted of SMF and RDF for this case will be several times larger than 10,000 km. This mentions that even we assume that the SMF and the RDF possess the complete opposite dispersion characteristic, the transmission using our scheme in real world will not so different from our calculated results.

Furthermore, in all our calculations the optical phase conjugator is assumed to be ideal. Practically, if we use the optical nonlinearity for producing the conjugated replica of the signal, the SNR of the signal will unavoidably decreases. This will cause poorer BER than the results we have shown in this paper.

Furthermore, in our calculations, we neglect the spatial fluctuation of local dispersion and the stimulated Brillouin scattering (SBS) effect [1]. The two effects can also cause significant signal distortion in OPC systems. For the systems where the dispersion fluctuation period is shorter than the nonlinear length: L_{nl} , the dispersion fluctuation has a little influence on signal transmission because, the dispersion fluctuation can be averaged out in the nonlinear scale. Then, the signal almost feels the average dispersion rather than the dispersion fluctuation while propagating in such systems. On the other hand, the dispersion variation whose period is comparable or longer than L_{nl} will cause significant signal distortion. Since the nonlinear coefficient of RDF is larger than that of SMF, the dispersion fluctuation on the RDF will result more severe degradation than that occurs in the SMF.

The signal distortion caused by the dispersion fluctuation can be reduced by using the transmission fibers with a relatively large dispersion. Since the combination of SMF and RDF yields large local fiber dispersion, moreover, in all calculations, we set the average dispersion value: D_{av} at -1 ps/km/nm, we believe that the influence of dispersion fluctuation is sufficiently suppressed in our proposed systems.

On the other hand, for the problem induced from the SBS, we have estimated the SBS threshold powers [33], [34] of the RDF for several data rates used in our simulations because the RDF is more

nonlinear than the SMF. The SBS thresholds for the case of 100-Gbit/s, 160-Gbit/s, and 200-Gbit/s data are approximately 51 mW, 81 mW, and 102 mW, respectively. Therefore, we can conclude that the SBS can be neglected for all values of the signal input powers used in our calculations.

5. CONCLUSIONS

In this report, performance improvement of ultra-long-haul high-bit-rate optical transmission system using midway OPC was studied. The serious limitations of OPC system is mainly resulted from TOD and SI effect. We have shown that the accumulation characteristic of the TOD in OPC transmission systems is almost linear as long as the GVD length is much shorter than the nonlinear length. This fact gave us a possibility to install only one of the linear TOD compensator at any point in the system for perfect TOD compensation. By assuming the ideal TOD compensator, the computer simulation result has shown the possibility of 100Gbit/s, 10,000km transmission based on TOD compensated OPC systems.

We have presented the derivation of the analytical expression of the sideband instability (SI) induced from periodic signal power variation and periodic dispersion management considering when two different fibers are connected together to form the dispersion compensation link. Three possible dispersion management systems were considered: (a) system where dispersion management period is larger than amplifier spacing, (b) system where the two lengths are equal, and (c) system where amplifier spacing is larger than dispersion management period.

We found that SI frequency depends on the larger period between the amplifier spacing and the dispersion management period. The larger the variation period becomes, the SI frequency will arise closer to carrier frequency. Moreover, the gain of SI appears to be reduced with the increase of local fiber second-order dispersion (SOD). This is because the increase in the local SOD virtually shifts the order of SI to higher order resulting in the difficulty of phase-match process. The computer simulations were made and their results were in a good agreement with the derived theory.

In WDM systems that use relatively narrow channel spacing, we demonstrated that even the dispersion map is properly designed to achieve low SI gain, SI causes signal distortion to specific channels that fall just on the low order SI frequency, especially the first order. Additionally to WDM system design rules, the channel allocation must avoid the SI position in such a way that none of the channel should be lied at. The computer simulations have confirmed that BER of WDM systems whose channel location is re-arranged to

avoid SI give a significant improvement of the transmission performance.

Next we proposed for the first time the simultaneous suppression of the two main problems, TOD and SI, in OPC transmission systems by employing higher-order dispersion management fiber link consisting of SMF and RDF. In order to implement the combination of SMF and RDF on OPC systems, we demonstrated that it is necessary to use symmetric dispersion profile with respect to mid-point of the system to reduce SI gain together with the accumulation of the interplay between SPM and each fiber local dispersion. According to the numerical computation results, the 100Gbit/s OPC systems using the SMF+RDF-dispersion-managed link without optimizing the dispersion map has achieved the transmission length at BER=10^{-9} over 2,000 km longer than system where SI is not suppressed even the nonlinear length of the system is set comparable to the amplifier spacing.

Next, we have introduced the system design approaches to achieve the maximum system performance considering the determination of dispersion management period l_d and the corresponding signal input power. Such maximum performance can be achieved by using optimum input power which will be found at relatively low value for the case $l_d > l_f$ and at relatively high value for the case $l_d < l_f$. The computer simulation results have demonstrated that the 10,000km transmission of 100Gbit/s, 160Gbit/s and even the data rate as high as 200Gbit/s become possible by the dispersion-managed OPC system whose dispersion map is properly designed.

Since all the systems considered in this work are single channel transmission systems, for future works, we suggest the study on the use of higher-order dispersion-managed OPC scheme on long-haul WDM transmission systems. In this case, design strategies for signal channel allocation that avoids the position of SI should be considered. Furthermore, the expansion of the bandwidth of OPC device should also be studied in order to support such ultra broadband transmission.

REFERENCES

[1] G. P. Agrawal, *Nonlinear Fiber Optics*. New York: Academic Press, 1993.

[2] R. W. Tkach, A. R. Chaplyvy, F. Forghieri, A. H. Gnauck, and R. M. Derosier, " Four-photon mixing and high-speed WDM systems, " *J. Lightwave Technol.*, vol. 13, pp. 841-849, 1995.

[3] N. Kikuchi, K. Sekine, and S. Sasaki, " Analysis of cross-phase modulation (XPM) effect on WDM transmission performance, " *Electron. Lett.*, vol. 33, pp. 653-654, 1997.

[4] D. Marcuse, " Single-channel operation in very long nonlinear fibers with optical amplifiers at zero dispersion , " *J. Lightwave Technol.*, vol. 9, pp. 356-361, 1991.

[5] N. Kikuchi and S.Sasaki, " Fiber nonlinearity in dispersion-compensated conventional fiber transmission, " *Electron. Lett.*, vol. 32, pp. 570-572, 1996.

[6] R. J. Nuyts, Y. K. Park, and P. Gallion, " Dispersion equalization of a 10Gbit/s repeatered transmission system using dispersion compensating fibers, " *J. Lightwave Technol.*, vol. 15, pp. 31-41, 1997.

[7] X. Wang, K. Kikuchi, and Y. Takushima, " Analysis of dispersion-managed optical fiber transmission system using non-return-to-zero pulse format and performance restriction from third-order dispersion, "*IEICE Trans. Electron.*, vol.E82-C, no.8, pp.1407-1413, 1999.

[8] M. Murakami, T. Matsuda, H. Maeda, and T. Imai, " Long-haul WDM transmission using higher order fiber dispersion management, " *J. Lightwave Technol.*, vol. 18, no. 9, pp. 1197-1204, 2000.

[9] M. Murakami, K. Suzuki, H. Maeda, T. Takahashi, A. Naka, N. Ohkawa, and M. Aiki, " High speed TDM-WDM techniques for long-haul submarine optical amplifier systems, " *Optic. Fiber Technol.*, vol. 3, no. 4, pp. 320-338, 1997.

[10] N. S. Bergano, C. R. Davidson, M. A. Mills, P. C. Corbett, R. Menges, J. L. Zyskind, J. W. Shulhoff, A. K. Srivastava, and C. Wolf, " Long-haul transmission using 10Gb/s channels: 160Gb/s(16x10Gb/s) 6000km demonstration, " in *Proc. OAA'97*, Postdeadline paper PD-9.

[11] M. Morimoto, I. Kobayashi, H. Hiramatsu, K. Mukasa, R. Sugizaki, Y. Suzuki, Y. Kamikura, " Development of dispersion compensation

cable using reverse dispersion fiber, " in *Proc. of Fifth Asia-Pacific Conference on Communications, 1999 and Fourth Optoelectronics and Communications Conference (APCC/OECC '99)*, vol. 2, pp. 1590-1593, 1999

[12] M. Kazunori, T. Yagi, " Dispersion flat and low nonlinear optical link with new type of reverse dispersion fiber (RDF-60), " in *Proc. Opt. Fiber Comm. (OFC'2001)*, Anaheim, CA, Mar. 17-22, 2001, paper TuH7

[13] T. Naito, N, Shimojoh, T. Tanaka, H. Nakamoto, M. Doi, T. Ueki, and M. Suyama, " 1 Terabit/s WDM transmission over 10,000km, " in *Proc. European Conf. on Opt. Commun. (ECOC'99)*, Nice France, Sept. 26-30, 1999, PD2-1, pp. 24-25.

[14] T. Yamamoto, E. Yoshida, K. R. Tamura, K. Yonenaga, and M. Nakazawa, " 640-Gbit/s optical TDM transmission over 92 km through a dispersion-managed fiber consisting of single-mode fiber and " reverse dispersion fiber, " *IEEE Photon. Technol. Lett.*, vol. 12, pp. 353-355, 2000.

[15] M. Nakazawa, T. Yamamoto, and K. R. Tamura, " 1.28Tbit/s-70km OTDM transmission using third- and Fourth-order simultaneous dispersion compensation with a phase modulator, " *Electron. Lett.*, vol. 36, no. 24, pp. 2027-2029, 2000.

[16] C. Lorattanasane and K. Kikuchi, " Design theory of long-distance optical transmission systems using midway optical phase conjugation, " *J. Lightwave Technol.*, vol. 15, pp. 948-955, 1997.

[17] K. Pasu, A. Tuptim, and K. Kikuchi, " Feasibility of 100-Gb/s 10000-km single-channel optical transmission by midway optical phase conjugation in corporated with third-order dispersion compensation, " *IEEE Photon. Technol. Lett.*, vol. 13, no. 4, pp. 293-295, 2001.

[18] S. Watanabe and M. Shirasaki, " Exact compensation for both chromatic dispersion and Kerr effect in a transmission fiber using optical phase conjugation, " *J. Lightwave Technol.*, vol. 14, pp. 243-248, 1996.

[19] K. Pasu and A. Tuptim, " Sideband instability in the presence of periodic power variation and periodic dispersion management, " in *Proc. Opt. Fiber Comm. (OFC'2001)*, Anaheim, CA, Mar. 17-22, 2001, paper WDD32

[20] K. Pasu, A. Tuptim, and K. Kikuchi, " Complete analysis of sideband instability in chain of periodic dispersion-managed fiber

link and its effect on higher-order dispersion-managed long-haul wavelength division multiplexed systems, " *IEEE/OSA J. Lightwave Technol.*, vol. 20, no. 11, pp. 1895-1907, 2002.

[21] F. M. Madani and K. Kikuchi, " Design theory of long-distance WDM dispersion-managed transmission system, " *J. Lightwave Technol.*, vol. 17, pp. 1326-1335, 1999.

[22] K. Tanaka, T. Tsuritani, N. Edagawa, and M. Suzuki, " 320Gbit/s (32x10.7Gbit/s) error-free transmission over 7,280km using dispersion flattened fiber link with standard SMF and slope compensating DCF, " in *Proc. ECOC'1999*, Nice, France, Sep. 26-30, 1999, pp. II-180-181

[23] T. Tsuritani, N. Takeda, K. Imai, K. Tanaka, A. Agata, I. Morita, H. Yamauchi, N. Edagawa, and M. Suzuki, " 1Tbit/s (100x10.7Gbit/s) transoceanic transmission using 30nm-wide broadband optical repeaters with A_{eff} -enlarged positive dispersion fibre and slope-compensating DCF, " in *Proc. European Conf. on Opt. Commun. (ECOC'99)*, Nice France, Sept. 26-30, 1999, PD2-1, pp. 38-39.

[24] H. Nakamoto, T. Tanaka, N. Shimojoh, T. Naito, I. Yokota, A. Sugiyama, T. Ueki, and M. Suyama, " 1.05Tbit/s WDM transmission over 8,186km using distributed Raman amplifier repeaters, " in *Proc. Opt. Fiber Comm. (OFC'2001)*, Anaheim, CA, Mar. 17-22, 2001, paper TuF6

[25] E. Shibano, S. Nakagawa, T. Kawazawa, H. Taga, and K. Goto, " 96x11.4Gbit/s transmission over 3,800km using C-band EDFA and non-zero dispersion shifted fiber, " in *Proc. Opt. Fiber Comm. (OFC'2001)*, Anaheim, CA, Mar. 17-22, 2001, paper TuN2

[26] F. Matera, A. Mecozzi, M. Romagnoli and M. Settembre, " Sideband instability induced by periodic power variation in long distance fiber links, " *Opt. Lett.*, 18, pp. 1499-1501, 1993.

[27] C. Kurtzke and K. Peterman, " Impact of fiber four-photon mixing on the design of n-channel megameter optical communication systems, " in *Proc. Opt. Fiber Comm. (OFC'93)*, San Jose, CA, Feb. 21-26, 1993, paper FC3.

[28] C. Kurtzke, " Suppression of fiber nonlinearities by appropriate dispersion management, " *IEEE Photon. Technol. Lett.*, vol. 5, no. 10, pp. 1250-1253, 1993.

[29] K. Kikuchi, C. Lorattanasane, F. Futami, and S. Kaneko, " Observation of quasi-phase matched four-wave mixing assisted by

periodic power variation in a long-distance optical amplifier chain, " *IEEE Photon. Technol. Lett.*, vol. 7, no. 11, pp. 1378-1380, 1995.

[30] N. J. Smith and N. J. Doran, "Modulation instability in fibers with periodic dispersion management, " *Opt. Lett.*, vol. 21, pp. 570-572, 1996.

[31] T. Okano, T. Ooishi, T. Kato, Y. Yokoyama, M. Yoshida, Y. Takahashi, Y. Makio, and M. Nishimura, " Optimum dispersion of non-zero dispersion shifted fiber for high bit rate DWDM systems, " in *Proc. Opt. Fiber Comm. (OFC'2001)*, Anaheim, CA, Mar. 17-22, 2001, paper TuH4

[32] C. Lorattanasane and K. Kikuchi, " Parametric instability of optical amplifier noise in long-distance optical transmission systems, " *J. Quantum Electron.*, vol. 33, pp. 1068-1074, 1997.

[33] Y. Aoki, K. Tajima, and I. Mito, " Input power limits of single-mode optical fibers due to stimulated Brillouin scattering in optical communication systems, " *J. Lightwave Technol.*, vol. 6, pp. 710-719, 1988.

[34] D. A. Fishman and J. A. Nagel, " Degradations due to stimulated Brillouin scattering in multigigabit intensity-modulated fiber-optic systems, " *J. Lightwave Technol.*, vol. 11, pp. 1721-1728, 1993.

PUBLICATIONS

International Periodical Journals

- K. Pasu, A. Tuptim, and K. Kikuchi, " Complete analysis of sideband instability in chain of periodic dispersion-managed fiber link and its effect on higher-order dispersion-managed long-haul wavelength division multiplexed systems, " *OSA/IEEE J. Lightwave Technol.*, vol. 20, no. 11, pp. 1895-1907, 2002
- K. Pasu, A. Tuptim, and K. Kikuchi, "Simultaneous suppression of third-order dispersion and sideband instability in single-channel optical fiber transmission by midway optical phase conjugation employing higher-order dispersion management, *submitted to OSA/IEEE J. Lightwave Technol.*

Domestic Conferences

- K. Pasu, A. Tuptim, and K. Kikuchi, " Effect of Sideband Instability on Long-haul DWDM Optical Fiber Transmission Systems Employing Higher-Order Dispersion Management, " *in Proc. of 25th Electrical engineering conference (EECON25)*, 23-24 Nov 2000, Hadyai, Songkla, Thailand. (BEST PAPER AWARD)
- K. Pasu, A. Tuptim, and K. Kikuchi, "Simultaneous Suppression of Third-Order Dispersion and Sideband Instability in Long-Haul Ultra-High Speed Midway Optical Phase Conjugation Systems Using Higher-Order Dispersion Management, " *in Proc. of 25th Electrical engineering conference (EECON25)*, 23-24 Nov 2000, Hadyai, Songkla, Thailand.

ISSN 0733-8724

Journal of Lightwave Technology

November 2002

Volume 20

Number 11

JLTEDG

IEEE

A JOINT IEEE / OSA PUBLICATION

OSA
Optical Society of America

PAPERS

Networks/Switching

Systems/Subsystems

Fibers/Cables

Active Components

Passive Components

Theory

Complete Analysis of Sideband Instability in Chain of Periodic Dispersion-Managed Fiber Link and Its Effect on Higher Order Dispersion-Managed Long-Haul Wavelength-Division Multiplexed Systems

Pasu Kaewplung, Tuptim Angkaew, *Member, IEEE*, and Kazuro Kikuchi, *Member, IEEE, Member, OSA*

Abstract—**We present for the first time a complete theoretical analysis of sideband instability (SI) that occurs when two kinds of fibers with different characteristics are concatenated to form a dispersion-managed fiber link. In the analysis, the following three cases are taken into account: case (a) when a dispersion-management period is larger than an amplification period, case (b) when the two lengths are equivalent, and case (c) when a dispersion-management period is smaller than an amplification period.**

We find that the SI gain peak appears at frequencies determined by the larger of the two variation periods. Moreover, for all three cases, the magnitude of the SI gain reduces with the increase in strength of dispersion management.

Next, we focus on the fiber link using the combination of standard single-mode fiber and reverse dispersion fiber, which is widely used for simultaneously compensating second- and third-order dispersion. By computer simulation, it is shown that in wavelength-division-multiplexed systems, SI still induces significant degradation in channels located at frequencies where SI induced from other channels arises. By reallocating the channel frequency to avoid the SI frequency, the transmission performance is improved significantly.

Index Terms—**Optical amplifiers, optical fiber communication, optical fiber dispersion, optical Kerr effect, wavelength-division multiplexing.**

I. Introduction

A. General Background

FOUR-WAVE mixing (FWM) and cross-phase modulation (XPM) in optical fibers have been recognized as the main problems that cause signal waveform distortion in wavelength-division-multiplexed (WDM) systems [1]–[3]. FWM induces signal energy transfer among channels, while, through XPM, temporal intensity variation of every channel modulates the phase of other copropagating channels. In fact, the use of nonzero dispersion for signal transmission yields relatively different propagating group velocity among channels, referred to as walkoff, which dramatically results in the reduction of channel crosstalk induced from both FWM and XPM. For this purpose, the second-order dispersion (SOD) management method has been proposed and demonstrated [4]–[7]. Through this method, fiber sections are periodically arranged in such a way that the signal carrier wavelengths alternatively fall in normal and anomalous dispersion region, while, for each period, the total fiber exhibits zero or near zero dispersion on average. Therefore, signal pulse propagating in the link will always experience nonzero dispersion, while its width is almost preserved at each compensation period due to low average dispersion.

However, such an approach can manage only SOD in only one channel. Therefore, in WDM systems, signal channels far from the average zero-dispersion wavelength experience different amounts of dispersion accumulation along the entire system length because of the existence of the dispersion slope or third-order dispersion (TOD).

It has been predicted that the existence of TOD limits the available passband of the WDM systems with data rates of more than 10 Gbit/s [8]–[10]. For further expansion in both capacity and distance, dispersion management to eliminate both SOD and TOD will be one of the key issues. For this purpose, special dispersion compensating fiber called reverse dispersion fiber (RDF) [11], [12] has been proposed and has demonstrated its potential. Since RDF exhibits low negative TOD with large negative SOD, we can achieve the dispersion flattened fiber link with low average SOD by combining RDF with standard single-mode fiber (SMF) in each compensation interval. The use of such a higher order dispersion compensation fiber link in combination with the optimization of channel spacing realizes the simultaneous reduction of FWM, XPM, and TOD. Transmission experiments show that using the combination of SMF and RDF can achieve a data rate as high as 1 Tbit/s (104 × 10 Gbit/s) WDM transmission over 10 000 km [13].

B. Purpose of This Paper

In this paper, we demonstrate that the additional signal distortion to long-haul higher order dispersion-managed WDM

Manuscript received January 8, 2002; revised August 8, 2002. This work was supported by Chulalongkorn University, Bangkok, Thailand, under the Ratchadaphisek Somphot Fund.

P. Kaewplung and T. Angkaew are with the Department of Electrical Engineering, Faculty of Engineering, Chulalongkorn University, 10330 Bangkok, Thailand (e-mail: pasu@ee.eng.chula.ac.th).

K. Kikuchi is with the Research Center for Advanced Science and Technology, University of Tokyo, Meguro-ku, 153-8904 Tokyo, Japan (e-mail: kikuchi@ginjo.rcast.u-tokyo.ac.jp).

Digital Object Identifier 10.1109/JLT.2002.806365

systems can occur via the quasi-FWM phase-match process assisted by periodic variation of the signal power in the chain of lossy fiber intervals and lumped amplifiers incorporated with periodic dispersion management. This parametric process, which occurs in both normal and anomalous dispersion regions, is called sideband instability (SI). Through this process, the signal carrier transfers its energy to specific sideband frequencies, which grow up exponentially with transmission distance.

It has been shown theoretically that in order to avoid the XPM-induced signal waveform distortion for 10-Gbit/s-based 10 000-km WDM transmission, the use of channel spacing larger than 100 GHz is preferable [14]. Several long-haul transmission experiments also demonstrate attractive results using channel spacing around this value [8], [13], [15]. With this relatively large channel spacing, the first-order SI, which usually exhibits larger gain than higher orders, will not arise inside one's channel bandwidth. Therefore, the problem induced from SI has not yet appeared and can be ignored for such transmissions.

However, with system distance shorter than 10 000 km, the possibility of using smaller channel spacing for signal transmission has been shown [16]–[18]. In this situation, if two different channels produce SI at the same frequency, SI will cause a serious problem to the channels whose carriers are placed just at that frequency, especially for the frequency where the first-order SI arises.

Historically, Matera *et al.* first theoretically showed the occurrence of SI in long-distance systems through the periodic signal amplification [19]. Kurtzke and Peterman briefly discussed the impact of SI on multichannel long-distance optical communication systems [20], [21]. In their works, by computer simulations, a serious channel signal distortion was observed when the SI resonance frequency superpositions on the channel frequency. Kikuchi *et al.*experimentally observed SI in an optical amplifier chain using a recirculating fiber loop [22]. Smith and Doran predicted that the periodic dispersion management also leads to the occurrence of SI. They also demonstrated that the gain of SI could be reduced by strong dispersion management [23]. Recently, we have presented a part of the derivation of SI under the existence of both periodic power variation and periodic dispersion variation [24].

However, none of the previous works has included the periodic variation of fiber parameters such as fiber loss coefficient and fiber nonlinear coefficient, which is practically necessary to consider when two different fibers are connected together to form a dispersion-managed transmission line. Moreover, to avoid the problem of SI in WDM systems, it is important to study SI in more detail, and the exact analytical expression of SI must be derived.

C. Organization of This Paper

This paper makes the first complete theoretical analysis of SI focusing on the case when two different characteristic fibers are connected together. In our analysis, not only the periodic power variation but also the periodic dispersion management, periodic fiber loss coefficient variation, and periodic nonlinear coefficient variation are included. In Section II, we derive the analytical SI gain and the SI frequency considering three cases: a) when a dispersion-management period is larger than an amplifier spacing, b) when the two lengths are equal, and c) when an amplifier spacing is larger than a dispersion-management period. In Section III, the accuracy of the derived theory is evaluated by computer simulations.

Section IV focuses on dispersion-managed transmission system consisting of SMF and RDF. Our computer simulation results show that when two or more channels produce SI at the same frequency, SI significantly causes a serious problem to the channel whose carrier is positioned just at that superposition resonance frequency. We also demonstrate that by rearranging the channel position or channel spacing in such a way that none of the SI resonance frequency falls inside the channel signal bandwidth, the transmission performance is significantly improved. Finally, this paper is summarized in Section V.

II. Derivarion of Sideband Instability in the Presence of Periodic Power Variation and Periodic Dispersion Management

In long-haul and high-capacity fiber transmission systems, the power of the optical signal must be kept high in order to obtain good signal-to-noise ratio (SNR) at a receiver. In such high-power systems, by amplification process, the periodic power variation produces a periodic variation of fiber refractive index through the nonlinear Kerr effect of an optical fiber. By this process, it seems like a grating is virtually constructed in the transmission fiber. As shown in Fig. 1, a parametric resonance between the virtual grating and the signal will occur at the signal sideband component whose wave number is half of the wave number of this virtual grating, resulting in exponential growth of that component with transmission length [19]. This phenomenon is known as the sideband instability, which causes signal waveform distortion if SI arises at frequency inside the signal bandwidth since it cannot be eliminated by using an optical bandpass filter.

Quantitatively, the occurrence of SI can be explained in terms of a quasi-phase-matched FWM process that is assisted by the virtual grating induced by the periodic power variation as the condition [19]

$$k_+ + k_- = 2k_0 + k_f. \tag{1}$$

In (1), the wave number of the signal, which acts as a pump, is $k_0 = -\gamma\bar{P} + \beta(\omega_0)$; and the sideband wave numbers are $k_+ = k_- = 1/2\beta_2\omega_n^2 + \beta(\omega_0)$, where $\beta(\omega_0)$ is the wave number at the central carrier frequency ω_0. k_f is the wave number of the virtual grating, which is given as

$$k_f = \frac{2\pi n}{l_f} \tag{2}$$

where $n = 0, \pm 1, \pm 2, \ldots$, and l_f is the amplifier spacing. The sideband frequency ω_n shifted from the carrier frequency at which SI arises is obtained from (1) and (2) as

$$\omega_n = \pm\sqrt{\frac{1}{|\beta_2|}\left(k_f n - 2\,\mathrm{sgn}\,(\beta_2)\,\gamma\bar{P}\right)} \tag{3}$$

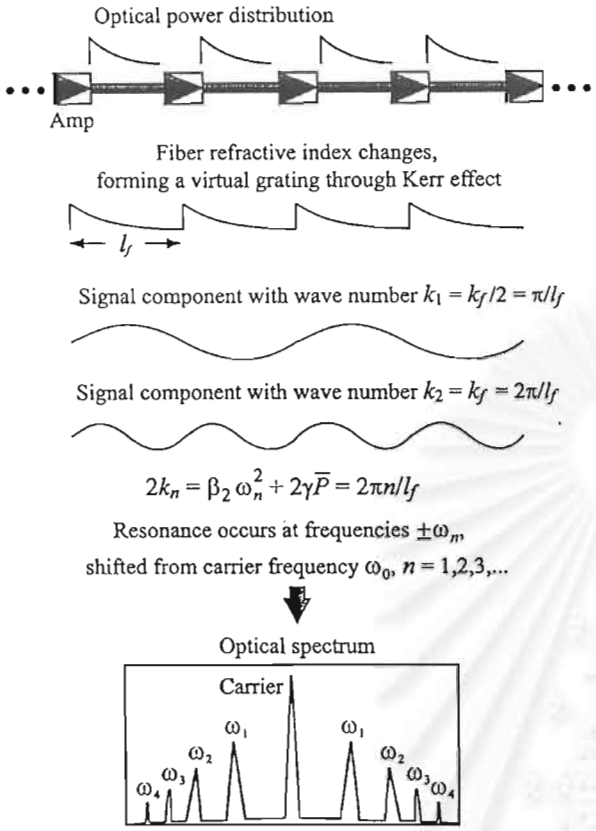

Fig. 1. Occurrence of sideband instability. A virtual grating is formed through fiber loss and periodic amplification via Kerr effect. A resonance between this virtual grating and propagating signal gives rise to an exponential growth with transmission length of the signal carrier sideband components whose wave vector matches that of the virtual grating.

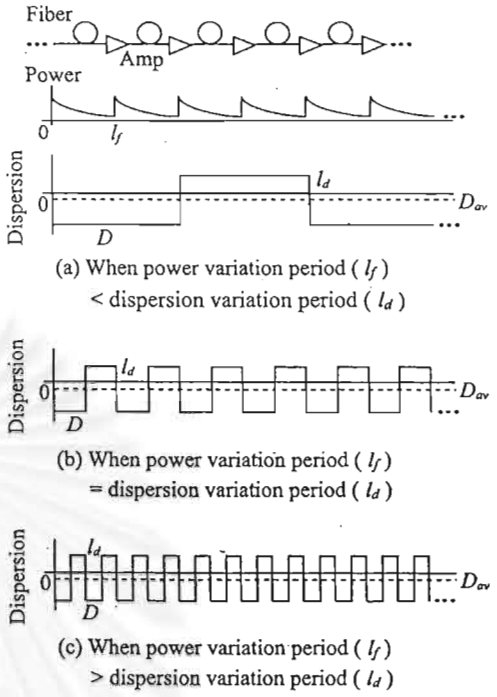

Fig. 2. Models of dispersion-management system used for analytical derivation. The signal power and fiber dispersion change periodically with transmission length. The fiber link consists of two different characteristic fibers with the same length. Three possible cases are modeled: a) when the dispersion compensation period l_d is longer than the amplifier span l_f, b) when the two scales become equal, and c) when $l_d < l_f$.

where $\bar{P}$ is the path-averaged signal power. The power gain $\lambda(\omega_n)$ of SI at each n-order resonance frequency is

$$\lambda(\omega_n) = 2P_0|F_n| \tag{4}$$

where P_0 denotes the signal input power and F_n the n-order of the Fourier series coefficient of the periodic function $\alpha(z)$ whose period is equal to l_f.

In fact, not only the periodic power variation but also all of the periodic perturbation under the Kerr effect—such as the periodic dispersion variation, the periodic fiber loss coefficient variation, and the periodic fiber nonlinear coefficient variation—can lead to the occurrence of SI. To obtain the general expression of SI considering all of the periodic perturbation, we should start the analytical derivation based on the models of dispersion-management systems illustrated in Fig. 2. In Fig. 2, the signal power and the fiber dispersion is assumed to change periodically with transmission length. As we aim to concentrate to dispersion-managed transmission system consisting of SMF and RDF, the fiber link is composed of two different characteristic fibers with the same length. Therefore, the dispersion profile is the simplest type, where the dispersion varies every half-period with the same amount plus and minus around a given average dispersion value. Each fiber has its own nonlinear coefficient and fiber loss, which is assumed periodic by the period equivalent to the dispersion-management period. We consider here three possible cases: a) when the dispersion-management period is longer than the amplifier span, b) when the two scales become equal, and c) when the dispersion-management period is shorter than the amplifier span.

The analysis starts from the nonlinear Schrodinger equation [1] for the signal envelope function $U(z,t)$

$$\frac{\partial U}{\partial Z} = -\frac{\alpha(z)}{2}U - \frac{j}{2}\left(\beta_{2\mathrm{av}} + \beta_{2\mathrm{fl}}(z)\right)\frac{\partial^2 U}{\partial t^2} + j\gamma(z)|U|^2 U. \tag{5}$$

In (5), the GVD is separated in two parts: the constant average $\beta_{2\mathrm{av}}$ and the fluctuation part $\beta_{2\mathrm{fl}}(z)$. The fiber loss coefficient $\alpha(z)$, the nonlinear coefficient $\gamma(z)$, and $\beta_{2\mathrm{fl}}(z)$ are the functions of z that are assumed periodic with the same period equivalent with the dispersion-management period. It should be noted that the GVD parameter β_2 relates to the common dispersion parameter D by

$$D = -\frac{\omega_0}{\lambda_0}\beta_2 \tag{6}$$

where ω_0 denotes the carrier frequency and λ_0 the carrier wavelength.

At each amplifier, the span loss is compensated so that we can assume that the optical field propagating in each amplification period has the form

$$U(z,t) = u(z,t)\exp\left(-\frac{1}{2}\alpha(z)z\right). \tag{7}$$

Inserting (7) into (5), we obtain

$$\frac{\partial u}{\partial Z} = -\frac{j}{2}\left(\beta_{2\mathrm{av}} + \beta_{2\mathrm{fl}}(z)\right)\frac{\partial^2 u}{\partial t^2} + jf(z)|u|^2 u \tag{8}$$

where $f(z) = \gamma(z)\exp(-\alpha(z)z)$ is the periodic function whose period is equal to the amplifier spacing. Next, we perturb (8) by a small amplitude fluctuation a added to the steady solution of (8)

$$u(z,t) = \left(\sqrt{P_0} + a\right)\exp\left(jP_0\int_0^z f(z')dz'\right) \tag{9}$$

where P_0 denotes the input peak power and a is defined as

$$a(z,t) = \frac{1}{2}\{a(z,\omega)\exp(j\omega t) + a(z,-\omega)\exp(-j\omega t)\}. \tag{10}$$

Substituting (9) and (10) back to (8), we obtain one set of two differential equations as shown in (11) at the bottom of the page, where the subscript * indicates the counterpart complex conjugate. By introducing the transformation shown in (12) at the bottom of the page, (11) becomes

$$\frac{\partial}{\partial Z}\begin{bmatrix} b(z,\omega) \\ b^*(z,-\omega)\end{bmatrix} = j\begin{bmatrix} \frac{1}{2}\beta_{2\mathrm{av}}\omega^2 + f(z)P_0 & g(z)P_0 \\ -g^*(z)P_0 & -\frac{1}{2}\beta_{2\mathrm{av}}\omega^2 - f^*(z)P_0\end{bmatrix}\cdot\begin{bmatrix} b(z,\omega) \\ b^*(z,-\omega)\end{bmatrix} \tag{13}$$

where

$$g(z) = f(z)\exp\left(-j\omega^2\int_0^z \beta_{2\mathrm{fl}}(z')dz'\right). \tag{14}$$

By this transformation, we can remove the fast oscillations in the field envelope, so that only those changes that accumulate over the period of $\beta_{2\mathrm{fl}}(z)$ are left. The key step of this analysis is to expand $f(z)$ and $g(z)$ as complex Fourier series

$$f(z) = \sum_{n=-\infty}^{\infty} F_n \exp(jk_f nz)$$
$$g(z) = \sum_{n=-\infty}^{\infty} G_n \exp(jk_g nz) \tag{15}$$

where k_f and k_g are the fundamental wave constants of $f(z)$ and $g(z)$ and F_n and G_n denote the Fourier series coefficients of $f(z)$ and $g(z)$.

A. The Case When the Dispersion Compensation Period is Larger Than the Amplifier Spacing

First, we consider case a) when the dispersion-management period l_d is larger than the amplifier spacing l_f. The wave constant k_g in this case can be written as $k_g = 2\pi/l_d = k_d$, where $l_d = 2pl_f$, so that $k_f = 2pk_d$ and $p = 1, 2, 3, \ldots$. To get close to the resonance of the nth Fourier component of the perturbation, we introduce the variable transformation

$$\begin{bmatrix} b(z,\omega) \\ b^*(z,-\omega)\end{bmatrix} = \begin{bmatrix} \exp\left(j\frac{1}{2}k_d nz\right) & 0 \\ 0 & \exp\left(-j\frac{1}{2}k_d nz\right)\end{bmatrix}\cdot\begin{bmatrix} c(z,\omega) \\ c^*(z,-\omega)\end{bmatrix} \tag{16}$$

Inserting (15) and (16) into (13) and equating only the coefficients of $\exp(jk_d nz/2)$ and $\exp(-jk_d nz/2)$ (for the complex conjugate counterpart), we obtain (17), shown at the bottom of the page, where F_0 and G_n denote the fundamental and the nth order coefficient of Fourier series of $f(z)$ and $g(z)$, respectively.

From the eigenvalues of (17), we obtain the power gain $\lambda(\omega)$ for the $n$order SI effect as

$$\lambda(\omega) = \sqrt{4P_0^2|G_n|^2 - \left(k_d n - \beta_{2\mathrm{av}}\omega^2 - P_0|F_0|\right)^2}. \tag{18}$$

At each order of SI, λ appears at its peak at frequencies defined by

$$\omega_n = \pm\sqrt{\frac{1}{|\beta_{2\mathrm{av}}|}\left(k_d n - 2\,\mathrm{sgn}\left(\beta_{2\mathrm{av}}\right)P_0|F_0|\right)}. \tag{19}$$

$$\frac{\partial}{\partial Z}\begin{bmatrix} a(z,\omega) \\ a^*(z,-\omega)\end{bmatrix} = j\begin{bmatrix} \frac{1}{2}\left(\beta_{2\mathrm{av}} + \beta_{2\mathrm{fl}}(z)\right)\omega^2 + f(z)P_0 & f(z)P_0 \\ -f^*(z)P_0 & -\frac{1}{2}\left(\beta_{2\mathrm{av}} + \beta_{2\mathrm{fl}}(z)\right)\omega^2 - f^*(z)P_0\end{bmatrix}\begin{bmatrix} a(z,\omega) \\ a^*(z,-\omega)\end{bmatrix} \tag{11}$$

$$\begin{bmatrix} a(z,\omega) \\ a^*(z,-\omega)\end{bmatrix} = \begin{bmatrix} \exp\left(j\frac{\omega^2}{2}\int_0^z \beta_{2\mathrm{fl}}(z')dz'\right) & 0 \\ 0 & -\exp\left(j\frac{\omega^2}{2}\int_0^z \beta_{2\mathrm{fl}}(z')dz'\right)\end{bmatrix}\begin{bmatrix} b(z,\omega) \\ b^*(z,-\omega)\end{bmatrix} \tag{12}$$

$$\frac{\partial}{\partial Z}\begin{bmatrix} c(z,\omega) \\ c^*(z,-\omega)\end{bmatrix} = j\begin{bmatrix} -\frac{1}{2}k_d n + \frac{1}{2}\beta_{2\mathrm{av}}\omega^2 + P_0F_0 & P_0G_n \\ -P_0G_n^* & \frac{1}{2}k_d n - \frac{1}{2}\beta_{2\mathrm{av}}\omega^2 - P_0F_0^*\end{bmatrix}\begin{bmatrix} c(z,\omega) \\ c^*(z,-\omega)\end{bmatrix} \tag{17}$$

It is remarkable from (19) that SI occurs at frequencies determined by the dispersion-management period l_d and by the averaged GVD $\beta_{2\mathrm{av}}$ independent of the fluctuation part $\beta_{2\mathrm{fl}}$. For larger l_d, the SI gain position moves closer to signal carrier frequency, which may cause more severe signal waveform distortion. On the other hand, the peak of SI gain at the $n$order resonance frequency $\lambda(\omega_n)$ depends on $\beta_{2\mathrm{av}}$ through ω_n in $|G_n|$ according to (14) and (19).

To obtain the expression of the SI gain, F_0 and G_n have to be derived. F_0 can be calculated from

$$F_0 = \frac{1}{l_d}\int_0^{l_d} f(z)dz = \frac{1}{l_d}\int_0^{l_d} \gamma(z)\exp(-\alpha(z)z)dz \quad (20)$$

since this paper considers the periodical dispersion compensation, which is constructed by the combination of two fibers in equal length. Each fiber exhibits different values of α and γ, which are assumed to be constant along each fiber length. In each compensation interval, let α_1 and γ_1 represent the fiber loss coefficient and the nonlinear coefficient of the first fiber and α_2 and γ_2 represent the fiber loss coefficient and the nonlinear coefficient of the second fiber, respectively. F_0 is obtained through

$$\begin{aligned} F_0 =& \frac{1}{l_d}\sum_{i=0}^{p-1}\left\{\int_{il_d/(2p)}^{l_d/(2p)+il_d/(2p)} \gamma_1\exp\left(-\alpha_1 z\right)dz \right. \\ &\left. + \int_{l_d/2+il_d/(2p)}^{l_d/2+l_d/(2p)+il_d/(2p)} \gamma_2\exp\left(-\alpha_2 z\right)dz\right\} \\ =& p\left\{\gamma_1\left(\frac{1-\exp\left(-\alpha_1\frac{l_d}{2p}\right)}{\alpha_1 l_d}\right)\right. \\ &\left. + \gamma_2\left(\frac{1-\exp\left(-\alpha_2\frac{l_d}{2p}\right)}{\alpha_2 l_d}\right)\right\}. \end{aligned} \quad (21)$$

By assuming that $\beta_{2\mathrm{fl}}(z)$ follows the profile shown in Fig. 2, we have

$$\int_0^z \beta_{2\mathrm{fl}}(z')dz' = \begin{cases} \beta_{2\mathrm{fl}} z, z = \left[0, \frac{l_d}{2}\right) \\ \beta_{2\mathrm{fl}}\left(l_d - z\right), z = \left[\frac{l_d}{2}, l_d\right]. \end{cases} \quad (22)$$

Substituting (22) into the exponential part of (14), G_n can be analytically obtained through the Fourier integration

$$\begin{aligned} G_n =& \frac{1}{l_d}\sum_{i=0}^{p-1}\int_{il_d/(2p)}^{ld/(2p)+il_d/(2p)} \gamma_1\exp\left(-\alpha_1 z\right) \\ &\cdot\exp\left(-j\beta_{2\mathrm{fl}}\omega^2 z\right)\exp\left(-jk_d n z\right)dz \\ &+ \frac{1}{l_d}\sum_{i=0}^{p-1}\int_{l_d/2+il_d/(2p)}^{l_d/2+ld/(2p)+il_d/(2p)} \gamma_2\exp\left(-\alpha_2 z\right) \\ &\cdot\exp\left(-j\beta_{2\mathrm{fl}}\omega^2\left(l_d - z\right)\right)\exp\left(-jk_d n z\right)dz. \end{aligned} \quad (23)$$

Because $f(z)$ is periodical over each fiber length with the period of $[il_d/(2p), il_d/(2p) + l_d/(2p))$ for $i = 0, 1, 2, \ldots$, it satisfies the following relations:

$$\begin{aligned} f\left(\frac{il_d}{2p}\right) =& \gamma\exp\left(-\alpha\frac{il_d}{2p}\right) = 1 \\ f\left(\frac{l_d}{2p} + \frac{il_d}{2p}\right) =& \gamma\exp\left(-\alpha\frac{l_d}{2p}\right) \\ f\left(\frac{l_d}{2} + \frac{il_d}{2p}\right) =& \gamma\exp\left(-\alpha\left(\frac{l_d}{2} + \frac{il_d}{2p}\right)\right) = 1 \\ f\left(\frac{l_d}{2} + \frac{l_d}{2p} + \frac{il_d}{2p}\right) =& \gamma\exp\left(-\alpha\frac{l_d}{2p}\right). \end{aligned} \quad (24)$$

Applying the above conditions to (23), we obtain (25) as shown at the bottom of the page.

At resonance frequency ω_n where the n-order SI occurs, the n-order SI gain becomes $2P_0|G_n|$. Fig. 3 plots the $n = 1, 2$, and 3-order SI gain peaks at ω_n as a function of local SOD D, calculated by (25) with $l_f = 40$ km, $l_d = 80$ km. P_0 is assumed to be 5 mW, D_{av} is -5 ps/km/nm, and α_1 and γ_1 of fiber #1 are 0.2 dB and 1.6 $\mathrm{W^{-1}km^{-1}}$. For fiber #2, α_2 and γ_2 are 0.25 dB and 4.8 $\mathrm{W^{-1}km^{-1}}$, respectively. It should be noted that D exhibits a negative value when the arrangement of fiber link changes the order of fiber installation to fiber #2, fiber #1 instead of fiber #1, fiber #2.

The gain characteristics shown in Fig. 3 for all three orders appear to be decreased and periodically reduced to minimum points with the increase in fiber local SOD. The reduction of SI gain with the increase of local SOD has been predicted by Smith and Doran [23]. However, the reason for explaining this phenomena has not been clearly mentioned yet. According to (23), it is obvious that

$$\begin{aligned} G_n =& \gamma_1\left\{\frac{1-\exp\left(-\alpha_1\frac{l_d}{2p}\right)\exp\left(-j\left(\beta_{2\mathrm{fl}}\omega^2 + k_d n\right)\frac{l_d}{2p}\right)}{\alpha_1 l_d + j\left(\beta_{2\mathrm{fl}}\omega^2 + k_d n\right)l_d}\right\}\sum_{i=0}^{p-1}\exp\left(-j\left(\beta_{2\mathrm{fl}}\omega^2 + k_d n\right)\frac{il_d}{2p}\right) \\ &+ \gamma_2\left\{\frac{\exp\left(j\left(\beta_{2\mathrm{fl}}\omega^2 - k_d n\right)\frac{l_d}{2}\right) - \exp\left(-\alpha_2\frac{l_d}{2p}\right)\exp\left(j\left(\beta_{2\mathrm{fl}}\omega^2 - k_d n\right)\left(\frac{l_d}{2} + \frac{l_d}{2p}\right)\right)}{\alpha_2 l_d - j\left(\beta_{2\mathrm{fl}}\omega^2 - k_d n\right)l_d}\right\} \\ &\cdot\sum_{i=0}^{p-1}\exp\left(j\left(\beta_{2\mathrm{fl}}\omega^2 - k_d n\right)\frac{il_d}{2p}\right) \end{aligned} \quad (25)$$

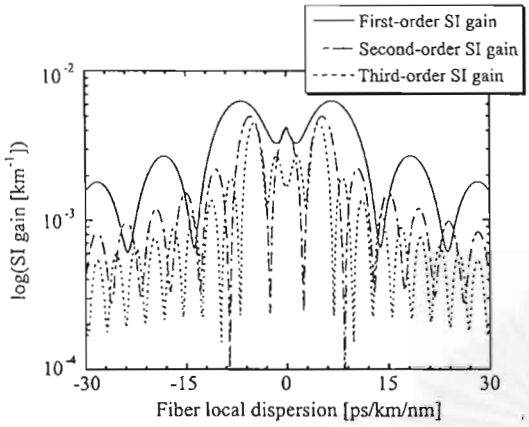

Fig. 3. Theoretical $n = 1, 2$, and 3-order SI gain peaks at resonance frequency ω_n as a function of local SOD D, calculated with $l_f = 40$ km, $l_d = 80$ km, $P_0 = 5$ mW, and $D_{\text{av}} = -5$ ps/km/nm. D exhibits a negative value when the arrangement of fiber link changes the order of fiber installation to RDF-SMF instead of SMF-RDF. The gain characteristics for all three orders appear to be decreased and periodically reduced to minimum points with the increase in D.

the reduction of SI gain does not come from the linear addition and cancellation of the two Fourier components: one induced from the periodic power variation $P_0\alpha(z)$ and the other from the periodic GVD variation $\beta_{2\text{fl}}(z)$. To understand the reason, we should rewrite $l_d = 2l_f(p = 1)$ and $\beta_{2\text{fl}}\omega_n^2 = ck_d$, where c denotes a real number larger than zero. Then (23) can be written as shown in (26) at the bottom of the page.

Equation (26) indicates that for the n-order SI, by increasing the local GVD $|\beta_{2\text{fl}}|$, the corresponding c is increased, resulting in the increase of wave constant k_f by the factor of $(c + n)/2$ for the first term and $(c-n)/2$ for the second term, respectively. Each order of the SI gain, which becomes smaller for large k_f, is correspondingly reduced. In other words, the first term of (26) is similar to the formula of Fourier integration used for obtaining the $(c + n)/2$-order Fourier coefficient of $f(z)$ when the period is l_f and, for the second term, the $(c - n)/2$-order Fourier coefficient. Therefore, this also can be interpreted as meaning that the increase of local GVD $|\beta_{2\text{fl}}|$ virtually shifts the order of SI induced from the power variation to higher order, which exhibits lower gain than the lower order. Furthermore, the SI gain falls down to minimum points when the virtual order numbers $(c + n)/2$ and $(c - n)/2$ together become an integer. In Fig. 3, agreeing with our prediction, the SI gain reduces to minimum points when $(c + n)/2$ and $(c - n)/2$ become $|c| = 3, 5, 7, \ldots$ for the first order, $|c| = 4, 6, 8, \ldots$ for the second order, and $|c| = 5, 7, 9, \ldots$ for the third order, respectively.

B. The Case When the Dispersion Compensation Period Becomes Equal to or Shorter Than the Amplifier Spacing

In this section, we consider the case when l_d is equal to or shorter than l_f. The wave constant k_g for this case becomes $k_f = 2\pi/l_f$. l_f is assumed to satisfy $l_f = pl_d$, where $p = 1, 2, 3, \ldots$. The analysis approach for this case is similar to that of the previous section. By only replacing k_d in (15) with k_f, the power gain $\lambda(\omega)$ for n-order SI effect becomes

$$\lambda(\omega) = \sqrt{4P_0^2 |G_n|^2 - (k_f n - \beta_{2\text{av}}\omega^2 - P_0 |F_0|)^2} \quad (27)$$

which exhibit each peak of the SI order at frequencies determined by

$$\omega_n = \pm\sqrt{\frac{1}{|\beta_{2\text{av}}|}(k_f n - 2\,\text{sgn}(\beta_{2\text{av}})\, P_0 |F_0|)}. \quad (28)$$

From (28), the frequencies where SI arises are determined by the wave constant k_f, which is constant even if the dispersion-management period l_d is changed. This means that for $l_d \le l_f$, SI will almost arise at the same frequencies independent of the change in l_d, which is different from the previous case. For this case, F_0 can be obtained by (29) as shown at the bottom of the page. It should be noted that, in fact, ω_n slightly depends on the change of l_d through F_0 in (28) and (29). For example, computing the first-order SI frequency by substituting the same fiber paramerters as the calculation of Fig. 3 into (28) and (29), when we reduce l_d from 40 km (l_f) to 1 km, the first-order SI frequency only moves 0.3 GHz closer to the carrier frequency. Therefore, such a small amount of frequency shift is negligible compared to the shift of SI position caused by the change of k_f.

$$|G_n| = \left| \begin{array}{c} \frac{2}{l_f}\int_0^{l_f} \gamma_1 \exp(-\alpha_1 z)\exp\left(-j\frac{(c+n)}{2}k_f z\right) dz \\ +\frac{2}{l_f}\exp(-j(c+n)\pi)\int_0^{l_f} \gamma_2 \exp(-\alpha_2 z)\exp\left(j\frac{(c-n)}{2}k_f z\right) dz \end{array} \right| \quad (26)$$

$$\begin{aligned} F_0 &= \frac{1}{l_f}\sum_{i=0}^{p-1}\left\{\int_{il_d}^{l_d/2+il_d} \gamma_1 \exp(-\alpha_1 z)\, dz + \int_{l_d/2+il_d}^{l_d+il_d} \gamma_2 \exp(-\alpha_2 z)\, dz\right\} \\ &= \sum_{i=0}^{p-1}\left\{\gamma_1\left(\frac{\exp(-\alpha_1 il_d) - \exp\left(-\alpha_1\left(\frac{l_d}{2}+il_d\right)\right)}{\alpha_1 l_f}\right) + \gamma_2\left(\frac{\exp\left(-\alpha_2\left(\frac{l_d}{2}+il_d\right)\right) - \exp(-\alpha_2(l_d+il_d))}{\alpha_2 l_f}\right)\right\}. \end{aligned} \quad (29)$$

G_n, for this case, can be analytically obtained through the series of Fourier integration

$$G_n = \frac{1}{l_f}\sum_{i=0}^{p-1}\int_{il_d}^{l_d/2+il_d} \gamma_1 \exp(-\alpha_1 z) \cdot \exp\left(-j\beta_{2\text{fl}}\omega^2 z\right)\exp(-jk_f n z)\,dz + \frac{1}{l_f}\sum_{i=0}^{p-1}\int_{l_d/2+il_d}^{l_d+il_d} \gamma_2 \exp(-\alpha_2 z) \cdot \exp\left(-j\beta_{2\text{fl}}\omega^2 (l_d - z)\right)\exp(-jk_f n z)\,dz. \quad (30)$$

As $\exp\left(-j\beta_{2\text{fl}}\omega^2 z\right)$ in $g(z)$ repeats periodically p times over each l_f

$$\begin{aligned}\exp\left(-j\beta_{2\text{fl}}\omega^2 i l_d\right) &= 1\\ \exp\left(-j\beta_{2\text{fl}}\omega^2\left(\frac{l_d}{2}+il_d\right)\right) &= \exp\left(-j\beta_{2\text{fl}}\omega^2\frac{l_d}{2}\right)\\ \exp\left(-j\beta_{2\text{fl}}\omega^2\left(l_d-\left(\frac{l_d}{2}+il_d\right)\right)\right) &= \exp\left(-j\beta_{2\text{fl}}\omega^2\frac{l_d}{2}\right)\\ \exp\left(-j\beta_{2\text{fl}}\omega^2\left(l_d-(l_d+il_d)\right)\right) &= 1. \end{aligned} \quad (31)$$

Carrying out the integration in (30) by the assistance of (31) gives (32) as shown at the bottom of the page.

Fig. 4 shows the relations between the $n = 1, 2$, and 3-order SI gains and D at resonance frequency ω_n. All parameters used in Fig. 4 are the same as the plot in Fig. 3 except that l_d is set equal to l_f at 40 km. The gain characteristics in Fig. 4 are similar in shape to Fig. 3 where the gain decreases and periodically reduces to minimum points with the increase in D.

A similar characteristic is also obtained for the case of $l_d < l_f$, as shown in Fig. 5, where l_d is reduced to 10 km. However, in order to achieve a magnitude of SI gain as low as in the above two cases, relatively large D is required.

One interesting thing observed from Figs. 3 ($l_d > l_f$), 4 ($l_d = l_f$), and 5 ($l_d < l_f$) is that the gain characteristic in Fig. 3 is symmetrical with respect to $D = 0$ while those of Figs. 4 and 5 are not symmetrical. This can be explained as follows. As described above, when the sign of D is reversed, the order of the fiber installation is changed from fiber #1, fiber #2 to fiber #2, fiber #1. For the case of Figs. 4 and 5, at least two pieces of fibers are used for constructing the transmission line between two amplifiers. This means that the fiber that locates at the output of amplifier where the signal power is still high is replaced with the other fiber, which has different α, different γ, and different sign of D. Therefore, the gain characteristics in Figs. 4 and 5 become asymmetrical when the order of the two fibers is changed. On the other hand, for the case of Fig. 3, only one fiber is installed

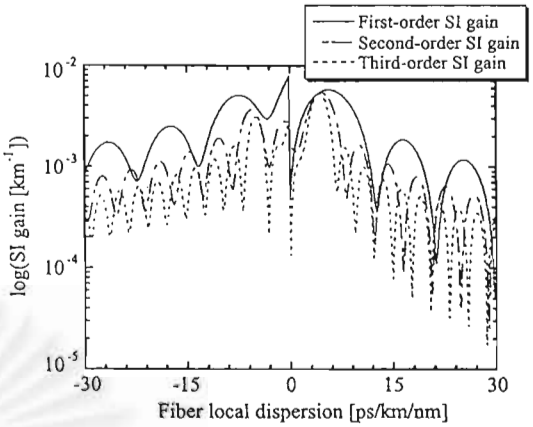

Fig. 4. Relations between the $n = 1, 2$, and 3-order SI gain peaks and D at resonance frequency ω_n. All parameters used in this figure are the same as the plot in Fig. 3 except that l_d is set equal to l_f at 40 km. The SI gain characteristics for all three orders are similar to Fig. 3 where the gain decreases and periodically reduces to minimum points with the increase in D.

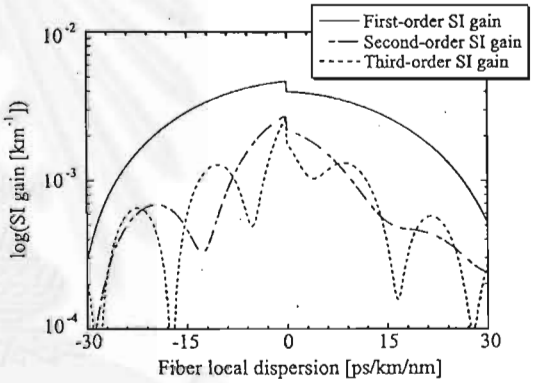

Fig. 5. Theoretical $n = 1, 2$, and 3-order SI gain peaks at resonance frequency ω_n as a function of D when l_d is set at 10 km and l_f is still 40 km. Other parameters are the same as used for Fig. 3. All three orders are similar to Figs. 3 and 4 where the gain decreases and periodically reduces to minimum points with the increase in D. However, in order to achieve a magnitude of SI gain as low as in the above two cases, relatively large D is required.

over the entire length of one amplifier spacing. Therefore, the arrangement of the two fibers will not result in any differences in the gain characteristic.

Quantitatively, $|G_n|$ calculated from (25) by replacing α_1 and γ_1 with α_2 and γ_2 and replacing α_2, γ_2, and $\beta_{2\text{fl}}$ with α_1, γ_1, and $-\beta_{2\text{fl}}$ is equivalent to that obtained directly from (25). On the other hand, the replacement of $\alpha_1, \gamma_1, \beta_{2\text{fl}}$ with $\alpha_2, \gamma_2, -\beta_{2\text{fl}}$ in (32) yields different $|G_n|$ compared to $|G_n|$ obtained directly

$$G_n = \gamma_1\left\{\frac{1-\exp\left(-\alpha_1\frac{l_d}{2}\right)\exp\left(-j\left(\beta_{2\text{fl}}\omega^2+k_f n\right)\frac{l_d}{2}\right)}{\alpha_1 l_f + j\left(\beta_{2\text{fl}}\omega^2+k_f n\right)l_f}\right\}\sum_{i=0}^{p-1}\exp(-\alpha_1 i l_d)\exp(-jk_f n i l_d) + \gamma_2\left\{\frac{\exp\left(-\alpha_2\frac{l_d}{2}\right)\exp\left(j\left(\beta_{2\text{fl}}\omega^2-k_f n\right)\frac{l_d}{2}\right)-\exp(-\alpha_2 l_d)\exp(-jk_f n l_d)}{\alpha_2 l_f - j\left(\beta_{2\text{fl}}\omega^2-k_f n\right)l_f}\right\}\sum_{i=0}^{p-1}\exp(-\alpha_2 i l_d)\exp(-jk_f n i l_d) \quad (32)$$

from (32) without the replacement. Furthermore, for the case of $l_d \leq l_f$, even both fiber #1 and fiber #2 possess equivalent values of α and γ, when the order of the two fibers is reversed. Only the difference in the sign of D leads to the different magnitude of SI gain since the power variation on each fiber is not the same.

It should be emphasized that in this paper, we focus only on the higher order dispersion-managed transmission line consisting of SMF and RDF. Since SMF and RDF possess almost equivalent absolute values of SOD and TOD with opposite signs, our analysis model shown in Fig. 2 is well matched with the practical transmission line composed of SMF and RDF. However, it is still worth studying SI induced from the dispersion-managed line, which consists of fibers with different lengths and different amount of dispersion shifted from the average dispersion value.

Fig. 6(a) shows the model of the dispersion-managed fiber link composed of fiber #1 and fiber #2, whose lengths are unequal. The most practical case where $l_d = l_f$ is considered. In Fig. 6(a), x is the length of fiber #1 and $l_f - x$ is the length of fiber #2. D_1 and D_2, respectively, denote the local dispersion of fiber #1 and fiber #2 shifted from the average dispersion D_{av}. To make the accumulated dispersion vanish at each l_d, D_2 can be written as the function of D_1 and x as

$$D_2 = -\frac{D_1 x}{l_f - x}. \tag{33}$$

Following the above derivation for the case $l_d - l_f$, we found that SI also occurs at the frequency determined by (28) but, for this case, F_0 is obtained as

$$\begin{aligned} F_0 =& \frac{1}{l_f}\left\{\int_0^x \gamma_1 \exp(-\alpha_1 z)\,dz + \int_x^{l_f} \gamma_2 \exp(-\alpha_2 z)\,dz\right\} \\ =& \gamma_1\left(\frac{1-\exp(-\alpha_1 x)}{\alpha_1 l_f}\right) \\ &+ \gamma_2\left(\frac{\exp(-\alpha_2 x) - \exp(-\alpha_2 l_f)}{\alpha_2 l_f}\right). \end{aligned} \tag{34}$$

On the other hand, $|G_n|$ can be obtained as

$$\begin{aligned} G_n =& \frac{1}{l_f}\int_0^x \gamma_1 \exp(-\alpha_1 z)\exp\left(-j\beta_{21}\omega^2 z\right) \\ &\cdot \exp(-jk_f n z)\,dz \\ &+ \frac{1}{l_f}\int_x^{l_f} \gamma_2 \exp(-\alpha_2 z) \\ &\cdot \exp\left(-j\omega^2\{(\beta_{21}-\beta_{22})x + \beta_{22} z\}\right) \\ &\cdot \exp(-jk_f n z)\,dz \end{aligned} \tag{35}$$

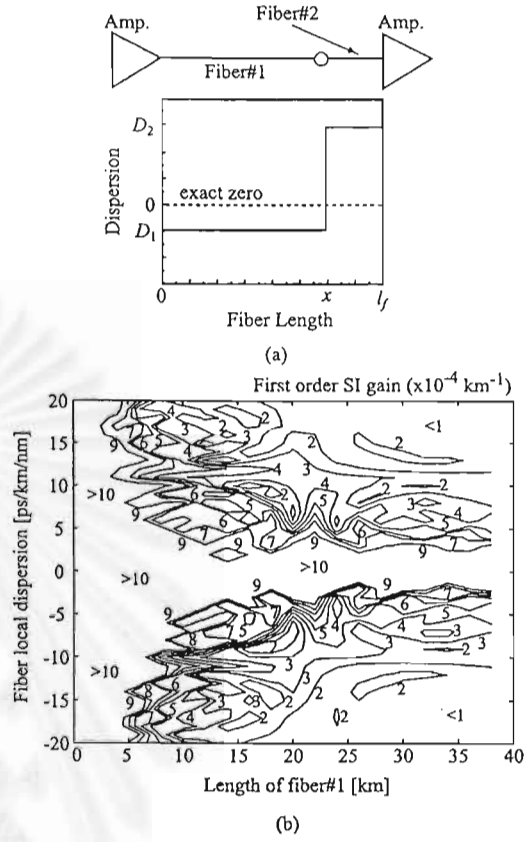

Fig. 6. Model of dispersion-managed transmission line and its corresponding SI gain contour map. (a) shows the model of dispersion-managed transmission line composed of fiber #1 and fiber #2, whose lengths are unequal. (b) shows the contour map of the first-order SI gain peak as function of D_1 and x. The gain map indicates that the use of fiber #1, which has large local dispersion with relatively long length, can significantly reduce the SI gain.

where β_{21} and β_{22} are local GVD parameters of fiber #1 and fiber #2, respectively. Completing the integrations in (35) by using (6) and (33), we have (36), shown at the bottom of the page.

Assuming that both fiber #1 and fiber #2 exhibit equivalent α and γ, then G_n depends on D_1 and x. To see the variation of SI gain with the change of both D_1 and x, the gain contour map should be used. Fig. 6(b) shows the contour map of the first-order SI gain peak as a function of D_1 and x. To obtain Fig. 6(b), $D_{\text{av}} = -0.5$ ps/km/nm, $\alpha = 0.2$ dB/km, $\gamma = 2.6$ W^{-1}km^{-1}, and $l_d = l_f = 40$ km are used. The gain map in Fig. 6(b)

$$\begin{aligned} G_n =& \gamma_1\left\{\frac{1-\exp(-\alpha_1 x)\exp\left(-j\left(\beta_{21}\omega^2 + k_f n\right)x\right)}{\alpha_1 l_f + j\left(\beta_{21}\omega^2 + k_f n\right) l_f}\right\} \\ &+ \gamma_2 \exp\left(-j\omega^2\left(\frac{\beta_{21} l_f}{l_f - x}\right)x\right) \\ &\cdot\left\{\frac{\exp(-\alpha_2 x)\exp\left(j\left(\omega^2\left(\frac{\beta_{21}x}{l_f-x}\right) - k_f n\right)x\right) - \exp(-\alpha_2 l_f)\exp\left(j\left(\omega^2\left(\frac{\beta_{21}x}{l_f-x}\right) - k_f n\right) l_f\right)}{\alpha_2 l_f - j\left(\omega^2\left(\frac{\beta_{21}x}{l_f-x}\right) - k_f n\right) l_f}\right\} \end{aligned} \tag{36}$$

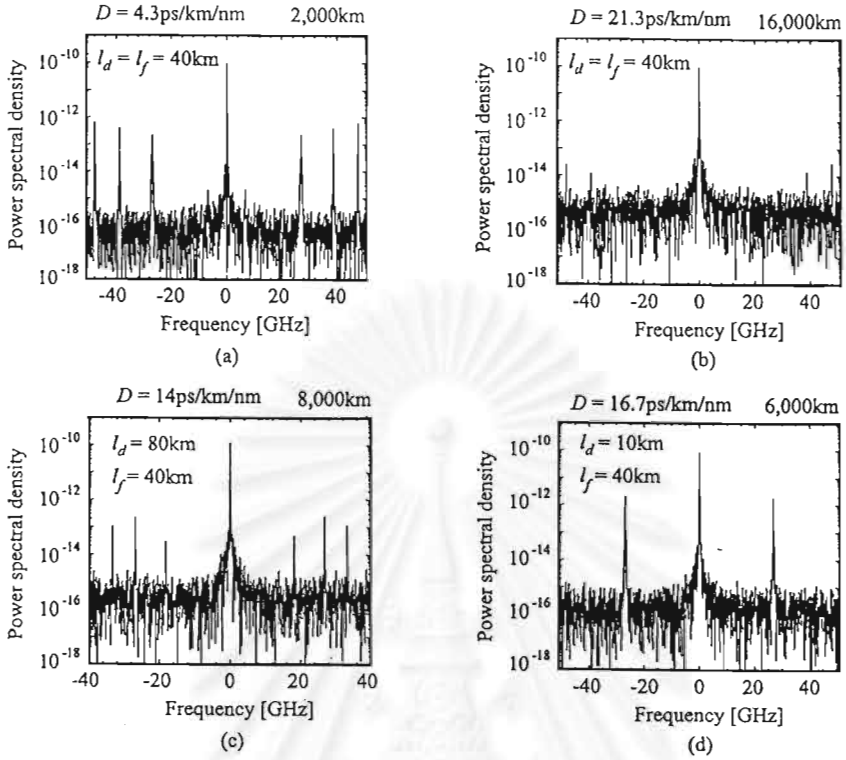

Fig. 7. Numerical simulation results show the spectrum of optical CW signal and ASE noise transmitted in dispersion-management transmission line using SMF and RDF with periodic signal amplification. (a) 2000-km-transmitted CW spectrum for $l_d = l_f = 40$ km with $D = 4.3$ ps/km/nm. (b) 16 000-km-transmitted CW spectrum for $l_d = l_f = 40$ km with $D = 21.3$ ps/km/nm. (c) 8000-km-transmitted CW spectrum for $l_f = 40$ km, $l_d = 80$ km with $D = 14$ ps/km/nm. (d) 6000-km-transmitted CW spectrum for $l_f = 40$ km, $l_d = 10$ km with $D = 16.7$ ps/km/nm. All simulation results, for both SI gain and SI frequency, are in a good agreement with the theoretical gain shown in Figs. 3–5.

indicates that the use of fiber #1 that has large local dispersion with relatively long length can significantly reduce the SI gain. Quantitatively, the length of fiber #1 should be longer than 10 km and the local dispersion $|D_1|$, which can be both normal and anomalous dispersion, should be larger than 5 ps/km/nm to assure a first-order SI gain smaller than 10^{-3} km^{-1}.

For all cases, it should be noted that when D_{av} is set in an anomalous dispersion region, the modulation instability (MI), which can be interpreted as the zero-order SI, occurs and is only slightly reduced by relatively large D.

Recently, the fabrication of optical fiber with designed dispersion value has been realized [25]. This enables us to construct a dispersion-managed transmission fiber with appropriate value of dispersion in order to suppress SI effect for a given system.

III. Computer Simulations

To confirm the validity of the proposed theory, we have performed some numerical simulations using a continuous-wave (CW) signal and amplified spontaneous emission (ASE) noise as a sideband frequency source. It should be noted that the CW is used for the convenience of observing the gain and the position of SI. The main parameters used in the simulations are the same as those used in Figs. 3–5. The TODs of fiber #1 and fiber #2 are set at 0.06 and -0.06 ps/km/nm^2, respectively. Since the two fibers have equal length, the accumulated TOD is canceled at each dispersion compensation interval. At the output of each amplifier, the ASE noise is added to the signal through the process of amplification with noise figure of 5.3 dB (n_{sp}=1.7). The propagation of the optical signal is calculated by solving the nonlinear Schrodinger equation by the split-step Fourier method [1].

The results of the numerical simulations for several cases in terms of transmitted optical spectrum are shown in Fig. 7. The transmitted CW spectrum for $l_d = l_f = 40$ km with $D = 4.3$ and 21.3 ps/km/nm are shown in Fig. 7(a) and (b), respectively. Fig. 7(c) and (d) shows the results for the case $l_d > l_f$ with $D = 14$ ps/km/nm and $l_d < l_f$ with $D = 16.7$ ps/km/nm, respectively. According to Fig. 4, at $D = 4.3$ ps/km/nm, the first-, second-, and third-order SI all exhibit high gain with almost the same value. However, at $D = 21.3$ ps/km/nm, all three orders of SI appear at minimum value.

As expected, in all figures, the computer simulation results of both SI gain and SI frequency are in a good agreement with the theoretical gain shown in Figs. 3–5 together with (19) and (28), confirming the accuracy of our analytical derivation. For high SI gain as in Fig. 7(a), SI arises obviously even in relatively short transmission length (2000 km). On the other hand, in order to observe SI for large D, a transmission distance as long as 16 000 km is required to serve the gain as shown in Fig. 7(b), 8000 km in Fig. 7(c), and 6000 km in Fig. 7(d). This informs us that strong dispersion-management fiber using the combination of SMF and RDF can be used to suppress SI.

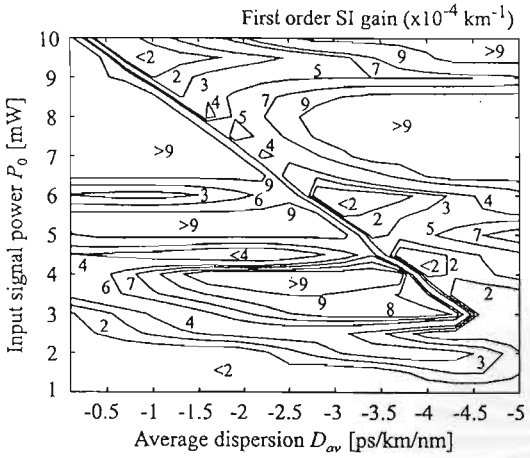

Fig. 8. Gain contour map of the first order of SI concerning the dispersion-managed transmission line consisting of SMF and RDF for $l_d = l_f = 40$ km and $|D| = 17$ ps/km/nm with positive sign for the SMF and minus sign for the RDF.

When l_d is determined, then, it is helpful to use an SI gain contour map to design the operating $D_{\rm av}$ and P_o at the point where the SI gain becomes as low as possible. If we consider a practical case when $l_d = l_f$, assuming that the local SOD is fixed at a given value, the magnitude of SI gain now only depends on P_o and $D_{\rm av}$. Fig. 8 shows the gain contour map of the first order of SI concerning the dispersion-managed transmission line using the combination of SMF and RDF. It should be noted that we should concentrate on the first-order SI because, practically, the low order of SI is easier to phase-match and causes more serious problems in the long-haul transmission than other high orders. The SMF and RDF parameters used for the calculation are the same as those used for fiber #1 and fiber #2, respectively. In the contour map, $|D|$ is assumed to be 17 ps/km/nm with positive sign for the SMF and minus sign for the RDF.

In Fig. 8, for low P_0, which is referred to relatively short transmission, SI possesses relatively low gain over a wide range of $D_{\rm av}$. For high power transmission, using low $D_{\rm av}$ can avoid the SI gain and, at the same time, move the SI position out of the signal carrier. However, at some points of P_0, the SI gain exhibits large value even at very low $D_{\rm av}$—for example, SI gain as high as 9×10^{-4} km^{-1} arises from $P_0 = 5$ mW at $D_{\rm av} = -0.5$ ps/km/nm. To achieve the maximum performance of the system, these operating points should be avoided. It should be noted that when this periodic dispersion management using SMF and RDF is not applied to the system, the first-order SI induced from only periodic amplification in dispersion-shifted fiber chain exhibits gain larger than 10^{-3} km^{-1} even when $P_0 > 2$ mW is used.

IV. Effect of SI on Long-Haul WDM Transmission Systems

In a dispersion-managed transmission system consisting of SMF and RDF, all channels experience almost the same amount of $D_{\rm av}$. Thus, each channel produces its own SI that occurs at frequency shifted from carrier frequency by the same amount of frequency shift with almost the same gain. If two different channels produce SI at the same frequency, SI will cause a serious problem for the channels whose carriers are placed just at that frequency, especially for the frequency where the first-order SI arises.

To confirm our mention, we perform computer simulations of the transmission of four-wavelength CW signal and ASE noise. In the first calculation, we focus on the case when the first-order SI gain generated from two separated channels enhances each other and positions on the other two channels. In the calculations, l_d is set equal to l_f at 40 km, and other SMF and RDF parameters are the same as those used in other calculations described above. According to the contour map in Fig. 8, to investigate the problem of SI even when the system is operating with condition that yields relatively low SI gain, we select $P_0 = 3$ mW and $D_{av} = -0.5$ ps/km/nm, which yields first-order SI gain of about 2×10^{-4} km^{-1}. Using (28) and the calculation parameters, the first-order SI will arise at ± 77.4 GHz shifted from each carrier frequency. Next, we place four channels at frequencies of -116.1, -38.7, 38.7, and 116.1 GHz shifted from the zero-dispersion wavelength 1550 nm, respectively. By this arrangement, SI produced from channel #1 and channel #3 will arise just at the position of channel #2 carrier. Similarly, SI induced from channel #2 and channel #4 will occur just at the position of channel #3.

Fig. 9(b) shows the spectrum of the four-channel CW signal transmitted over 4000 km compared with its initial shape shown in Fig. 9(a). By this channel allocation, the serious distortion of CW spectrum is clearly observed. To avoid this problem, it is necessary to arrange the channel allocation in such a way that none of the channel is placed on the SI frequency. Fig. 9(c) and (d), respectively, shows the initial four-channel CW signal spectrum and its shape after 4000-km transmission simulated by the same parameters as Fig. 9(b). The channel spacing in this calculation is decreased 10 GHz, resulting in the shift of SI frequency out of signal bandwidth. In contrast to Fig. 9(b), where the SI occurs just at the channel position, the output spectrum in Fig. 9(d) has less distortion than Fig. 9(b) when compared with its input shape, confirming the achievement of avoiding the effect of SI. In fact, as FWM among channels is easy to phase-match when the channel spacing becomes smaller [1], the decrease in channel spacing should have led to more signal distortion. However, the transmitted spectrum in Fig. 9(b) appears in more severe distorted shape than that of Fig. 9(d). This can be interpreted as meaning that the effect of SI plays a more significant role in determining the transmission performance than the interchannel FWM for this condition.

To explore the effect of SI on WDM transmission in more detail, we perform the calculation of the bit error rate (BER) of the four-channel WDM system using pseudorandom 32-bit Gaussian return-to-zero (RZ) pulse train as an input optical signal whose bit rate of each channel is equal to 10 Gbit/s. At the end of the system, the accumulated $D_{\rm av}$ is postcompensated by multiplying the complex amplitude of the signal with a negative amount of linearly accumulated phase shift caused by $D_{\rm av}$. We assume the use of a bandwidth-adjustable optical bandpass filter (OBPF) in front of the receiver to select the passband channel. This OBPF is also always adjusted to obtain

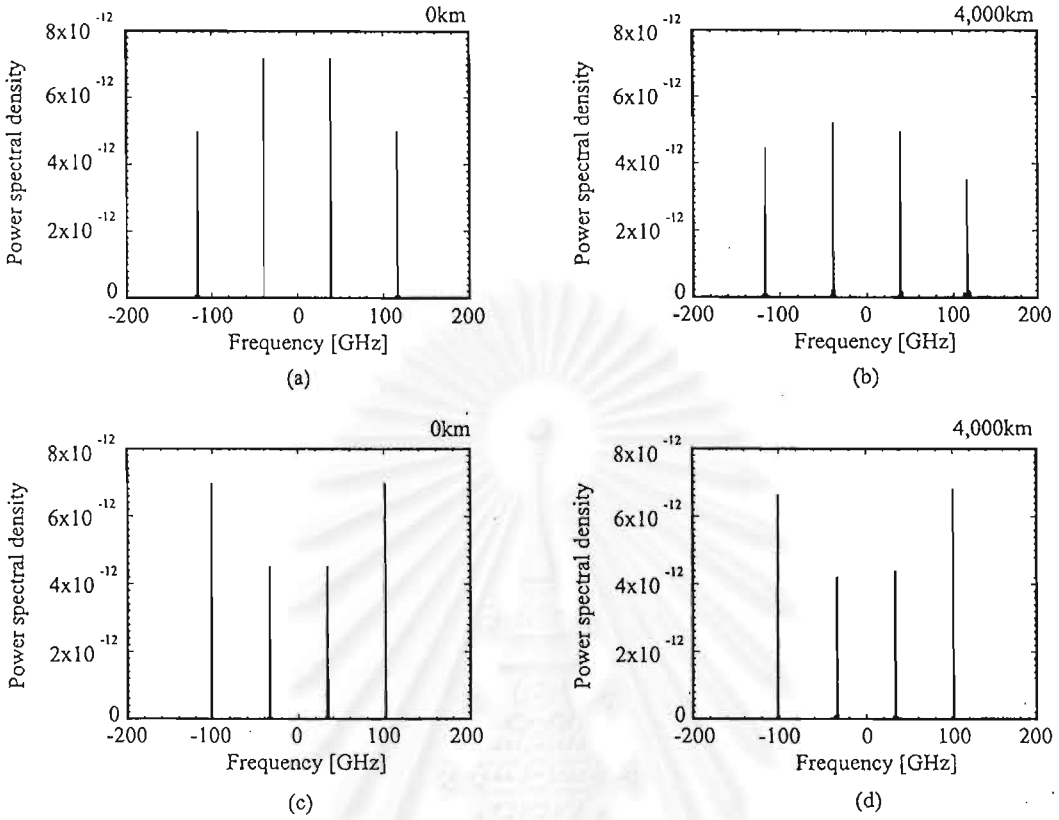

Fig. 9. Optical spectrum of four-channel CW signal shown in linear scale. l_d is set equal to l_f at 40 km, $P_0 = 3$ mW, and $D_{av} = -0.5$ ps/km/nm. In (a) and (b), the channel spacing is set at ± 77.4 GHz, where two of the first-order SIs from neighbor channels arise just at channel #2 and channel #3 carrier positions. (a) Initial shape and (b) 4000-km-transmitted spectrum. By this channel allocation, serious distortion of CW spectra is clearly observed. (c) and (d), respectively, show the initial and 4000-km-transmitted CW spectra simulated by decreasing 10 GHz to shift SI frequency out of signal bandwidth. The transmitted spectrum in (b) appears in more severe distorted shape than (d) because of SI.

minimum BER. The receiver is modeled by a 6.5-GHz-cutoff sixth-order Bessel–Thompson low-pass filter followed by BER detector. To obtain the numerical BER of the detected signal, the simulation is repeated 128 times for the same pseudorandom pulse train. The numerical Q factor of every bit is then individually calculated at the maximum eye-opening point of the bit period. Based on the assumption of Gaussian noise distribution, the numerical BERs are computed from the bit numerical Q factors and averaged over the entire bits [7].

Fig. 10(a) and (b), respectively, shows the calculated BER curves of channel #2 and channel #3 as a function of transmission distance simulated by $P_0 = 3$ mW and $D_{av} = -0.5$ ps/km/nm with different channel spacing setting. The BER curves obtained from the system whose signal carriers are placed on the position where the SI arises (shown by circles) drop more rapidly than those obtained from 10-GHz-decreased channel spacing (shown by squares). If we defined the maximum transmission distance obtained at the distance where the BER reaches 10^{-9} as shown by the dotted line, the systems where the channel allocation is arranged to avoid the position of SI yield significantly longer transmission length. We also simulated the system with $P_0 = 5$ mW and $D_{av} = -0.5$ ps/km/nm that yields high SI gain. The result showed more severe degradation of BER for channel carriers positioned just on SI frequency and, on the contrary, an obvious improvement when a channel allocation is done to avoid the SI frequency. This confirms the necessity of avoiding SI in higher order dispersion-management long-haul WDM transmission systems.

V. Conclusion

In this paper, we have presented the derivation of the analytical expression of the SI induced from periodic signal power variation and periodic dispersion management when two different fibers are connected together to form the dispersion compensation link. Three possible dispersion-management systems were considered: a) where dispersion-management period is larger than amplifier spacing, (b) where the two lengths are equal, and (c) where amplifier spacing is larger than dispersion-management period.

We found that SI frequency depends on the larger period between the amplifier spacing and the dispersion-management period. The larger the variation period becomes, the closer the SI frequency will arise to carrier frequency. Moreover, the gain of SI appears to be reduced with the increase of local fiber second-order dispersion. This is because the increase in the local SOD virtually shifts the order of SI to higher order, resulting in the difficulty of phase-match process. The computer simulations

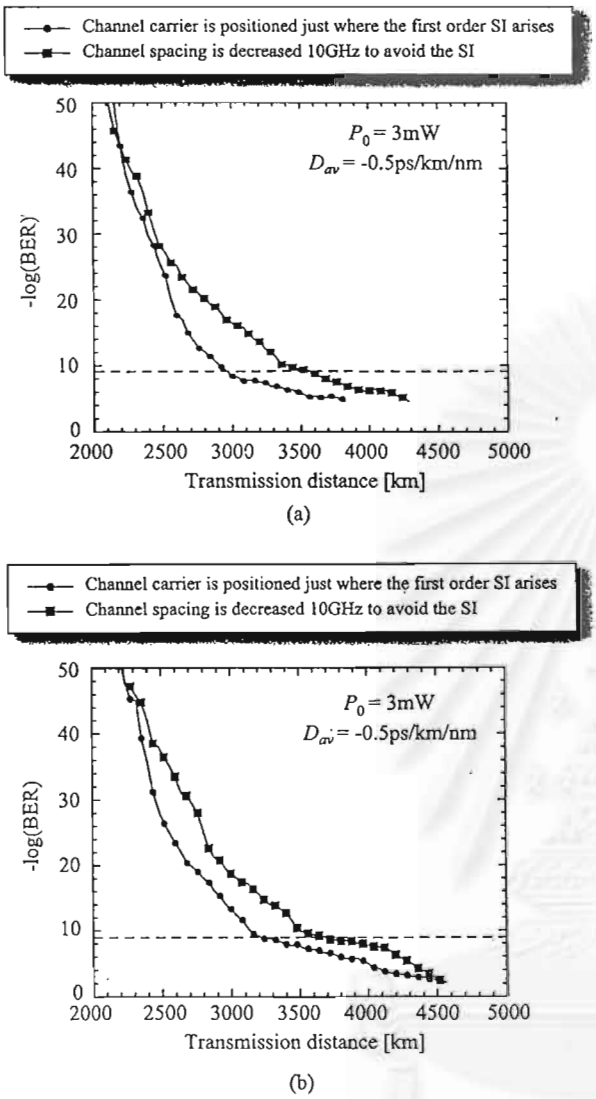

Fig. 10. BER as a function of transmission distance calculated from the (4 × 10)-Gbit/s 32-bit RZ signal for different channel spacings. (a) and (b) show BER curves of channel #2 and channel #3, respectively. In both (a) and (b), circles show BER obtained from the system whose signal carriers are placed on the position where the SI arises while squares show BER obtained from 10-GHz-decreasing channel spacing. At BER = 10^{-9} (shown by an across dotted line), the systems where the channel allocation is rearranged to avoid the position of SI give significantly longer transmission length.

were made, and their results were in good agreement with the derived theory.

In WDM systems that use relatively narrow channel spacing, we demonstrated that even when the dispersion map is properly designed to achieve low SI gain, SI causes signal distortion to specific channels that fall just on the low-order SI frequency, especially the first order. Additionally to WDM system design rules, the channel allocation must avoid the SI position in such a way that none of the channel should be lied at. The computer simulations have confirmed that the BER of WDM systems whose channel location is rearranged to avoid SI gives a significant improvement in the transmission performance.

REFERENCES

[1] G. P. Agrawal, *Nonlinear Fiber Optics*. New York: Academic Press, 1993.

[2] R. W. Tkach, A. R. Chaplyvy, F. Forghieri, A. H. Gnauck, and R. M. Derosier, "Four-photon mixing and high-speed WDM systems," *J. Lightwave Technol.*, vol. 13, pp. 841–849, 1995.

[3] N. Kikuchi, K. Sekine, and S. Sasaki, "Analysis of cross-phase modulation (XPM) effect on wdm transmission performance," *Electron. Lett.*, vol. 33, pp. 653–654, 1997.

[4] D. Marcuse, "Single-channel operation in very long nonlinear fibers with optical amplifiers at zero dispersion," *J. Lightwave Technol.*, vol. 9, pp. 356–361, 1991.

[5] N. Kikuchi and S. Sasaki, "Fiber nonlinearity in dispersion-compensated conventional fiber transmission," *Electron. Lett.*, vol. 32, pp. 570–572, 1996.

[6] R. J. Nuyts, Y. K. Park, and P. Gallion, "Dispersion equalization of a 10 Gbit/s repeatered transmission system using dispersion compensating fibers," *J. Lightwave Technol.*, vol. 15, pp. 31–41, 1997.

[7] X. Wang, K. Kikuchi, and Y. Takushima, "Analysis of dispersion-managed optical fiber transmission system using nonreturn-to-zero pulse format and performance restriction from third-order dispersion," *IEICE Trans. Electron.*, vol. E82-C, no. 8, pp. 1407–1413, 1999.

[8] M. Murakami, T. Matsuda, H. Maeda, and T. Imai, "Long-haul WDM transmission using higher order fiber dispersion management," *J. Lightwave Technol.*, vol. 18, no. 9, pp. 1197–1204, 2000.

[9] M. Murakami, K. Suzuki, H. Maeda, T. Takahashi, A. Naka, N. Ohkawa, and M. Aiki, "High speed TDM-WDM techniques for long-haul submarine optical amplifier systems," *Opt. Fiber Technol.*, vol. 3, no. 4, pp. 320–338, 1997.

[10] N. S. Bergano, C. R. Davidson, M. A. Mills, P. C. Corbett, R. Menges, J. L. Zyskind, J. W. Shulhoff, A. K. Srivastava, and C. Wolf, "Long-haul transmission using 10 Gb/s channels: 160 Gb/s(16 × 10 Gb/s) 6000 km demonstration," presented at the Proc. OAA'97, Postdeadline paper PD-9.

[11] M. Morimoto, I. Kobayashi, H. Hiramatsu, K. Mukasa, R. Sugizaki, Y. Suzuki, and Y. Kamikura, "Development of dispersion compensation cable using reverse dispersion fiber," in *Proc. 5th Asia-Pacific Conf. Communications 1999 and 4th Optoelectronics and Communications Conf. (APCC/OECC '99)*, vol. 2, 1999, pp. 1590–1593.

[12] M. Kazunori and T. Yagi, "Dispersion flat and low nonlinear optical link with new type of reverse dispersion fiber (RDF-60)," in *Proc. Opt. Fiber Commun. (OFC2001)*, Anaheim, CA, Mar. 17–22, 2001, paper TuH7.

[13] T. Naito, N. Shimojoh, T. Tanaka, H. Nakamoto, M. Doi, T. Ueki, and M. Suyama, "1 Terabit/s WDM transmission over 10 000 km," in *Proc. Eur. Conf. Opt. Commun. (ECOC'99)*, vol. PD2-1, Nice, France, Sept. 26–30, 1999, pp. 24–25.

[14] F. M. Madani and K. Kikuchi, "Design theory of long-distance WDM dispersion-managed transmission system," *J. Lightwave Technol.*, vol. 17, pp. 1326–1335, 1999.

[15] K. Tanaka, T. Tsuritani, N. Edagawa, and M. Suzuki, "320 Gbit/s (32 × 10.7 Gbit/s) error-free transmission over 7,280 km using dispersion flattened fiber link with standard SMF and slope compensating DCF," in *Proc. ECOC'1999*, Nice, France, Sept. 26–30, 1999, pp. II-180–II-181.

[16] T. Tsuritani, N. Takeda, K. Imai, K. Tanaka, A. Agata, I. Morita, H. Yamauchi, N. Edagawa, and M. Suzuki, "1 Tbit/s (100 × 10.7 Gbit/s) transoceanic transmission using 30 nm-wide broadband optical repeaters with A_{eff}-enlarged positive dispersion fiber and slope-compensating DCF," in *Proc. Eur. Conf. Opt. Commun. (ECOC'99)*, vol. PD2-1, Nice, France, Sept. 26–30, 1999, pp. 38–39.

[17] H. Nakamoto, T. Tanaka, N. Shimojoh, T. Naito, I. Yokota, A. Sugiyama, T. Ueki, and M. Suyama, "1.05 Tbit/s WDM transmission over 8,186 km using distributed Raman amplifier repeaters," in *Proc. Opt. Fiber Commun. (OFC2001)*, Anaheim, CA, Mar. 17–22, 2001, paper TuF6.

[18] E Shibano, S. Nakagawa, T. Kawazawa, H. Taga, and K. Goto, "96 × 11.4 Gbit/s transmission over 3,800 km using C-band EDFA and nonzero dispersion shifted fiber," in *Proc. Opt. Fiber Commun. (OFC2001)*, Anaheim, CA, Mar. 17–22, 2001, paper TuN2.

[19] F. Matera, A. Mecozzi, M. Romagnoli, and M. Settembre, "Sideband instability induced by periodic power variation in long distance fiber links," *Opt. Lett.*, vol. 18, pp. 1499–1501, 1993.

[20] C. Kurtzke and K. Peterman, "Impact of fiber four-photon mixing on the design of n-channel megameter optical communication systems," in *Proc. Opt. Fiber Commun. (OFC'93)*, San Jose, CA, Feb. 21–26, 1993, paper FC3.

[21] C. Kurtzke, "Suppression of fiber nonlinearities by appropriate dispersion management," *IEEE Photon. Technol. Lett.*, vol. 5, no. 10, pp. 1250–1253, 1993.

[22] K. Kikuchi, C. Lorattanasane, F. Futami, and S. Kaneko, "Observation of quasiphase matched four-wave mixing assisted by periodic power variation in a long-distance optical amplifier chain," *IEEE Photon. Technol. Lett.*, vol. 7, no. 11, pp. 1378–1380, 1995.
[23] N. J. Smith and N. J. Doran, "Modulation instability in fibers with periodic dispersion management," *Opt. Lett.*, vol. 21, pp. 570–572, 1996.
[24] K. Pasu and A. Tuptim, "Sideband instability in the presence of periodic power variation and periodic dispersion management," in *Proc. Opt. Fiber Commun. (OFC2001)*, Anaheim, CA, Mar. 17–22, 2001, paper WDD32.
[25] T. Okano, T. Ooishi, T. Kato, Y. Yokoyama, M. Yoshida, Y. Takahashi, Y. Makio, and M. Nishimura, "Optimum dispersion of nonzero dispersion shifted fiber for high bit rate DWDM systems," in *Proc. Opt. Fiber Commun. (OFC2001)*, Anaheim, CA, Mar. 17–22, 2001, paper TuH4.

Pasu Kaewplung was born in Bangkok, Thailand, in December 1971. He received the B.S. and M.S. degrees in electrical engineering from Yokohama National University, Yokohama, Japan, in 1996 and 1998, respectively. He is currently pursuing the Ph.D. degree in electrical engineering at Chulalongkorn University, Bangkok.

From April 1998 to March 2000, he conducted research at the Research Center for Advanced Science and Technology (RCAST), University of Tokyo, Japan. In April 2000, he joined the Department of Electrical Engineering, Chulalongkorn University, as a Lecturer. His research activities have been devoted to long-distance large-capacity optical fiber transmission systems, dispersion compensations, and the applications of nonlinear optical effects.

Tuptim Angkaew (S'81–M'92) was born in Bangkok, Thailand, in 1961. She received the B.Eng. degree in electrical engineering from King Mongkut's Institute of Technology Ladkrabang, Thailand, in 1984. She received the master's and doctoral degrees in electrical communication engineering from Osaka University, Osaka, Japan, in 1987 and 1990, respectively.

In 1990, she joined the Department of Electrical Engineering, Chulalongkorn University, Bangkok, as a Lecturer. She is currently an Assistant Professor there. She has been engaged in research on computational electromagnetics, finite-element analysis, and analysis of optical components in optical communication systems.

Kazuro Kikuchi (M'90) was born in Miyagi Prefecture, Japan, on March 6, 1952. He received the B.S. degree in electrical engineering in 1974 and the M.S. and Ph.D. degrees in electronic engineering from the University of Tokyo, Tokyo, Japan, in 1976 and 1979, respectively.

In 1979, he joined the Department of Electronic Engineering at the University of Tokyo. In 1997, he moved to the Research Center for Advanced Science and Techonology (RCAST) at the same university. From April 1986 to March 1987, he was on leave of absence from the University of Tokyo with Bell Communications Research (Bellcore), NJ. Since 1979, his work has focused on the optical communication system. He is currently involved in ultrafast optical devices and their system applications.

Dr. Kikuchi is a Member of the Optical Society of America and the Institute of Electronics, Information and Communication Engineers (IEICE) of Japan.

การประชุมวิชาการ
ทางวิศวกรรมไฟฟ้า ครั้งที่ 25

25th Electrical Engineering Conference

(EECON - 25)

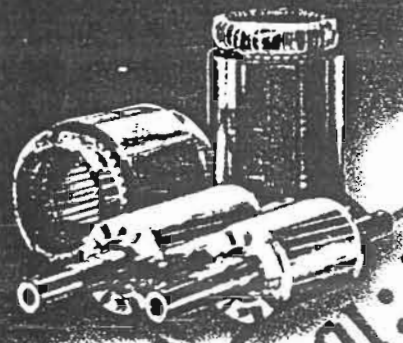

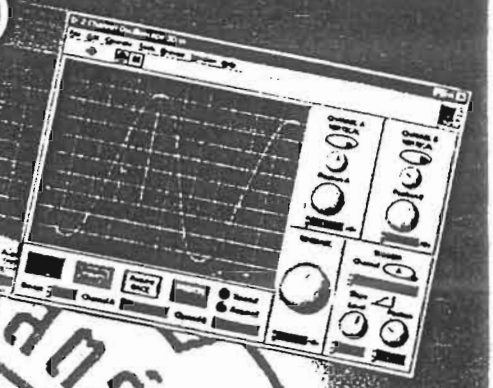

21-22 พฤศจิกายน 2545

ณ ภาควิชาวิศวกรรมไฟฟ้า คณะวิศวกรรมศาสตร์
มหาวิทยาลัยสงขลานครินทร์

สาขาบทความ

- ไฟฟ้าสื่อสาร (CM)
- อิเล็กทรอนิกส์ (EL)
- ประมวลผลสัญญาณดิจิตอล (DS)
- วิศวกรรมคอมพิวเตอร์และเทคโนโลยีสารสนเทศ (CP)
- งานวิจัยที่เกี่ยวข้องกับวิศวกรรมไฟฟ้า (GN)

ดำเนินการจัดการประชุมโดย
ภาควิชาวิศวกรรมไฟฟ้า คณะวิศวกรรมศาสตร์
มหาวิทยาลัยสงขลานครินทร์

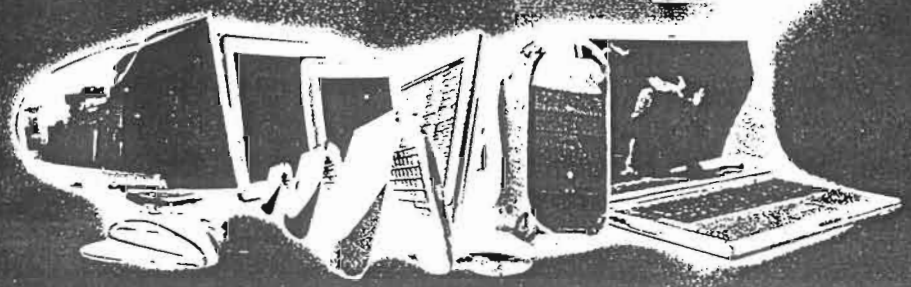

กลับไปสารบัญหลัก

บทความดีเด่น

สารบัญ

สาขาไฟฟ้าสื่อสาร

Effect of Sideband Instability on Long-haul DWDM Optical Fiber Transmission Systems Employing Higher-Order Dispersion Management

Pasu Kaewplung[1], Tuptim Angkaew[1], and Kazuro Kikuchi[2]
1. Department of Electrical Engineering, Faculty of Engineering, Chulalongkorn University,
Phayathai Rd., Pathumwan, Bangkok 10330, Thailand
Phone (66-2)218-6907, Fax (66-2)218-6912, E-mail : pasu@ee.eng.chula.ac.th
2. Research Center for Advanced Science and Technology (RCAST), University of Tokyo,
Komaba, Meguro-ku, Tokyo, 153-8904, JAPAN
Phone: (81-3)5452-5123, Fax: (81-3)5452-5125, E-mail : kikuchi@ginjo.rcast.u-tokyo.ac.jp

Abstract

We present for the first time an analytical expression of sideband instability (SI) that occurs when two kinds of fibers with different characteristics are concatenated to form a dispersion-managed fiber link. We focus on the fiber link using the combination of standard single-mode fiber (SMF) and reverse dispersion fiber (RDF), which is widely used for simultaneously compensating second-order dispersion (SOD) and third-order dispersion (TOD). By computer simulation, it is shown that, in dense-wavelength-division-multiplexed (DWDM) systems, SI still induces significant degradation in channels located at frequencies where SI induced from other channels arises. By re-allocating the channel frequency to avoid the SI frequency, the transmission performance is improved significantly.

Keywords: optical fiber transmission, wavelength division multiplexing, fiber nonlinearity, four-wave mixing, sideband instability, dispersion, third-order dispersion, dispersion management.

1. Introduction

Second-order dispersion (SOD) management method has been proposed and demonstrated for reducing four-wave mixing (FWM) and cross-phase modulation (XPM) effect in wavelength-division multiplexed (WDM) systems [1], [2]. However, such an approach can manage only SOD in only one channel. Therefore, in WDM systems, signal channels far from the average zero-dispersion wavelength experience different amount of dispersion accumulation along the entire system length because of the existence of the dispersion slope or third-order dispersion (TOD) [3].

It has been predicted that the existence of the third-order dispersion (TOD) of optical fibers limits the available passband of the WDM systems with the data rates of over 10Gbit/s [4]. For further expansion both in capacity and distance, dispersion management to eliminate both SOD and TOD will be one of the key issues. For this purpose, the special dispersion compensating fibers called reverse dispersion fiber (RDF) [5], [6] has been proposed and demonstrated its potential. Since RDF exhibits low negative TOD with large negative SOD, we can achieve the dispersion flattened fiber link with low average SOD by combining RDF with standard single-mode fiber (SMF) in each compensation interval. The use of such higher-order dispersion compensation fiber link in combination with the optimization of channel spacing realizes the simultaneously reduction of FWM, XPM, and TOD. Transmission experiment shows that using the combination of SMF and RDF can achieve the data rate as high as 1Tbit/s (104channels x 10Gbit/s) WDM transmission over 10,000km [7].

In this paper, we demonstrate that the additional signal distortion to long-haul higher-order-dispersion-managed WDM systems can occur via the quasi FWM phase-match process assisted by periodic variation of the signal power in the chain of lossy fiber intervals and lumped amplifiers incorporated with periodic dispersion management. This parametric process, which occurs in both normal and anomalous dispersion region, is called sideband instability (SI) [8]-[11]. Through this process, signal carrier transfers its energy to specific sideband frequencies which grow up exponentially with transmission distance.

This paper is organized as follows. In section 2, the complete analytical expression of SI focusing on the case when two different characteristic fibers connected together has been shown for the first time following our derivation approach described in [11]. In our analytical expression, not only the periodic power variation but the periodic dispersion management, periodic fiber loss coefficient variation, and periodic nonlinear coefficient variation are also included. In section 3, we focus on dispersion managed transmission system consisting of SMF and RDF. Our computer simulation results show that, when two or more channels produce SI at the same frequency, SI significantly causes a serious problem to the channel whose carrier is positioned just at that superposition resonance frequency. We also demonstrate that, by re-arranging the channel position or channel spacing in such a way that none of the SI resonance frequency falls inside the channel signal bandwidth, the transmission performance is significantly improved. Finally, the summary of this paper is made at section 4.

2. Analytic expressions of SI frequencies and gains induced by periodic dispersion management fiber link

In long haul and high-capacity fiber transmission systems, the power of the optical signal must be kept high in order to obtain good signal-to-noise ratio (SNR) at a receiver. In such high power systems, by amplification process, the periodic power variation

produces a periodic variation of fiber refractive index through the nonlinear Kerr effect of an optical fiber. By this process, it seems like a grating is virtually constructed in the transmission fiber. A resonance between the virtual grating and the signal will occur at the signal sideband component whose wave vector matches the wave vector of this virtual grating resulting in exponential growth of that component with transmission length. This phenomenon is known as the sideband instability (SI) [8], which causes signal waveform distortion if SI arises at frequency inside the signal bandwidth since it cannot be eliminated by using optical bandpass filter.

The models of dispersion management transmission line used in this paper is illustrated in Fig. 1. As we aim to concentrate to dispersion managed transmission system consisting of SMF and RDF, the fiber link is composed of two different characteristic fibers with the same length. Therefore, the dispersion profile is the simplest type where the dispersion varies every half of period with the same amount plus and minus around a given average dispersion value. Each fiber has its own nonlinear coefficient and the fiber loss, which is assumed periodic by the period equivalent to the dispersion management period.

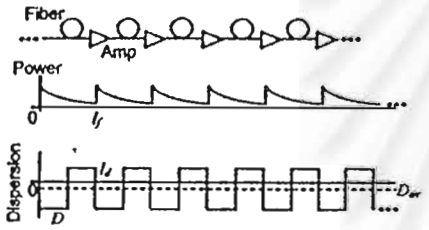

Fig. 1: Dispersion management transmission line model. The fiber link is composed of two different characteristic fibers but equal in length.

By additionally including periodic variation of fiber loss coefficient and nonlinear coefficient and following our derivation of SI in the presence of periodic power variation and periodic dispersion variation in [11], the n-order SI frequency ω_n shifted from carrier frequency can be obtained as

$$\omega_n = \pm\sqrt{\frac{1}{|\beta_{2av}|}\left(k_f n - 2\,\mathrm{sgn}(\beta_{2av})P_0|F_0|\right)}\,, \qquad (1)$$

which is derived from the case that the amplification period l_f is set equivalent to the dispersion management period l_d. In Eq. (1), P_0 denotes the input signal power, $k_f = 2\pi/l_f$, β_{2av} the average group velocity dispersion (GVD). It should be noted that the GVD parameter β_2 relates to the dispersion parameter D by $D = -\omega_0\beta_2/\lambda_0$, where ω_0 and λ_0, respectively, denote the carrier frequency and the carrier wavelength. In Eq. (1), F_0 is obtained from

$$F_0 = \gamma_1\left(\frac{1-\exp(-\alpha_1 l_d/2)}{\alpha_1 l_d}\right) + \gamma_2\left(\frac{\exp(-\alpha_2 l_d/2)-\exp(-\alpha_2 l_d)}{\alpha_2 l_d}\right), \qquad (2)$$

where α_1 and γ_1 represent the fiber loss coefficient and the nonlinear coefficient of the first fiber, whereas α_2 and γ_2 the fiber loss coefficient and the nonlinear coefficient of the second fiber in the link, respectively. The n-order SI gain $\lambda(\omega_n)$ appearing at resonance frequency ω_n becomes

$$\lambda(\omega_n) = 2P_0\left|\begin{array}{l}\frac{1}{l_f}\int_0^{\frac{l_d}{2}}\gamma_1\exp(-\alpha_1 z)\exp\left(-j(C+n)k_f z\right)dz \\ +\frac{1}{l_f}\exp(-\alpha l_f/2)\exp(-j(C+n)\pi) \\ \int_{\frac{l_d}{2}}^{l_d}\gamma_2\exp(-\alpha_2 z)\exp\left(j(C-n)k_f z\right)dz\end{array}\right|, \qquad (3)$$

where C denotes a real number larger than zero and $Ck_f = \beta_{2fl}\omega_n^2$, where β_{2fl} is the fiber local GVD differing from β_{2av}. Equation (3) indicates that, for the n-order SI gain, by increasing fiber local SOD through the increasing in C, the wave constant k_f is virtually shifted to $(C+n)$ for the first term and to $(C-n)$ for the second term. Intrinsically, the resonance at higher k_f exhibits lower gain, therefore, to increase fiber local SOD will lead to the reduction of SI gain. Since the SMF-RDF based fiber link yields large local SOD, sufficient low SI gain is also expectable. From Eq. (1), it is remarkable that the position of n-order SI frequency is determined only by β_{2av} without the dependence on β_{2fl}. On the other hand, $\lambda(\omega_n)$ depends not only on β_{2fl} but also on β_{2av} through ω_n according to Eq. (1) and (3).

Equation (3) can be utilized to calculate the gain map of the first order SI concerning the SMF+RDF combination based fiber link, which is useful for determining the operating P_0 and D_{av}. Figure 2 shows the gain contour map of the first order of SI concerning the dispersion managed transmission line using the combination of SMF and RDF. In obtaining Fig. 2, we substitute SMF parameters α_1 =0.2dB/km, γ_1 =1.6W^{-1}km^{-1} and RDF parameters α_2 =0.25dB/km, γ_2 =4.8W^{-1}km^{-1} [2] into Eq. (3), and assume the fiber local SOD $|D|$ =17ps/km/nm with positive sign for the SMF and minus sign for the RDF, following by setting l_d equivalent to l_f at 40km. It should be noted that we should concentrate to the first order SI because, practically, the low order of SI is easier to be phase-matched and causes problem in the long haul transmission than other high orders. In Fig. 2, for low

P_0, which is referred to relatively short transmission, SI possesses relatively low gain over a wide range of D_{av}. For high power transmission, using low D_{av} can avoid the SI gain and, at the same time, move the SI position out of the signal carrier. However, at some points of P_0, the SI gain exhibits large value even at very low D_{av}, for examples, SI gain as high as 9×10^{-4}km^{-1} arises from P_0 = 5mW at D_{av} = -0.5ps/km/nm. In order to achieve the maximum performance of the system, these operating points should be avoided. It should be noted when this periodic dispersion management using SMF and RDF is not applied to the system, the first order SI induced from only periodic amplification in dispersion-shifted fiber chain exhibits high gain larger than 10^{-3}km^{-1} even P_0 > 2mW is used.

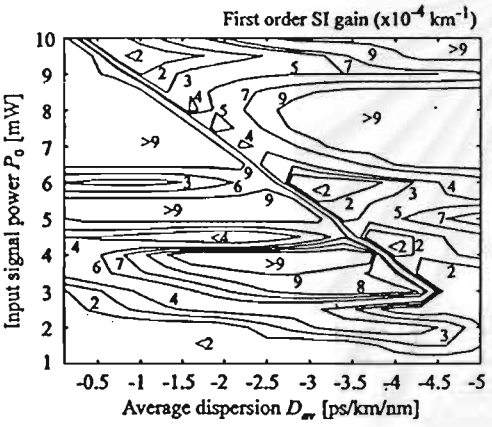

Fig. 2: Gain contour map of the first order of SI concerning the dispersion managed transmission line consisting of SMF and RDF for $l_d = l_f$ = 40km and $|D|$ = 17ps/km/nm with positive sign for the SMF and minus sign for the RDF.

3. Effect of SI on long-haul DWDM transmission systems

It has been shown theoretically that in order to avoid the XPM-induced signal waveform distortion for 10Gbit/s-based 10,000km WDM-transmission, the use of channel spacing larger than 100GHz is preferable [12]. Several long-haul transmission experiments also demonstrate attractive results using the channel spacing around this value [4], [7]. With this relatively large channel spacing, the first order SI, which usually exhibits large gain than higher orders, will not arise inside one's channel bandwidth. Therefore, the problem induced from SI has not been yet appeared and can be ignored for such transmissions.

However, with system distance shorter than 10,000km, the possibility of using smaller channel spacing for signal transmission has been shown [13], [14]. Moreover, to realize long-haul controversial dense wavelength division multiplexed (DWDM) transmission, the channel spacing has a tendency to be shortened closer to Nyquist limit. In this situation, for dispersion managed transmission system consisting of SMF and RDF, since all channels experience almost the same amount of D_{av}, each channel produces its own SI that occurs at frequency shifted from carrier frequency by the same amount of frequency shift with almost the same gain. If two different channels produce SI at the same frequency, SI will cause a serious problem to the channels whose carriers are placed just at that frequency especially for the frequency where the first order SI arises.

In order to confirm our mention, we perform computer simulations of the transmission of 4-wavelength CW signal and amplified spontaneous emission (ASE) noise. In the first calculation, we focus on the case when the first order SI gain generated from two separated channels enhances each other and positions on the other two channels. In the calculations, l_d is set equal to l_f at 40km and other SMF and RDF parameters are the same as those used in the calculation of Fig. 2. The propagation of optical signal is calculated by solving the nonlinear Schrodinger equation by using the split-step Fourier method [3].

According to the contour map in Fig. 2, to investigate the problem of SI even the system is operating with condition that yields relatively low SI gain, we select P_0 = 3mW and D_{av} = -0.5ps/km/nm, which yields the first order SI gain about 2×10^{-4}km^{-1}. Using Eq. (1) and the calculation parameters, the first order SI will arise at $\pm$ 77.4GHz shifted from each carrier frequency. Next, we place four channels at the frequencies –116.1GHz, -38.7GHz, 38.7GHz, and 116.1GHz shifted from the zero-dispersion wavelength 1,550nm respectively. By this arrangement, SI produced from channel#1 and channel#3 will arise just at the position of channel#2 carrier. Similarly, SI induced from channel#2 and channel#4 will occurs just at the position of channel#3.

Figure 3(b) shows the spectrum of the 4-channel CW signal transmitted over 4,000km comparing with its initial shape shown in Fig. 3(a). By this channel allocation, the serious distortion of CW spectrum is clearly observed. In order to avoid this problem, it is necessary to arrange the channel allocation in such a way that none of the channel is placed on the SI frequency. Figure 3(c) and (d) respectively shows the initial four-channel CW signal spectrum and its shape after 4,000km transmission simulated by the same parameters as Fig. 3(b). The channel spacing in this calculation is decreased 10GHz resulting in the shift of SI frequency out of signal bandwidth. Comparing to Fig. 3(b) where the SI occurs just at the channel position, the output spectrum in Fig. 3(d) appears in similar shape to the initial than the case of Fig. 3(b), confirming the achievement of avoiding the effect of SI. In fact, as FWM among channels is easy to be phase-matched when the channel spacing becomes smaller [3], the decrease in channel spacing should have led to more signal

distortion. However, the transmitted spectrum in Fig. 3(b) appears in more severe distorted shape than that of Fig. 3(d). This can be interpreted that the effect of SI plays a significant role in determining the transmission performance than the inter-channel FWM for this condition.

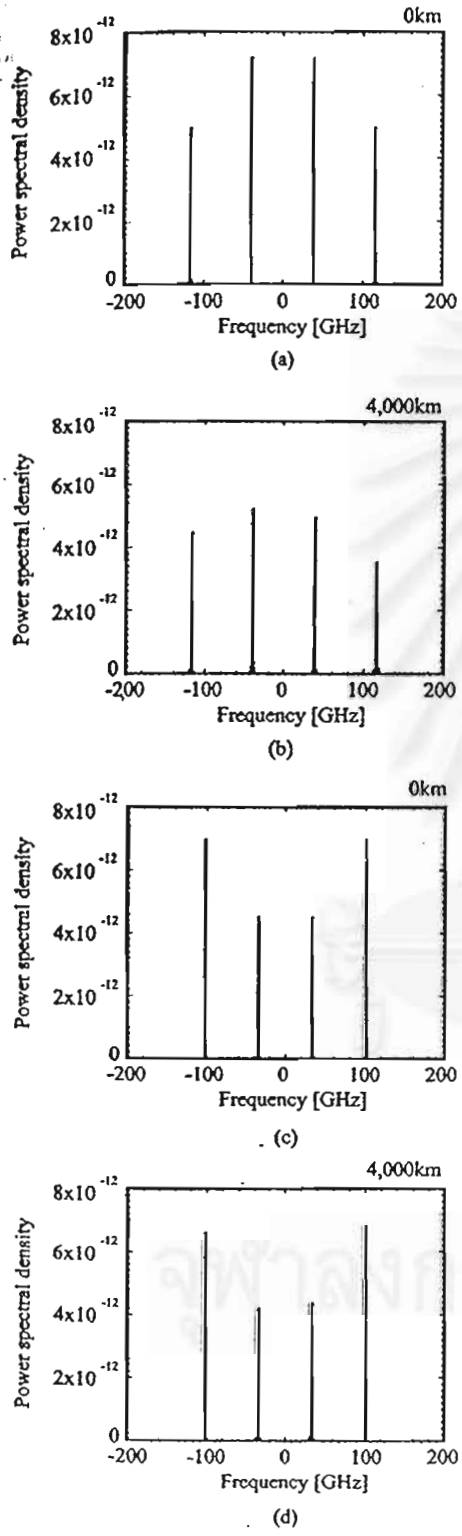

Fig. 3: Optical spectrum of 4-channel CW signal. P_0 = 3mW and D_{av} = -0.5ps/km/nm. In (a) and (b) the channel spacing is set at ± 77.4GHz where two of the first order SI from neighbor channels arise just at channel#2 and channel#3 carrier positions. (a) initial shape and (b) 4,000km-transmitted spectrum. By this channel allocation, serious distortion of CW spectrums is clearly observed. (c) and (d), respectively, shows the initial and 4,000km-transmitted CW spectrums simulated by decreasing 10GHz to shift SI frequency out of signal bandwidth. The transmitted spectrum in (b) appears in more severe distorted shape than (d) because of SI.

To explore the effect of SI on WDM transmission more details, we perform the calculation of the bit-error rate (BER) of the 4-channel WDM system using pseudorandom 32-bit Gaussian RZ pulse train as an input optical signal whose bit rate of each channel is equal to 10Gbit/s. At the end of the system, the accumulated D_{av} is post-compensated by multiplying the complex amplitude of the signal with a negative amount of linearly accumulated phase shift caused by D_{av}. We assume the use of a bandwidth-adjustable optical band-pass filter (OBPF) in front of the receiver to select the passband channel. This OBPF is also always adjusted to obtain minimum BER. The receiver is modeled by 6.5GHz-cutoff sixth-order Bessel-Thompson low-pass filter following by BER detector.

BER of detected signal is calculated by repeating 128times the transmission of the same pulse train and assuming Gaussian distribution of amplifier noise. Figure 4(a) and (b), respectively, shows the calculated BER curves of channel#2 and 3 as a function of transmission distance simulated by P_0 = 3mW and D_{av} = -0.5ps/km/nm with different channel spacing setting. The BER curves obtained from the system whose signal carriers are placed on the position where the SI arises (shown by circles) drop more rapidly than those obtained from 10GHz-decreased channel spacing (shown by squares). If we defined the maximum transmission distance obtained at the distance where the BER reaches 10^{-9} as shown by the across dotted line, the systems where the channel allocation is arranged to avoid the position of SI yield significantly longer transmission length. We also simulated the system with P_0 = 5mW and D_{av} = -0.5ps/km/nm that yields high SI gain. The result showed more severe degradation of BER for channel carriers positioned just on SI frequency and, on the contrary, an obvious improvement when a channel allocation is done to avoid the SI frequency. This confirms the necessity of avoiding SI in higher-order dispersion management long-haul WDM transmission systems.

4. Conclusion

In this paper, we have presented the analytical expression of the sideband instability (SI) induced from periodic signal power variation and periodic dispersion

management considering when two different fibers are connected together to form the dispersion compensation link.

In DWDM systems that use relatively narrow channel spacing, we demonstrated that even the dispersion map is properly designed to achieve low SI gain, SI causes signal distortion to specific channels that fall just on the low order SI frequency, especially the first order. Additionally to WDM system design rules, the channel allocation must avoid the SI position in such a way that none of the channel should be lied at. The computer simulations have confirmed that BER of WDM systems whose channel location is re-arranged to avoid SI give a significant improvement of the transmission performance.

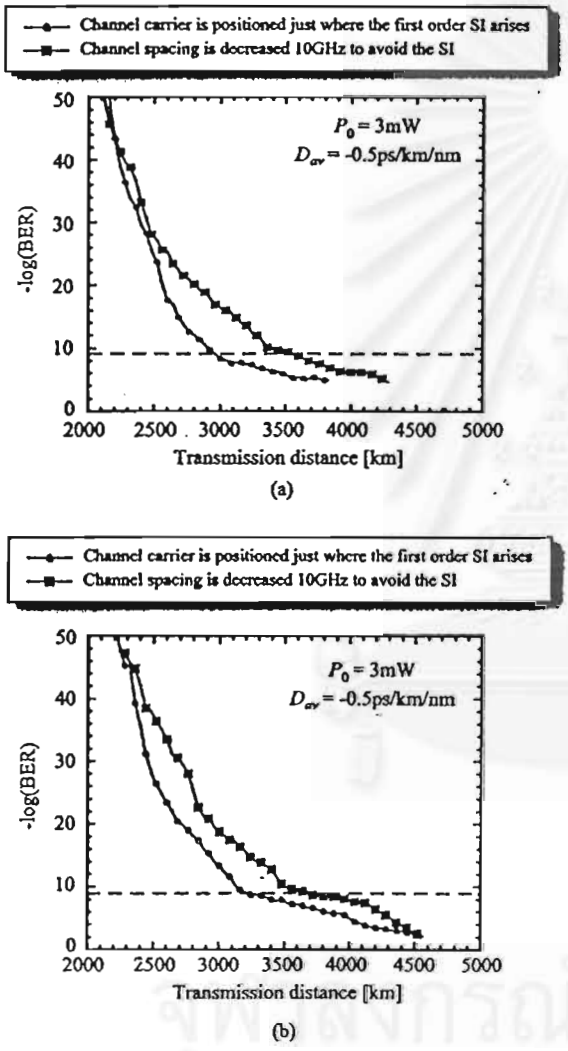

Fig. 4: BER as a function of transmission distance calculated from the 4x10Gbit/s 32-bit RZ signal for different channel spacings. (a) and (b) show BER curves of channel#2 and channel#3, respectively. In both (a) and (b), circles show BER obtained from the system whose signal carriers are placed on the position where the SI arises while squares show BER obtained from 10GHz-decreasing channel spacing. At BER = 10^{-9} (shown by an across dotted line) the systems where the channel allocation is re-arranged to avoid the position of SI give significantly longer transmission length.

References

[1] R. J. Nuyts, Y. K. Park, and P. Gallion, " Dispersion equalization of a 10Gbit/s repeatered transmission system using dispersion compensating fibers, " *J. Lightwave Technol.*, vol. 15, pp. 31-41, 1997.

[2] X. Wang, K. Kikuchi, and Y. Takushima, " Analysis of dispersion-managed optical fiber transmission system using non-return-to-zero pulse format and performance restriction from third-order dispersion, "*IEICE Trans. Electron.*, vol.E82-C, no.8, pp.1407-1413, 1999.

[3] G. P. Agrawal, *Nonlinear Fiber Optics.* New york: Academic Press, 1993.

[4] M. Murakami, T. Matsuda, H. Maeda, and T. Imai, " Long-haul WDM transmission using higher order fiber dispersion management, " *J. Lightwave Technol.*, vol. 18, no. 9, pp. 1197-1204, 2000.

[5] M. Morimoto, I. Kobayashi, H. Hiramatsu, K. Mukasa, R. Sugizaki, Y. Suzuki, Y. Kamikura, " Development of dispersion compensation cable using reverse dispersion fiber, " in *Proc. of Fifth Asia-Pacific Conference on Communications, 1999 and Fourth Optoelectronics and Communications Conference (APCC/OECC '99)*, vol. 2, pp. 1590-1593, 1999

[6] M. Kazunori, T. Yagi, " Dispersion flat and low nonlinear optical link with new type of reverse dispersion fiber (RDF-60), " in *Proc. Opt. Fiber Comm. (OFC'2001)*, Anaheim, CA, Mar. 17-22, 2001, paper TuH7

[7] T. Naito, N, Shimojoh, T. Tanaka, H. Nakamoto, M. Doi, T. Ueki, and M. Suyama, " 1 Terabit/s WDM transmission over 10,000km, " in *Proc. European Conf. on Opt. Commun. (ECOC'99)*, Nice France, Sept. 26-30, 1999, PD2-1, pp. 24-25.

[8] F. Matera, A. Mecozzi, M. Romagnoli and M. Settembre, " Sideband instability induced by periodic power variation in long distance fiber links, " *Opt. Lett.*, 18, pp. 1499-1501, 1993.

[9] K. Kikuchi, C. Lorattanasane, F. Futami, and S. Kaneko, " Observation of quasi-phase matched four-wave mixing assisted by periodic power variation in a long-distance optical amplifier chain, " *IEEE Photon. Technol. Lett.*, vol. 7, no. 11, pp. 1378–1380, 1995.

[10] N. J. Smith and N. J. Doran, "Modulation instability in fibers with periodic dispersion management, " *Opt. Lett.*, vol. 21, pp. 570-572, 1996.

[11] K. Pasu and A. Tuptim, " Sideband instability in the presence of periodic power variation and periodic dispersion management, " in *Proc. Opt. Fiber Comm. (OFC'2001)*, Anaheim, CA, Mar. 17-22, 2001, paper WDD32

[12] F. M. Madani and K. Kikuchi, " Design theory of long-distance WDM dispersion-managed transmission system, " *J. Lightwave Technol.*, vol. 17, pp. 1326-1335, 1999.

[13] H. Nakamoto, T. Tanaka, N. Shimojoh, T. Naito, I. Yokota, A. Sugiyama, T. Ueki, and M. Suyama, " 1.05Tbit/s WDM transmission over 8,186km using distributed Raman amplifier repeaters, " in *Proc. Opt. Fiber Comm. (OFC'2001)*, Anaheim, CA, Mar. 17-22, 2001, paper TuF6

[14] E. Shibano, S. Nakagawa, T. Kawazawa, H. Taga, and K. Goto, " 96x11.4Gbit/s transmission over 3,800km using C-band EDFA and non-zero dispersion shifted fiber, " in *Proc. Opt. Fiber Comm. (OFC'2001)*, Anaheim, CA, Mar. 17-22, 2001, paper TuN2

Simultaneous Suppression of Third-Order Dispersion and Sideband Instability in Long-Haul Ultra-High Speed Midway Optical Phase Conjugation Systems Using Higher-Order Dispersion Management

Pasu Kaewplung[1], Tuptim Angkaew[1], and Kazuro Kikuchi[2]
1. Department of Electrical Engineering, Faculty of Engineering, Chulalongkorn University, Phayathai Rd., Pathumwan, Bangkok 10330, Thailand
Phone (66-2)218-6907, Fax (66-2)218-6912, E-mail : pasu@ee.eng.chula.ac.th
2. Research Center for Advanced Science and Technology (RCAST), University of Tokyo, Komaba, Meguro-ku, Tokyo, 153-8904, JAPAN
Phone: (81-3)5452-5123, Fax: (81-3)5452-5125, E-mail : kikuchi@ginjo.rcast.u-tokyo.ac.jp

Abstract

In optical phase conjugation (OPC) systems, the third-order dispersion (TOD) of optical fibers and the nonlinear resonance at well-defined signal sideband frequencies called sideband instability (SI) mainly limit the transmission performance. We propose, for the first time, a scheme for simultaneous suppression of both TOD and SI in OPC systems using a higher-order dispersion-managed link consisting of standard single-mode fibers (SMFs) and reverse dispersion fibers (RDFs). Numerical simulation results show that 100Gbit/s transmission using OPC with SMF+RDF has achieved the transmission length at BER=10^{-9} over 2,000km longer than system where SI is not suppressed even the nonlinear length of the system becomes comparable with the amplifier spacing.

Keywords: optical fiber transmission, fiber nonlinearity, dispersion, third-order dispersion, dispersion compensation, optical phase conjugation.

1. Introduction

In ultra-high bit-rate optical-time-division multiplexed (OTDM) transmission systems, both second-order dispersion (SOD) and third-order dispersion (TOD) of transmission fibers must be completely compensated. Among available such dispersion compensation schemes, the special dispersion compensating fiber called reverse dispersion fiber (RDF) [1], [2] seems to be more practical and attractive than other TOD compensators owing to its low loss, low nonlinearity, and low polarization mode dispersion (PMD). By combining with conventional single-mode fiber (SMF) in each span, a dispersion flattened fiber link with low average SOD for simultaneously compensating both SOD and TOD is achieved. Several recent OTDM transmission experiments have demonstrated very attractive results of SMF+RDF combination based systems such as the transmission of 640Gbit/s over 92km [3] and even a data bit rate as high as 1.28Tbit/s over 70km [4].

As an alternative approach for ultra-high bit-rate long-haul transmission, midway optical phase conjugation (OPC) is an attractive solution to compensate for the distortion induced from the interplay between SOD and self-phase modulation (SPM) [5]. However, the ultimate performance of the OPC systems is also limited by TOD together with a nonlinear resonance at well-defined signal sideband frequencies induced by periodic signal power variation through amplification process called sideband instability (SI) effect [5]. Recently, we have demonstrated by numerical simulation that the single-channel 100Gbit/s, 10,000km transmission can be made possible by using the optimum signal power in the OPC system incorporated with TOD compensation [6].

For the SI effect, recently, our analysis has demonstrated a more practical way to suppress SI by only applying strong dispersion management [7], [8]. Therefore, by using such combination of SMF and RDF in the OPC system, the simultaneous suppression of both SI and TOD can be expected.

In this paper, we show, for the first time to our knowledge, the simultaneous suppression of TOD and SI in ultra-high bit-rate long-haul OPC transmission systems using the dispersion-managed fiber link consisting of SMF and RDF. This paper is organized as follows. Section 2 reviews our previous works about the TOD compensation scheme in OPC systems and the reduction of the SI gain by employing the combination of SMF and RDF. Our main contributions presented here commence from section 3. In this section, we discuss an implementation of dispersion management in OPC systems. We suggest that a symmetric dispersion profile with respect to the mid-point of the system is preferable in order to avoid nonlinear accumulation of amplifier noise when the system operates with relatively high signal intensity. The simulation result shows that, even the system is operating in the worst condition of SI, the 100Gbit/s OPC systems using SMF+RDF dispersion-managed link has improved transmission length at BER=10^{-9} over 2,000km longer than system where SI is not suppressed.

2. Simultaneously suppression of TOD and SI by combination of SMF and RDF

As described above, the performance of OPC transmission systems is mainly limited by TOD and SI effect. Without TOD compensation, a 10,000km transmission with data rate of 40Gbit/s was achieved by following optimum design strategies to avoid the effect of SI [5]. To increase the transmission bit-rate of the 10,000km OPC systems, it is necessary to suppress both

TOD and SI. In this section, we review and summarize our previous studies on the TOD compensation scheme in OPC systems [6] and the reduction of SI gain through periodic strong dispersion-managed fiber link [7], [8].

2.1 TOD compensation scheme in OPC systems

The accumulation characteristic of TOD in OPC systems can be discussed through three characteristic scales: the SOD length L_{d2}, the TOD length L_{d3}, and the nonlinear length L_{nl}, which are defined in [9]. In OPC systems, SOD exists along the entire transmission length; therefore, L_{d2} becomes many times shorter than L_{nl} for the case of high bit-rate transmission. When L_{d2} is much shorter than L_{nl} and L_{d3}, the signal pulses are rapidly broadened by SOD, and their peak power decreases after transmitting for several L_{d2}. This means that the broadened pulses almost do not experience the effect of fiber nonlinearity. Thus, in ultra-high-speed OPC systems, the accumulation of the TOD-induced phase shift increases almost linearly with the transmission length at an ordinary operating signal power. The linear TOD accumulation enables us to achieve perfect TOD compensation by placing only one compensator at any point in the line, or even freely installing distributed compensators without the necessity of concerning their intervals.

When TOD is perfectly compensated in OPC systems, the 100Gbit/s data transmission over 10,000km [6] can be made possible at the balance point of the improvement of signal-to-noise ratio (SNR) and the degradation from SI effect. In order to further improve the transmission performance of the TOD-compensated OPC system, the waveform distortion induced from SI effect must be overcome.

2.2 Reduction of Sideband instability gain by strong dispersion management

For long distance transmission, periodic lump amplification is used for maintaining good SNR at a receiver. The fiber loss and the periodic gain form a periodic signal power distribution along the system length, producing a periodic variation of the fiber refractive index through the nonlinear Kerr effect of an optical fiber. This process constructs a virtual grating in the transmission fiber. The resonance between the virtual grating and the signal will occur at signal sideband components whose wave vectors match with the wave vector of this virtual grating, resulting in exponential growth of those components with transmission length.

This phenomenon is known as sideband instability (SI), which causes signal waveform distortion if SI arises at frequencies inside the signal bandwidth [10]. Since the signal power distribution in practical OPC systems is not symmetrical with respect to the mid-point, SI cannot be compensated and will accumulate to the end of the system length.

The gain of SI can be practically reduced by using a strong periodic dispersion-managed transmission line such as the combination of SMF and RDF, instead of uniform dispersion line [7]. This is because the increase in the local fiber dispersion virtually shifts the order of SI to higher orders resulting in the difficulty of phase-match process. Furthermore, the frequency where SI arises depends on the larger period between the amplifier spacing (l_f) and the dispersion management period (l_d). The larger the variation period becomes, the closer to the carrier frequency the SI frequency arises.

In order to show the reduction of SI gain through a periodic dispersion-managed line, here we calculate the gain contour map of the first-order SI focusing on the dispersion-managed transmission line consisting of SMF and RDF. The dispersion management profile is the simple type where one SMF and one RDF with equivalent length are only connected together. In each dispersion management period, SMF is placed before RDF at the output end of the amplifier. The placement of signal carrier frequency determines the values of the operating average dispersion D_{av} and the local dispersion D. In Fig. 1, the gain map is obtained as a function of l_d and an input signal power P_0 when D_{av} and D are given. It should be noted that we should concentrate to the first order SI because, practically, the low order of SI is easier to be phase-matched and causes more serious signal distortion in long haul transmission systems than higher order SI. The fiber loss coefficient α_1 and the fiber nonlinear coefficient γ_1 of SMF used for calculating the gain map are 0.2dB and $1.6W^{-1}km^{-1}$, respectively, while α_2, γ_2 representing those of RDF are 0.25dB and $4.8W^{-1}km^{-1}$, respectively. D_{av} is set at –1ps/km/nm and $|D|$ = 17ps/km/nm. Comparing with these gain maps, the magnitudes of the first, second, and third-order SI gains of a non-dispersion management system as a function of the input power is shown in Fig. 2. In this case, the transmission fiber is assumed to be a dispersion-shifted fiber (DSF) with α =0.2dB and γ = $2.6W^{-1}km^{-1}$.

In Fig. 1, for low P_0 (< 3mW), SI possesses very low gain over a wide range of l_d; thus, SI may not affect the signal transmission for relatively short distance systems. Even in high power transmission (from 3mW to 15mW), SI still exhibits relatively low gain ($<10^{-3}km^{-1}$) comparing with the gain shown in Fig. 2 at the same P_0. Without dispersion management, Fig. 2 indicates that the SI gain almost linearly increases with P_0 and exhibits a value larger than $10^{-3}km^{-1}$ even for P_0 = 2mW for the first-order SI.

The linear accumulation of TOD, together with the reduction of SI gain through strong dispersion management open a possibility of simultaneously

suppressing TOD and SI in OPC systems by using the higher-order dispersion management transmission line such as the combination of SMF and RDF.

Assuming that TOD and SI are perfectly suppressed in OPC systems, there remains the problem originated from the accumulation of the transmission of amplified spontaneous emission (ASE) noise which is enhanced during the transmission by parametric interaction between SOD and SPM [11]. Since the transmission of the ASE noise is not symmetrical with respect to the midpoint of the system. Thus, only part of the nonlinear enhancement can be compensated by OPC while there still exists the accumulated ASE noise, which is enhanced by the nonlinear interaction.

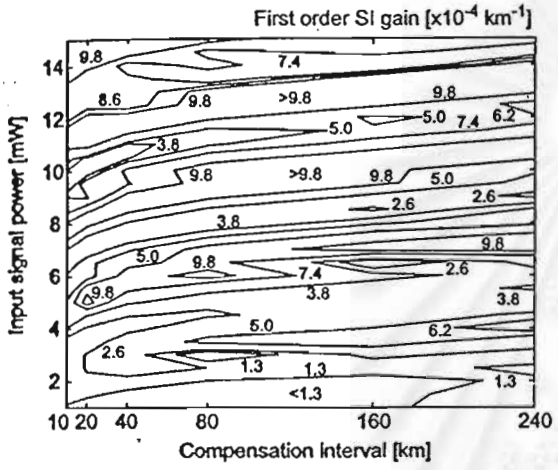

Fig. 1: Gain contour map of the first-order SI focusing on the dispersion-managed transmission line consisting of SMF and RDF. The gain is calculated as a function of l_d and an input signal power P_0 when an average dispersion D_{av} and a fiber local dispersion $|D|$ are set at −1ps/km/nm and 17ps/km/nm, respectively.

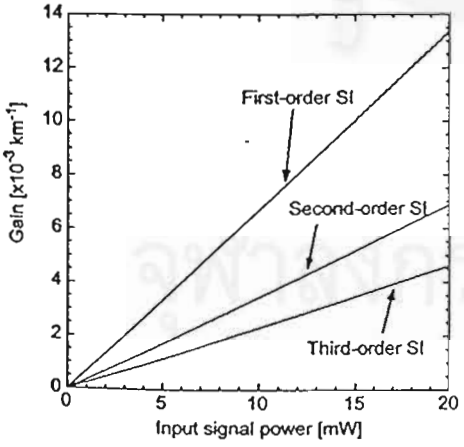

Fig. 2: Magnitudes of the first, second, and third-order SI gains arising from a non-dispersion management system. The gains are obtained as a function of signal input power. The transmission fiber is assumed to be only DSF with α =0.2dB and $\gamma = 2.6 W^{-1}km^{-1}$.

It should be noted that this fiber nonlinearity-enhanced ASE noise cannot be suppressed by the combination of SMF and RDF. However, its harm is expected to reduce through large fiber local dispersion with sufficiently large compensation period. This is because the signal pulses are rapidly broadened by SOD, therefore, they almost do not experience the effect of fiber nonlinearity.

3. Implementation of dispersion management on OPC systems

The most practical way available now to compensate TOD for ultra-high bit-rate long-haul transmission is probably the use of the dispersion-managed fiber link such as the combination of SMF and RDF. In the previous section, we have shown that SI induced from the periodic power variation can be suppressed by using periodic dispersion management with large local dispersion. Therefore, by using such combination of SMF and RDF in OPC systems, the simultaneous compensation of both TOD and SI can be expected. Moreover, the accumulation of D_{av} will be automatically compensated by OPC without post compensation used in ordinary dispersion management systems.

3.1 Possible installing dispersion profiles

Figure 3 illustrates two possible schemes to install dispersion management in the OPC transmission system. In Fig. 3(a), both periodic dispersion variation and periodic power variation are in uniform distributions along the entire system length. On the other hand, in Fig. 3(b), the order of SMF-RDF is reversed to RDF-SMF after the midway OPC yielding the symmetric distribution of the periodic dispersion variation with respect to the system mid-point.

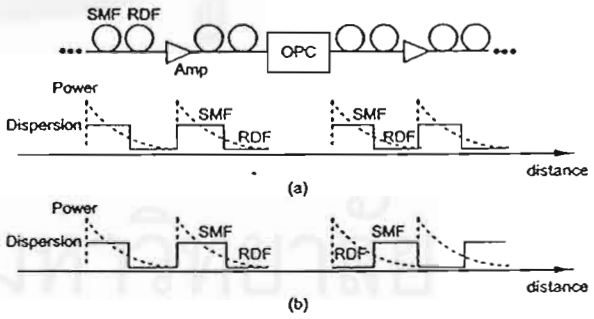

Fig. 3: Two possible ways for implementing the dispersion management in OPC transmission system. In (a) both periodic dispersion variation and periodic power variation are in uniform distributions along the entire system length. On the other hand, in (b), the order of SMF-RDF is reversed to RDF-SMF after the system mid-point, forming the symmetric

distribution of the periodic dispersion variation with respect to the system mid-point.

We suggest that the symmetric dispersion profile in Fig. 3(b) gives better transmission performance than the other profile especially for high power transmission. The reasons can be explained as follows. First, when the nonlinear length L_{nl} is longer than the periods of the variations, due to the uniform distributions in Fig. 3(a), each order of SI arises from one frequency determined by the two periodic perturbations and experiences the gain whose magnitude exponentially increases with the transmission length. On the other hand, for the dispersion management profile in Fig. 3(b), the system in the first half and second half produce their own SI at different frequencies whose separation depends on the difference in the nonlinear coefficient and the fiber loss coefficient between SMF and RDF. However, each resonance frequency experiences the SI gain only half of the system length, the signal distortion may not be so severe as that occurs from the dispersion profile in Fig. 3(a).

Second, for high power transmission, when L_{nl} becomes comparable or shorter than the compensation interval, the interplay between SPM and the local dispersion of each fiber occurs and causes additional signal waveform distortion. With this consideration, by constructing the symmetric dispersion compensation profile as shown in Fig. 3(b), part of the interaction between SPM and local dispersion of the fiber will be compensated by OPC whether the power variation distribution remains unchanged. Oppositely, for the profile in Fig. 3(a), this interaction will accumulate along the transmission length due to the asymmetric distribution with respect to mid-point of both periodic power variation and periodic dispersion compensation.

3.2 Computer simulations

In order to evaluate our proposed SI suppression method in OPC systems, we perform a computer simulation of the transmission of 100Gbit/s data composed of 32bit pseudorandom Guassian RZ pulses based on the system models in Fig. 3. In the calculation, we set $l_d = l_f$ at 40km. TOD is assumed to be 0.06ps/km/nm for SMF and -0.06ps/km/nm for RDF. Other SMF and RDF parameters used in this simulation are the same as used in Fig. 1. The optical amplifier produces ASE noise with noise figure of 5.3dB ($n_{sp} = 1.7$). The optical pulse at the midway of the system is conjugated by an ideal infinite-bandwidth optical phase conjugator.

When the combination of SMF and RDF is not applied for TOD compensation, the TOD compensator, placed only at the end of system, is assumed to be an ideal device that multiplies the complex amplitude of the signal with a negative amount of linearly accumulated phase shift caused by TOD. Also, for signal transmission in this case, DSF with the same parameters as the calculation in Fig. 2 is used.

To see the efficiency of the SI suppression more obviously, the input signal power P_0 is set at 21mW giving L_{nl} becomes equivalent to l_f. Also for all other cases, P_0 will be set at this value. Since SMF and RDF exhibit different values of α and γ, we calculate L_{nl} of the system employing SMF and RDF by using the average values of those parameters. With P_0=21mW, L_{nl} of the system constructed by SMF and RDF becomes approximately 36km, which is slightly shorter than that of DSF.

The bandwidth of the optical band-pass filter, which is placed at the output end of the fiber, is always adjusted to obtain the minimum BER. The propagation of the optical pulse is calculated by solving the nonlinear Schrodinger (NLS) equation by the split-step Fourier method [9]. The receiver is modeled by 65GHz-cutoff sixth-order Bessel-Thompson low-pass filter followed by a BER detector. The system performance is evaluated in terms of the bit-error rate (BER) calculated by repeating 128times the transmission of the same pulse train and assuming the Gaussian distribution of the amplifier noise.

Figure 4 shows the calculated BER as a function of transmission distance. According to the condition $L_{nl} = l_f$, when only TOD is compensated (shown by circles), the performance of the system is limited by SI and the nonlinear distortion from the interaction between SPM and local dispersion in each segment of fiber. Thus, BER of the system in this case rapidly decreases. When the dispersion management profile in Fig. 3(b) is employed to the system (shown by squares), BER curve drops significantly slow. Comparing to the case without the combination of SMF and RDF, by using SMF and RDF, the achievable transmission length at BER=10^{-9} can be extended approximately 2,000km longer.

Moreover, the BER curve of the system where TOD is neglected (shown by crosses) almost fits with that obtained from TOD-compensated system. This result mentions that this SI suppression method does not affect accumulation characteristics of TOD since l_d is still much shorter than the TOD length L_{d3} ($\approx$ 280km) so that in the TOD scale, the signal propagates as if there is no dispersion management ever be installed.

On the other hand, BER of the system employing the dispersion profile of Fig. 3(a) (shown by triangles) obviously becomes worse than others due to the reasons described above. Furthermore, the difference in transmission distance between the BER curve obtained from the system using the dispersion profile of Fig. 3(b) and the BER curve obtained from the system neglecting TOD and SI (shown by diamonds) mainly comes from part of the interaction between SPM and local fiber dispersion that cannot be perfectly compensated by OPC.